AD NUMBER: AD0517006
CLASSIFICATION CHANGES
TO: Unclassified
FROM: Confidential
LIMITATION CHANGES
TO: Approved for public release; distribution is unlimited.
FROM: Distribution authorized to US Government Agencies only; Export Control; 28 Aug 1971. Other requests shall be Air Force Rocket Propulsion Laboratory, Edwards AFB, CA 93523
AUTHORITY
U per GDS dtd 28 Aug 1983; ST-A per AFRPL ltr dtd 10 Mar 1986

GENERAL DECLASSIFICATION SCHEDULE

IN ACCORDANCE WITH
DOD 5200.1-R & EXECUTIVE ORDER 11652

SECURITY MARKING

The classified or limited status of this report applies to each page, unless otherwise marked.
Separate page printouts MUST be marked accordingly.

AFRPL - TR - 71 - 75

NOFORN
CONFIDENTIAL

(UNCLASSIFIED TITLE)

ACOUSTIC LINER DESIGN AND DEMONSTRATION FINAL REPORT

G. D. Garrison et al
Pratt & Whitney Aircraft
Division of United Aircraft Corporation
Florida Research and Development Center

Technical Report AFRPL-TR-71-75
August 1971

NOFORN

FOREIGN NATIONAL EMPLOYEES OF THE CONTRACTOR OR SUBCONTRACTOR(S), INCLUDING THOSE POSSESSING CANADIAN OR UNITED KINGDOM RECIPROCAL CLEARANCE, ARE NOT AUTHORIZED ACCESS TO CLASSIFIED INFORMATION RESULTING FROM, OR USED IN THE PERFORMANCE OF THIS CONTRACT UNLESS AUTHORIZED IN WRITING BY THE PROCURING CONTRACTING OFFICER.

Air Force Rocket Propulsion Laboratory
Air Force Systems Command
United States Air Force
Edwards Air Force Base, California

GROUP 4
DOWNGRADED AT 3 YEAR INTERVALS;
DECLASSIFIED AFTER 12 YEARS

NOFORN
CONFIDENTIAL

Printed in the United States of America

"When U. S. Government drawings, specifications, or other data are used for any purpose other than a definitely related Government procurement operation, the Government thereby incurs no responsibility nor any obligation whatsoever, and the fact that the Government may have formulated, furnished, or in any way supplied the said drawings, specifications, or other data, is not to be regarded by implication or otherwise, or in any manner licensing the holder or any other person or corporation, conveying any rights or permission to manufacture, use, or sell any patented invention that may in any way be related thereto."

AFRPL - TR - 71 - 75
28 August 1971

(UNCLASSIFIED TITLE)

ACOUSTIC LINER DESIGN AND DEMONSTRATION FINAL REPORT

G. D. Garrison, et al

Prepared Under

Contract F04611-69-C-0017

Air Force Rocket Propulsion Laboratory
Air Force Systems Command
United States Air Force
Edwards Air Force Base, California

Printed in the United States of America

FOREWORD

This report is submitted in compliance with the requirements of Contract F04611-69-C-0017 and presents the results of work accomplished at Pratt & Whitney Aircraft, Florida Research and Development Center under both of the two phases of the program. All work was performed during the period 15 November 1968 through 30 April 1971. This report was submitted on 9 June 1971.

The Air Force Project Number is 3058. The Program Structure Number (BPSN) is 623058. The Pratt & Whitney Aircraft Document Control Number is PWA FR-4515.

The Air Force Project Officer was 1st Lt. W. L. Pritz, AFRPL (RTSC). The following personnel of Pratt & Whitney Aircraft contributed to the technical effort and preparation of the report: P. L. Russell, C. D. Baldwin, A. P. Genchi, J. F. Presley, and J. W. Koenig. The Pratt & Whitney Aircraft Program Manager was Mr. G. D. Garrison.

This report is classified Confidential to prevent unauthorized disclosure of a relationship between two or more items and to protect a compilation of information and a complete analysis of the subject. All individual paragraphs are unclassified.

This report contains no classified information extracted from other classified documents.

This technical report has been reviewed and is approved.

Wayne L. Pritz, 1st Lt., USAF
Project Engineer, AFRPL (RTSC)

UNCLASSIFIED ABSTRACT

The objectives of this two-phase exploratory development program were (1) to demonstrate the effectiveness for suppressing combustion instability of a regeneratively cooled acoustic liner installed in flight-type hardware, and (2) to extend the acoustic liner design theory to include rocket chamber applications with high combustion gas velocities and high dynamic pressure amplitudes. Phase I consisted of the design, fabrication and firing of a fuel cooled, 15 thousand pound thrust chamber incorporating an integral acoustic liner, using an Agena injector known to be dynamically unstable with N_2O_4/50% N_2H_4-50% UDMH propellants. Before fabrication of the chamber was initiated, adequate suppression characteristics of the liner design were demonstrated in short duration tests of uncooled hardware. The uncooled test series included firings during which both the baseline heat transfer rates and the effects of liner apertures on the heat transfer rates were measured. Other uncooled firings were conducted to measure the dynamic stability characteristics of the potential flightweight liner design, to determine the minimum required liner length, and to supply data for the final liner design. Thirty uncooled firings and thirteen firings of the regeneratively cooled chamber were made; combustion in the regeneratively cooled chamber was demonstrated to be dynamically stable. The results under this phase of the program demonstrated that regeneratively cooled acoustic liners are feasible for flightweight thrust chamber applications. The necessary acoustic data for the Phase II theory extension were obtained from high Mach number cold flow impedance experiments, and from firings of an uncooled rocket motor using a technique based on the measurement of the complex pressure difference across the absorbing liner surface. The acoustic data formed the basis for appropriate theory extensions, and using the extended theory, two different types of resonant absorbing liners were designed for a spontaneously unstable, existing uncooled thrust chamber having a chamber Mach number of 0.32. Five firings were made with N_2O_4/50% UDMH-50% N_2H_4 propellants at a nominal thrust level of 5000 lb_f. The liners suppressed the most prevalent modes of combustion instability, but spontaneous pops triggered instability at frequencies greater than 6400 Hz. Both liners theoretically had sufficient absorption to suppress the high frequency modes. It was concluded that failure of the liners to suppress high frequency modes of instability in the particular test motor used was not caused by the high net flow past the liners, but was the result of errors from extrapolation of the liner design theory with frequency. Additional firings of the motor with liner elements instrumented for high frequency acoustic impedance measurements are recommended.

CONTENTS

ILLUSTRATIONS

ILLUSTRATIONS (Continued)

ILLUSTRATIONS (Continued)

ILLUSTRATIONS (Continued)

ILLUSTRATIONS (Continued)

TABLES

NOMENCLATURE

Symbol	Description	Units
A	Aperture Area	$in.^2$
c	Sonic Velocity	ft/sec
C_f	Aperture Flow Coefficient	
d	Aperture Diameter	in.
f	Frequency	Hz
k	Wave Number	ft^{-1}
L	Cavity Depth	in.
ℓ_{eff}	Aperture Effective Length	in.
M	Mach Number	
P	Pressure Amplitude (Peak Value)	$lb_f/in.^2$, db*, lb_f/ft^2
P_c	Chamber Pressure, Static	$lb_f/in.^2$
t	Liner Thickness	in.
u	Particle Velocity in Aperture (Peak Value)	ft/sec
V	Velocity	ft/sec
Z	Specific Acoustic Impedance	
α	Absorption Coefficient	
η_{c^*}	Combustion Efficiency	
θ	Specific Acoustic Resistance	
ρ	Density	lb_m/ft^3
σ	Open Area Ratio	
ϕ	Phase Difference	deg
χ	Specific Acoustic Reactance	

*Ref: 0.0002 microbar

Subscripts

0	Resonance
1	At Liner Facing
2	In Liner Cavity
a	Conditions in Aperture
c	Conditions in Combustion Chamber
C	Critical
n	No Flow
p	Past Flow
t	Through Flow
T	Theoretical

SECTION I
PROGRAM SUMMARY

A. BACKGROUND

With the completion of the first year of effort under Contract AF04-(611)-11387 (Reference 1), the capability of acoustic liners to suppress combustion instability in rocket thrust chambers was proved. From the results, it was recommended that the design analysis of rocket liners be based on the mean velocity of the combustion gas flowing past the liner. The theoretical maximum absorption that can be obtained with a liner is inversely proportional to the magnitude of the velocity past the apertures; therefore, the damping that can be achieved with resonant liners in rocket chambers having small (less than 1.5) contraction ratios could be insufficient to suppress combustion instability.

Work during the second year under that contract (Reference 2) was devoted to analysis and experimental evaluation of the effectiveness of film cooled, transpiration cooled, and ablative absorbing liners. Several convectively cooled liners have been successfully fired under various Air Force, NASA and Pratt & Whitney Aircraft research programs; however, all of these liners were water cooled. The fabrication of a pure regeneratively cooled liner for application in a flightweight motor had not been attempted.

Thus, the next logical steps in the investigation of acoustic liners for rocket chambers were to demonstrate the feasibility of regeneratively cooled resonant liners for flightweight chambers, and to investigate the effectiveness of absorbing liners in high Mach number combustion chambers.

B. OBJECTIVES

The objectives of the exploratory development program reported herein were (1) to demonstrate the effectiveness of a regeneratively cooled acoustic liner installed in flight type hardware, and (2) to extend the acoustic liner design theory to include rocket chamber applications with high combustion gas velocities and high dynamic pressure amplitudes.

C. APPROACH

To accomplish the objectives, a two-phase program was conducted. Phase I consisted of design, fabrication and firing tests of a regeneratively cooled thrust chamber incorporating an acoustic liner, using an Air Force supplied Agena injector with known instability characteristics. Before fabrication of the chamber was initiated, adequate suppression characteristics of the liner design were demonstrated in short duration tests of uncooled hardware. The uncooled test series included firings during which both the baseline heat transfer rates and the effects of liner apertures on the heat transfer were measured. Other uncooled firings were conducted to measure the dynamic stability characteristics of the potential flightweight liner design and to determine the minimum required liner length. In addition, to supply data for the final liner design, cavity gas temperatures were measured and the molecular weight of the gas was determined during several of the tests. A total of 30 uncooled firings were made. The regeneratively cooled chamber was subjected to 13 firings with N_2O_4/50% N_2H_4 - 50% UDMH propellants at a nominal thrust level of 15K. All tests of the regeneratively cooled chamber were dynamically stable.

The Phase II portion of the program was conducted to overcome uncertainties in the absorbing liner design theory and to extend the analytical model so that it is applicable to thrust chambers with gas velocities of up to 2000 ft/sec and with incident sound pressure levels of at least 210 db[1]. The necessary acoustic data were obtained from high Mach number, cold flow impedance experiments, and from hot tests of uncooled hardware. Both the cold flow data and the hot firing data were obtained using a technique based on the measurement of the complex pressure difference across the absorbing liner surface.

The acoustic data formed the basis for appropriate theory extensions, and using the extended theory, two new absorbing liners were designed for a series of high chamber Mach number verification tests. The verification tests were conducted with the uncooled thrust chamber fabricated under Contract AF04(611)-11387, Reference 1, after modifying the nozzle to produce a Mach number in the chamber of 0.32.

Five firings were made with N_2O_4/50% UDMH - 50% N_2H_4 propellants at a thrust level of 5000 lb_f. Combustion instability triggered by high amplitude, spontaneous pops occurred with both liners at frequencies of the fourth transverse mode and higher, i.e., greater than 6400 Hz. Theoretically, both liners had sufficient absorption to suppress the high frequency modes.

D. CONCLUSIONS AND RECOMMENDATIONS

From the results of this program the following conclusions and recommendations are made:

1. Combustion in the Agena motor is dynamically unstable with N_2O_4 oxidizer and 50% blended fuel.

2. A half-chamber length absorbing liner will cause combustion to be dynamically stable.

3. The chamber with the integral liners can be fuel cooled, regeneratively, with no loss in performance.

4. It is recommended that the use of regeneratively cooled chambers with integral acoustic liners be considered a solution for combustion instability problems in flightweight motors.

5. Failure of the Phase II acoustic liners to suppress high frequency modes of combustion instability in the particular test motor used was not caused by high flow past the liners.

6. To compute the theoretical absorption of the Phase II liners at frequencies greater than 3300 Hz extrapolations of the theory were necessary. It is therefore postulated that, because of error from these extrapolations, the actual absorption was not high enough to suppress the high frequency instability modes.

---

[1] In this report all pressures expressed in decibels (db) are based on a reference pressure of 0.0002 microbar.

7. Additional firings of the Phase II motor with the liners instrumented for high frequency, i.e., above 5000 Hz, impedance measurements are recommended.

This page intentionally left blank

SECTION II
PHASE I - REGENERATIVELY COOLED ACOUSTIC LINER DEMONSTRATION

A. GENERAL

The objective of the Phase I effort was to demonstrate the durability and effectiveness of a regeneratively cooled acoustic liner installed in flight-type hardware. Work toward this objective was begun by performing preliminary acoustic and cooling analyses. The acoustic analysis was performed to determine a liner configuration (aperture diameter, facing thickness, cavity volume and open area) suitable for application to a flightweight regeneratively cooled motor that would theoretically produce good absorbing characteristics. The preliminary cooling analysis was conducted to determine which of the propellants would be more suitable for use as the coolant and to determine the heat exchanger basic configuration, i.e., parallel or counterflow.

After the preliminary analyses were finished, a layout of the flightweight chamber was prepared. From the layout, uncooled hardware was designed for a series of short duration tests to demonstrate the combustion stability characteristics of the proposed flightweight design. Other uncooled hardware included liners and nozzles especially instrumented to measure the baseline heat transfer rates and the effects of liner apertures on the heat transfer.

Thirty firings were conducted with the uncooled hardware mated to the Agena injector to be used with the flightweight chamber. Conclusions drawn from the results of these tests were:

1. The motor operating with no liner at nominal conditions (500 psia, mixture ratio of 2) with N_2O_4/50% UDMH 50% N_2H_4 propellants, unless disturbed with an explosive device, would experience combination pressure oscillations of less than ±5% of chamber pressure.

2. Combustion disturbances induced by either radial or tangential pulse guns loaded with 50-grain C-4 explosive would cause peak-to-peak (P/P) oscillations of approximately 400 psi that would not damp.

3. A 6% open area, 1/2 chamber length liner would cause perturbations from pulse guns and nondirectional bombs to damp in approximately 0.015 sec or less.

4. The liner apertures had no significant effect on the wall heat flux.

5. Using the fuel as coolant had no adverse effect on motor stability.

The final design of the flightweight chamber was completed, detail drawings were prepared and sent to a vendor[2] for fabrication by electroforming. The

[2]Camin Laboratories, Inc., Brooklyn, New York

completed chamber was coated on the inside surfaces with a refractory, mated to the Agena injector and tested. The chamber was fired 13 times; after the fourth firing the chamber assembly was modified to correct a faulty seal between the fuel turnaround manifold and the cooled, acoustic liner pressure shell. Total run time was 117.2 sec; the last firing, the longest, was of 60 seconds duration. Combustion was disturbed with nondirectional bombs during 6 of the tests. The resulting perturbations decayed within 0.01 sec. From these results, it was concluded that regeneratively cooled chambers with integral acoustic liners are feasible for flightweight motor applications. A detailed discussion of work performed under this phase of the program follows.

B. DESIGN ANALYSES

1. Acoustic Preliminary Analysis

If the amount of absorption required to eliminate combustion instability were known and the frequency and intensity of the forces causing the instability were well established, the design of absorbing liners would be relatively simple. Unfortunately, this is not the case, and the designer is faced with the problem of providing a certain minimum absorption coefficient, the value of which is not too well known, over an arbitrary band of frequencies. Although the history of rocket engine absorbing liners indicates that only a small amount of absorption is required at a frequency of the first transverse mode of the combustion chamber, the designer of a liner for a new injector-thrust chamber application cannot be certain his requirements will be similar; thus he must design for the best possible absorption and bandwidth characteristics.

Good bandwidth performance is important for two reasons. First, typical acoustic liners of the Helmholtz-array type tend to possess resonant absorbing characteristics (i.e., high absorption coefficients are obtained near the resonant frequency of the assembly; however, at frequencies slightly different from resonance, the coefficients decrease to less than 50% of the peak value). The resonant frequency of the assembly can be determined with an accuracy no better than that of the assumed sonic velocity of the gas in the liner apertures and cavity. If the assumption is poor, peak absorption cannot be obtained, for the liner must operate with incident pressures at a frequency different from that of the resonant frequency for which it was designed. Second, in some instances the use of a resonant-type liner with poor bandwidth characteristics does not suppress the combustion instability, but causes it to shift to a different frequency with more or less the same pressure amplitudes. The additional wall impedance due to the presence of the liner apparently can cause a complete shift in the mode and type of pressure wave; e.g., from 1st tangential to 3rd longitudinal. No reliable techniques are available for predicting the effects of the liner impedance on the frequency of the potential instability. The obvious solution to both of the above problems is to design the liner so that high absorption is obtained over a range of frequencies corresponding to the most destructive modes; i.e., the first through the third transverse modes.

A review of the stability history of the Agena chamber fitted with either a S/N 7 or S/N 9 injector, the two injectors supplied for use in this program, and without baffles revealed that the 1st and 3rd transverse modes were the most predominate frequencies of instability (Reference 3). Frequencies corresponding to natural acoustic modes (up to the 2nd radial) were computed for the chamber

operating conditions which are described in table I. The results are shown in figure 1, in which frequency is plotted as a function of both mode and combustion gas sonic velocity; those velocities corresponding to combustion efficiencies (η_{c^*}) of 90, 96, and 100% are also identified. Frequencies for the most likely modes ranged from 2500 Hz to 5400 Hz.

The calculations necessary to determine absorption over this frequency range for a given set of liner parameters are not especially complex. However, to evaluate all potential liner configurations within the limitations imposed by engine geometry and by cooling requirements, use of a digital computer is required. The computer program published in Reference 4 was used in this analysis.

Table I. Flightweight Chamber Nominal Design Point

Thrust	15,000 lb_f
Chamber Pressure	500 psia
Mixture Ratio	2.0
Oxidizer	Nitrogen Tetroxide
Fuel	N_2H_4 and UDMH (50-50 blend)
Oxidizer Flow Rate	36 lb_m/sec
Fuel Flow Rate	18 lb_m/sec
Combustion Efficiency, assumed	96 %
Combustion Gas Temperature	5590 °R
Gas Constant	69
Specific Heat Ratio	1.22
Sonic Velocity, Combustion Gas	3890 ft/sec
Chamber Contraction Ratio	5.0
Nozzle Expansion Ratio	4.0
Chamber Length/Throat Diameter	3.0
Throat Diameter	5.15 in.
Chamber Internal Diameter	10.8 in.
Chamber Length	13.74 in.

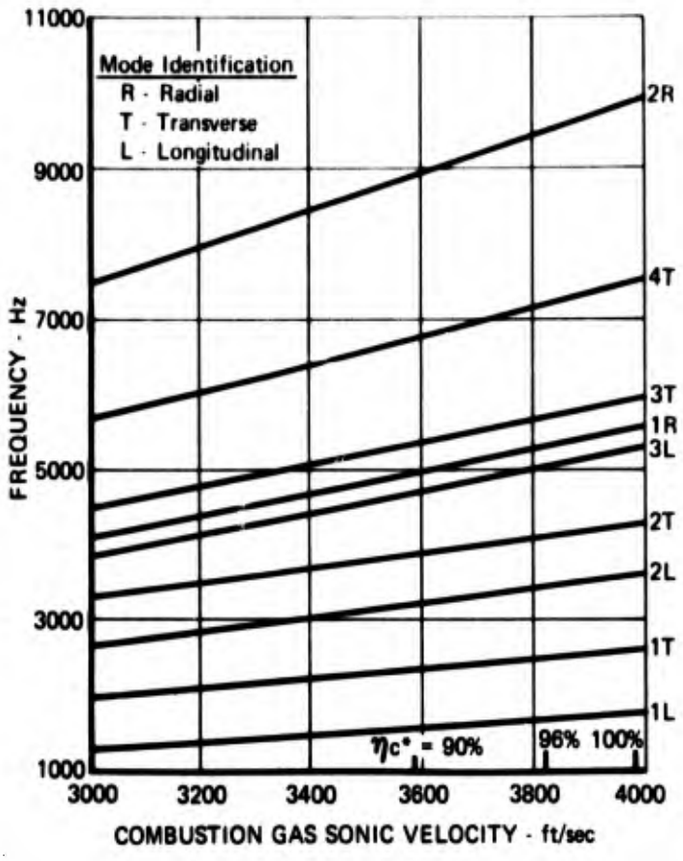

Figure 1. Frequency of Natural Acoustic Modes in Flightweight Chamber FD 53714

As in most practical liner designs, the range variation for liner thickness, backing cavity depth, open area ratio, and aperture diameter were fixed by cooling requirements, structural integrity, and fabrication cost. For example, the liner thickness variation was dictated by flightweight design and cooling criteria; a small annular gap was deemed necessary to minimize the stress on the pressure shell and to keep the overall chamber diameter small. The aperture diameter was varied only between 0.090 and 0.150 in. because drilling costs were considered prohibitive for diameters below 0.090 in. and aperture erosion from increased heat transfer on the downstream edge of the aperture could occur with diameters over 0.150 in.

A mean chamber velocity of 480 ft/sec and an incident pressure of 190 db were assumed as design points. Accurate estimations of the liner gas properties, sonic velocity, density, and viscosity are essential for a good acoustic liner design, but because these properties were unknown before hot firing test measurements were taken, the liner design was determined from a parametric analysis of liner geometric variables in which a wide range of aperture gas conditions were assumed (figure 2). The acoustic liner geometry chosen for the first test series from the results of this analysis is described in table II.

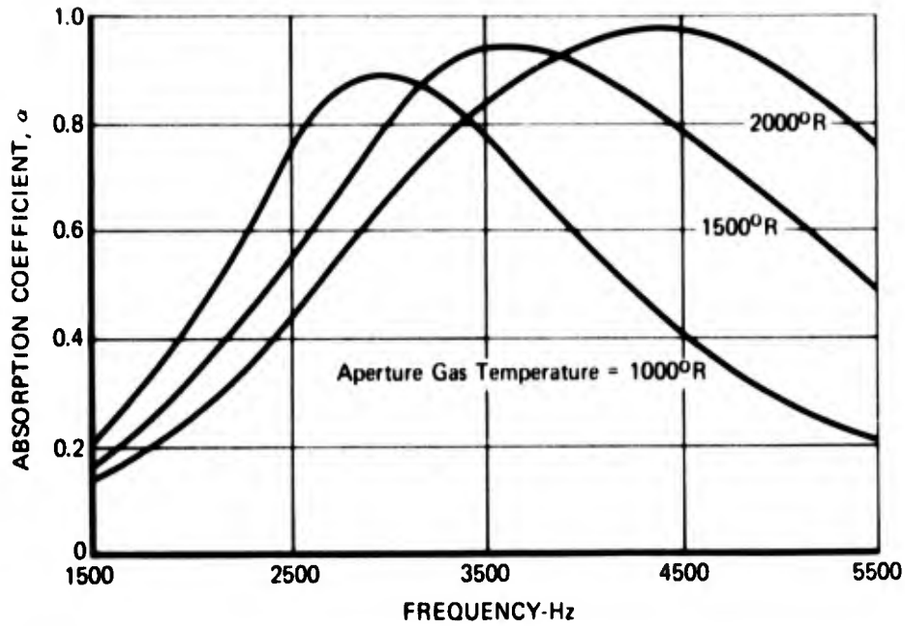

Figure 2. Results of Preliminary Acoustic Analysis FD 53715

Table II. Acoustic Liner Configuration for First Test Series

Liner thickness	0.20 in.
Backing cavity depth	0.60 in.
Aperture diameter	0.12 in.
Open area*	6.0 %

*Based on chamber area backed by acoustic cavity

2. Cooling Analysis

A preliminary cooling analysis was conducted to determine which propellant would be more suitable for use as a regenerative coolant, to define the basic heat exchanger configuration and to identify potential cooling problems associated with the design of the flightweight, acoustically lined thrust chamber described in table I. Regenerative cooling schemes using either the total oxidizer flow or total fuel flow and employing either a single pass counterflow or parallel flow arrangement were selected for consideration.

In the coolant passage of a heat exchanger using a coolant at subcritical pressure, nucleate boiling will occur at the heated surfaces whenever the wall temperature slightly exceeds the saturation temperature of the coolant. The bubbles that form on the heated surfaces and move into the coolant mainstream produce such a highly efficient heat transfer process that the heat flux can be increased significantly with only a small increase in the surface temperature. However, if the heat flux is increased beyond a certain point, the bubbles will start to coalesce and form a vapor film on the heated surface with an attendant

large decrease in the heat transfer coefficient. This is the point of transition to film boiling. For most liquids it causes an increase in the surface temperature that is great enough to cause failure of most commonly employed metals. Even with cryogenic liquids for which film boiling does not cause metal failure, the resulting film coefficients are so low that for all practical purposes the value of heat flux at this upper limit of nucleate boiling must be used as the design limit for regenerative cooling.

In the past, much effort has been devoted to the development of an analytical technique for predicting the upper limit heat flux for a given fluid from the knowledge of its physical and transport properties. Unfortunately, none of the existing methods have proved entirely valid, and the design of rocket engine heat exchangers must be based upon empirical correlations of experimental data. These experimental investigations have shown that the upper limit heat flux is influenced mostly by three system variables: pressure, bulk fluid temperature and velocity. With this information, the designer can achieve a successful regenerative cooling scheme if he can provide sufficient coolant flow to ensure that the local values of the upper limit heat flux exceed the corresponding local heat fluxes from the combustion gases to the wall everywhere in the motor.

The total heat rate that can be absorbed by a coolant at bulk temperatures below saturation is equal to the product of the flowrate, the specific heat, and the difference between saturation temperature and coolant inlet temperature. This total heat rate must be safely above the total expected heat-rejection rate from the combustion gases to the motor wall, since values of the upper limit heat flux decrease sharply as bulk temperatures approach saturation, becoming too low for successful cooling even in regions of very low heat flux. If, for a given engine design, the total heat capacity of the coolant is found to be marginal, the heat-rejection rate can be reduced by a refractory coating on the combustion chamber walls.

The variation of coolant bulk temperature along the thrust chamber wall was determined for both fuel and oxidizer assuming both counterflow and parallel flow arrangements. The results, shown in figure 3, were based on an axial variation of local combustion-side heat flux throughout the chamber and nozzle computed using the Simplified Bartz Equation (Reference 5) and assuming the combustion-side wall temperature to be 1700°R throughout the thrust chamber. Vapor pressure data indicated that either coolant would absorb the total heat load of the thrust chamber without experiencing a change of phase, and therefore remaining in the liquid state throughout the chamber.

The feasibility of cooling a regeneratively cooled thrust chamber using a coolant that is undergoing nucleate boiling can be determined for a first approximation by the coolant passage size necessary to maintain the local heat flux levels at or below the ultimate nucleate boiling heat flux of the coolant. This calculation must be performed in the throat region of the thrust chamber, the region of highest heat flux levels, and at the heat exchanger exit where, usually, the lowest ultimate heat flux occurs. If the resulting coolant passage dimensions render it impracticable to fabricate, or necessitate excessive coolant pressure losses, the cooling scheme is marginal.

For the preliminary analysis, coolant passage geometry was determined at three locations in the thrust chamber (near the injector, at the throat, and

at the exit of the nozzle) assuming three different wall materials (347 stainless steel, nickel 200, and aluminum) to explore the effect of coolant pressure and temperature and wall thermal conductivity on passage size. Both fuel and oxidizer were used as the coolant in the regenerative cooling arrangements described above. Rectangular coolant passages were selected initially for the calculations because of the relative simplicity of the equations associated with this geometry. The passage geometry at the throat was adjusted to enable the coolant to generate its ultimate nucleate boiling heat flux. It must be emphasized that assuming the heat flux to be the ultimate nucleate boiling heat flux for the coolant allows the passage configuration for the limiting case to be computed (for the analysis performed for the actual design of the flightweight chamber, Section II-D, no such assumption was necessary). The ultimate nucleate boiling heat flux was determined for the oxidizer by extrapolating the data of Reference 6 and for the fuel from the data of Reference 7. The bulk temperature of the coolant at any location was determined from figure 3 while the coolant pressure was estimated.

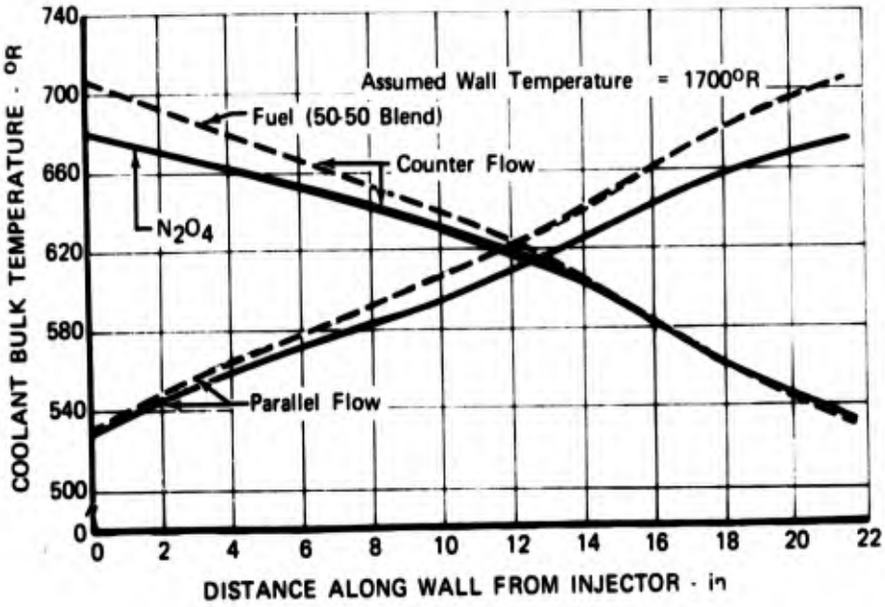

Figure 3. Computed Coolant Bulk Temperature Profiles for Regeneratively Cooled Motor FD 24902A

At the throat the rectangular passages were required to conform to the geometric restrictions that the passage depth be equal to the passage width. In the chamber and nozzle, the passage geometry was determined by requiring the passage depth, the number of passages, and the relation between passage width and the spacing between passages to remain constant throughout the thrust chamber. Again, these restrictions represent a simplification enabling cooling feasibility to be determined; different criteria were used in the final chamber design. With the restrictions, the passage width may be calculated as a function of thrust chamber radius and combustion-side wall thickness.

For both oxidizer and fuel, the ultimate nucleate boiling heat flux was computed for the coolant and compared with that existing at the location of interest. The resulting coolant passage geometry for rectangular and circular passages of equivalent flow area, along with other pertinent information, is

included in table III. From these calculations it was concluded that the coolant passage geometry necessary to maintain the heat flux levels below the ultimate nucleate boiling heat flux for either the oxidizer or fuel is such that the resulting coolant passages may be easily fabricated using existing technology. The correspondingly low coolant bulk velocities listed in table III are indicative of low pressure losses even in the presence of boiling.

The results of the preliminary cooling analysis indicated that it is feasible to cool a flightweight thrust chamber, acoustic liner combination operating under the conditions specified in table I employing a regenerative cooling system using either the total oxidizer flow or the total fuel flow in either a single-pass counterflow or parallel flow arrangement that may be constructed from a variety of materials. With reference to table III, and considering that the thrust chamber and liner must be flightweight and represent a least-risk design approach, the following recommendations were made:

1. Coolant: 50% N_2H_4 - 50% UDMH

   a. Advantages

      (1) Higher saturation temperatures resulting in reduced possibility of bulk vaporization and lower heat flux levels.

      (2) Lower flowrate, resulting in lcwer pressure drop.

      (3) Better boiling characteristics, resulting in higher ultimate heat flux margin.

      (4) Less risk of combustion along the heated surface in the event of a coolant leak into the chamber.

   b. Disadvantages

      (1) Larger coolant passages resulting in greater weight.

      (2) Greater stresses in coolant passages.

2. Flow arrangement: Single-pass counterflow using total fuel flow.

   a. Advantages

      (1) Less plumbing required, resulting in lighter weight.

      (2) Coolant flow-splitting is not required, increasing reliability and decreasing required accessories.

3. Wall material: Nickel 200

a. Advantages

(1) High thermal conductivity.

(2) Above-average strength characteristics.

(3) Compatible for use with fuel or oxidizer.

b. Disadvantages

(1) Relatively dense, increasing thrust chamber weight.

C. UNCOOLED TEST PROGRAM

1. Hardware

An uncooled test motor was designed and fabricated to demonstrate the suppression characteristics of the liner acoustic design and to obtain heat transfer data for the design of the regeneratively cooled flightweight liner. The motor utilized an existing Air Force supplied Agena Model S/N 9 injector. The nominal design conditions for the uncooled motor were the same as those of the flightweight chamber, table I. Figure 4 is a sketch of the uncooled motor assembly. The major parts of the assembly are the S/N 9 injector, the stainless steel combustion pressure shell, the stainless steel (or copper) exhaust nozzle, and various stainless steel and nickel acoustic liners.

A transient temperature analysis was conducted to determine satisfactory specifications for the uncooled acoustic liners and nozzles to be used to obtain heat transfer data. The acoustic liner thickness was assumed to be 0.2, 0.3, and 0.5 in. for the analysis. Nickel was chosen as the uncooled liner material because it would maintain a satisfactory level of structural integrity after the 2 sec firing time required to generate useful heat transfer data. The 0.20-in. thickness was found to be acceptable for heat transfer firings since it would reach only 1770°R after 2.0 sec at which time it would retain sufficient structural strength; and as discussed in the previous section, the 0.20-in. thickness was found to have acceptable absorption characteristics.

Copper was selected for the throat and nozzle material because of its high thermal conductivity. After 2-sec firing the hot wall temperature of a 1.0 in. thick nozzle was predicted to be 1900°R. The structural integrity of a copper nozzle at 1900°R is questionable, but since previous copper nozzles have been run to predicted hot wall temperatures of 2000°R without problem, the 1.0 in. thick copper nozzle was chosen for the uncooled heat transfer tests.

Table III. Results of Preliminary Cooling Analysis

	(1) Combustion Side Heat Flux (B/sec-in.^{2})	Ultimate Nucleate Boiling Heat Flux (B/sec-in.^{2})	Heated Surface Temp ($^\circ$R)	(2) Coolant-Side Wall Temp ($^\circ$R)	(3) Coolant Bulk Temp ($^\circ$R)	(4) Coolant Pressure (psia)	Rectangular Coolant Passage Width (in.)	Rectangular Coolant Passage Depth (in.)	Number of Rectangular Coolant Passages	Diameter of Equivalent Circular Passage (in.)	Coolant Flow Area (in.^{2})	Coolant Bulk Velocity (ft/sec)
I. COUNTERFLOW												
A. Chamber												
1. N_2O_4 Coolant												
a. 347 Stainless Steel	3.05	5.51	1010.	755.	652.	800.	.103	.0464	176.	.078	.00478	82.3
b. Nickel 200	3.15	6.06	838.	755.	652.	800.	.0871	.0392	208.	.066	.00342	97.6
c. Aluminum	3.20	6.31	782.	755.	652.	800.	.0812	.0366	223.	.062	.00298	104.3
2. 50% N_2H_4-50% UDMH Coolant												
a. Nickel 200	2.96	3.77	1130.	1040.	645.	800.	.203	.0917	89.	.154	.0186	32.8
B. Throat												
1. N_2O_4 Coolant												
a. 347 Stainless Steel	10.92	10.92	1530.	770.	573.	1000.	.0464	.0464	176.	.052	.00215	172.
b. Nickel 200	12.07	12.07	1040.	770.	573.	1000.	.0392	.0392	208.	.0442	.00153	204.
c. Aluminum	12.59	12.59	852.	770.	573.	1000.	.0366	.0366	223.	.0412	.00133	219.
2. 50% N_2H_4-50% UDMH Coolant												
a. Nickel 200	11.0	11.0	1486.	1080.	578.	1070.	.0917	.0917	89.	.1035	.0084	68.8
C. Nozzle Exit												
1. N_2O_4 Coolant												
a. 347 Stainless Steel	2.63	8.84	1000.	782.	530.	1200.	.0934	.0464	176.	.074	.00433	82.5
b. Nickel 200	2.73	9.39	840.	782.	530.	1200.	.079	.0392	208.	.063	.00310	97.9
c. Aluminum	2.75	9.63	805.	782.	530.	1200.	.0737	.0366	223.	.059	.00270	104.5
2. 50% N_2H_4-50% UDMH Coolant												
a. Nickel 200	2.51	6.18	1175.	1100.	530.	1200.	.1848	.0917	89.	.148	.0170	33.1
II. PARALLEL FLOW												
A. Throat												
1. N_2O_4 Coolant												
a. Nickel 200	12.77	12.77	798.	766.	647.	950.	.0316	.0316	305.	.0354	.00098	232.
2. 50% N_2H_4-50% UDMH Coolant												
a. Nickel 200	11.0	11.0	1486.	1080.	665.	1070.	.0876	.0876	93.	.099	.0077	74.9

(1) Corrected for wall temperature

(2) For N_2O_4 this value was set 20° in excess of coolant saturation temperature (Reference 8) and 50° in excess for 50% N_2H_4-50% UDMH

(3) This value determined from heat load based upon constant 1700°R heated surface temperature

(4) Estimated value

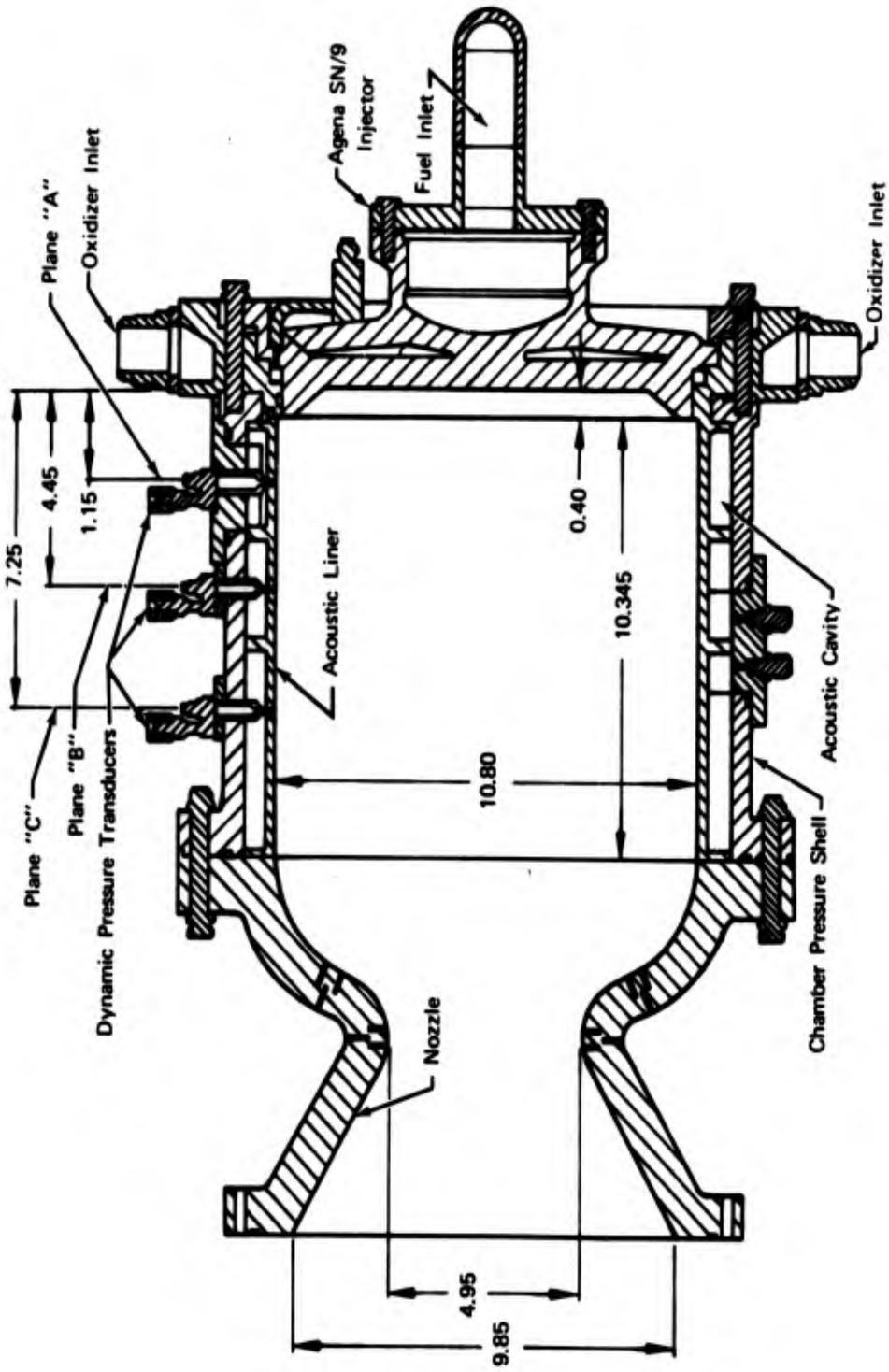

FD 53716

Figure 4. Uncooled Test Motor Assembly

The injector assembly, figures 5 and 6, was composed of a stainless steel oxidizer manifold and the Agena Model S/N 9 injector. Table IV is a summary of the characteristics of the injector faceplate orifice configuration. The injector was cold-flowed with water to visually investigate the injection pattern and to determine the differential pressures necessary to produce the required propellant flowrates. Photographs taken during the process showed that there would be no direct spray on the liner surfaces (see figure 7). At design point flowrates, the discharge coefficients were 0.57 on the fuel side and 0.60 on the oxidizer side; the corresponding differential pressures were 73 and 94 psi, respectively.

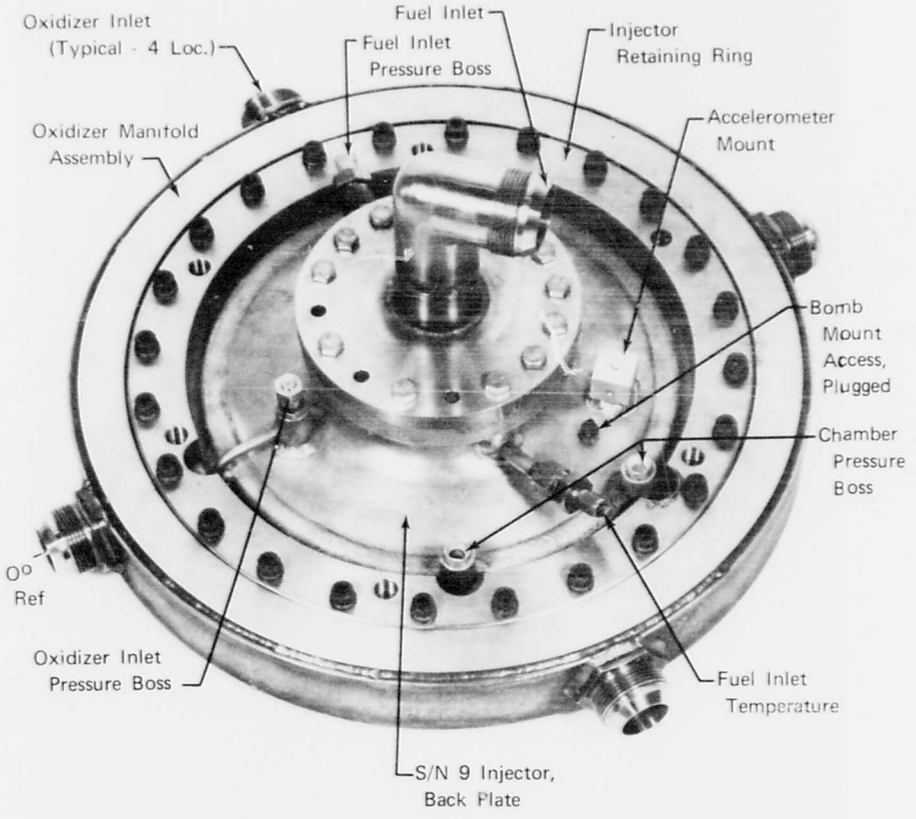

Figure 5. Modified Agena S/N 9 Injector Assembly - Rear View FE 83812A

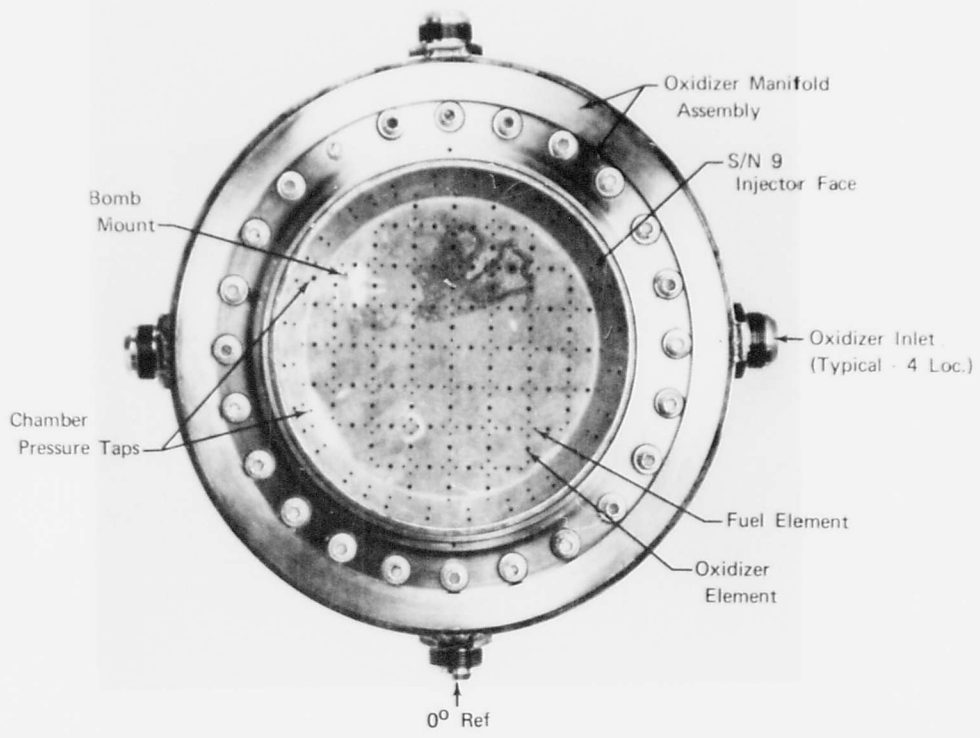

Figure 6. Modified Agena S/N 9 Injector Assembly - Face View FE 83813A

Table IV. S/N 9 Injector Faceplate Orifice Configuration

Orifice Type	Number of Orifices	Diameter, in.
Fuel Impingement	172	0.0635
Fuel Barrier	32	0.099
Fuel Film Cooling	32	0.0235
Oxidizer Core	88	0.118
Oxidizer Barrier	32	0.065

FE 83548A

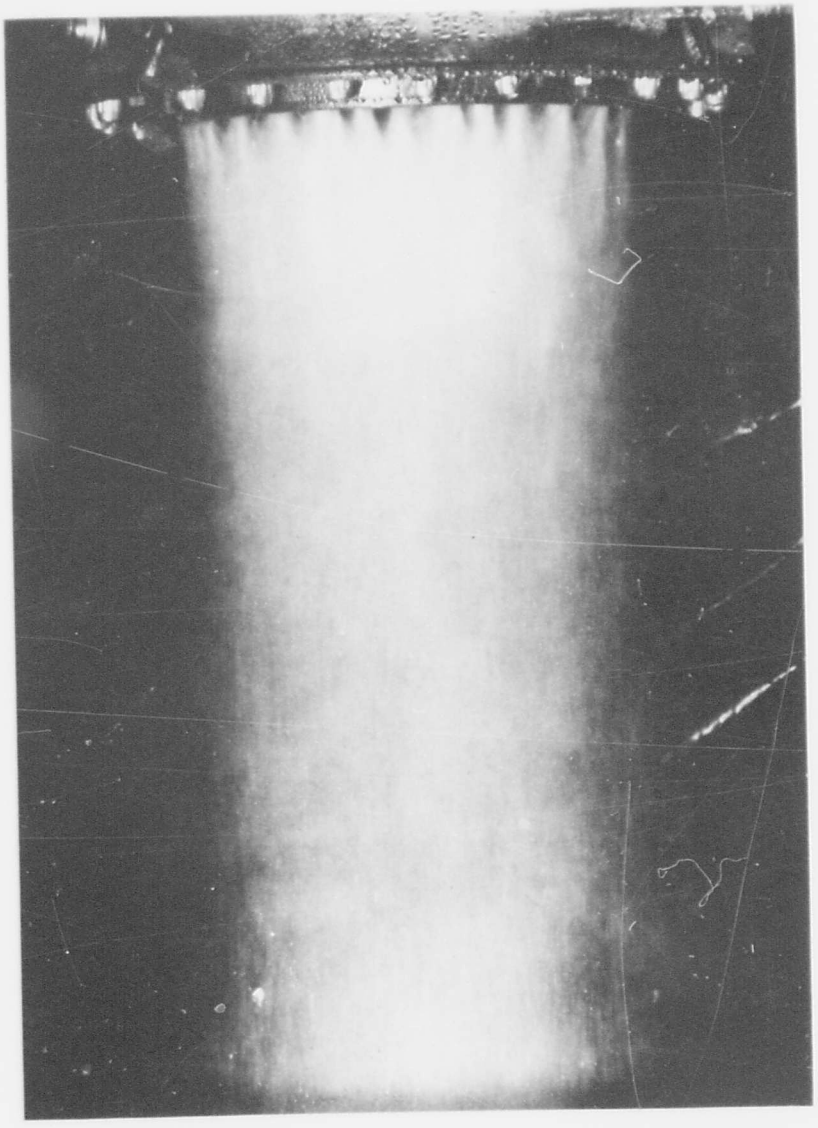

Figure 7. Water Flow Test of S/N 9 Injector Assembly

Only minor modifications were required to mate the S/N 9 injector to the chamber and manifold and to provide for mounting of the nondirectional bomb.

Figure 8 is a sketch of the bomb mounting scheme. The bomb was attached to the injector face using a tapered mount with a threaded end. A threaded hole in the injector, of location and depth such that there was no interference with either fuel or oxidizer passages, accepted the mount. A smaller hole, concentric with the threaded hole, provided the orifice plate feed-through for the detonator wire. The wiring hole at the injector face was sealed with epoxy potting (inside the bomb mount); a Conax packing gland was used at the backplate.

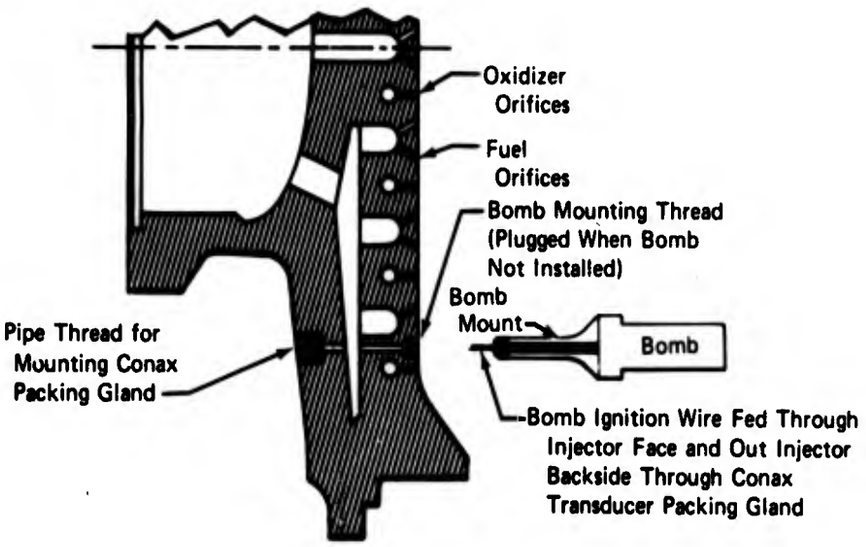

Figure 8. S/N 9 Injector Face Bomb Mounting Scheme FD 53717

The combustion chamber pressure shell walls were 0.5 in. thick with a 12.4 in. internal diameter, allowing installation of a 10.8 in. ID acoustic liner with 0.2 in. thickness and a 0.6 in. backing cavity depth. Two pressure shells were fabricated; one incorporated five rectangular ports designed to provide access to the liner wall, cavity and aperture thermocouples. Figures 9 and 10 are photographs of the pressure shell with access ports and a typical inspection port coverplate. The chamber walls were provided with adapters for mounting five Kistler 614A and one 615A dynamic pressure transducers for measuring combustion pressure oscillations in the chamber at the liner inner surface (five locations) and at one location in the liner backing cavity. The exact locations of the Kistler transducers are given in table V. As shown in figure 11, bosses for two pulse guns were incorporated; one with a tangential entry port and one with a radial entry port.

Figure 12 is a photograph of the two types of combustion disturbance devices, bombs and pulse guns, used with the uncooled motor; design sketches of the devices are presented in figures 13 and 14. Where applicable, the design of disturbance devices was based on criteria found in Reference 8. Both bombs and guns were loaded with C-4 explosive as the primary charge and electrically detonated with a 6 grain blasting cap. Two different types of barrels were fabricated so that the guns could be mounted either radially or tangentially.

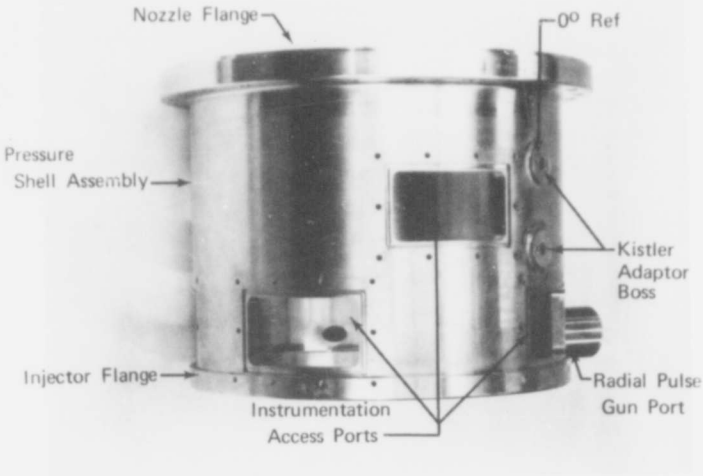

Figure 9. Uncooled Chamber Pressure Shell with Instrumentation Access Ports FE 83915A

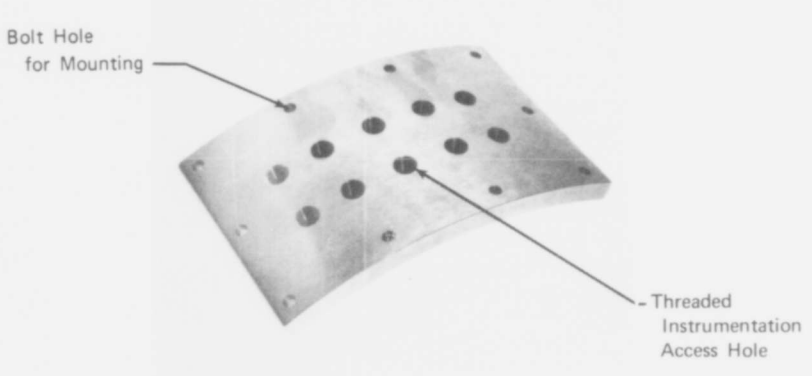

Figure 10. Typical Cover Plate for Instrumentation Access Port FE 83707A

Table V. Kistler Dynamic Pressure Transducer Locations

Location	Distance from Injector Face, in.	Angular Location, deg *
12:00 "A" Plane	1.15	0
3:00 "A" Plane	1.15	90
4:30 "A" Plane	1.15	135
4:46 "A" Plane**	1.15	142
12:00 "B" Plane	4.45	0
12:00 "C" Plane	7.25	0

*0° reference at top; looking from nozzle toward injector
**Cavity pressure transducer; other locations for chamber pressure

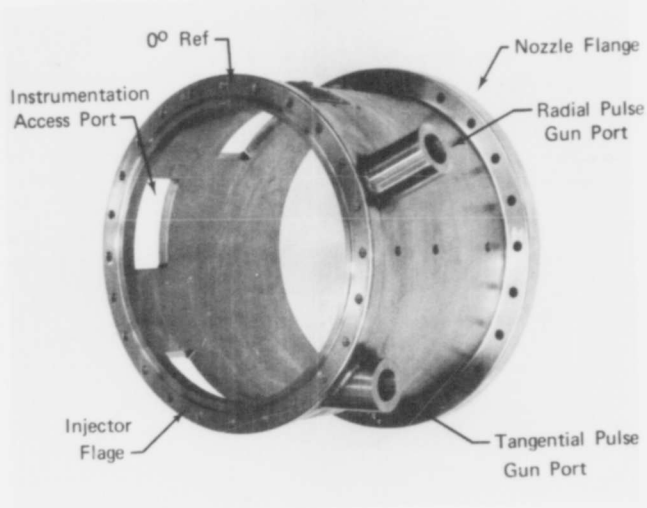

Figure 11. Pulse Gun Bosses Installed on Pressure Shell FE 83912A

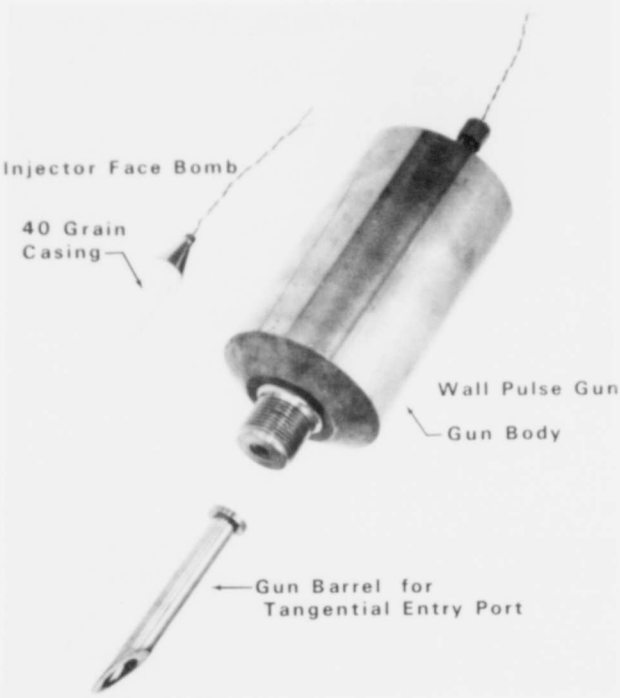

Figure 12. Combustion Disturbance Devices FD 49822

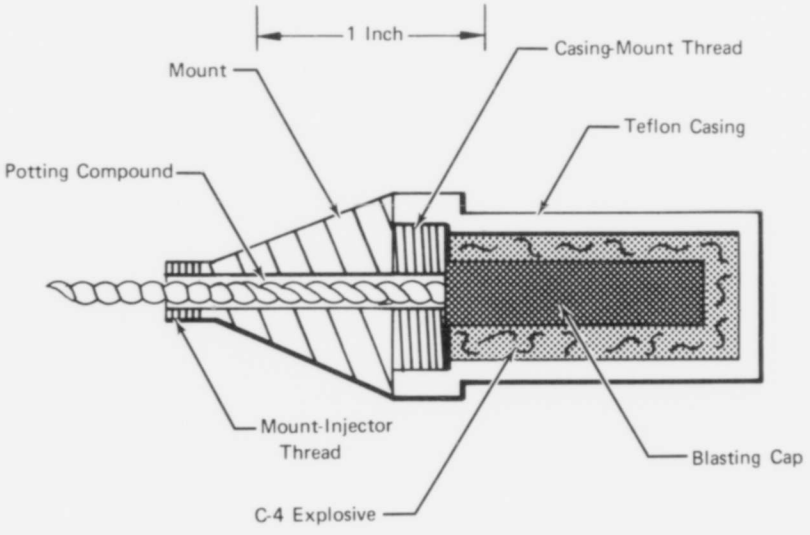

Figure 13. Injector Face Bomb FD 51849

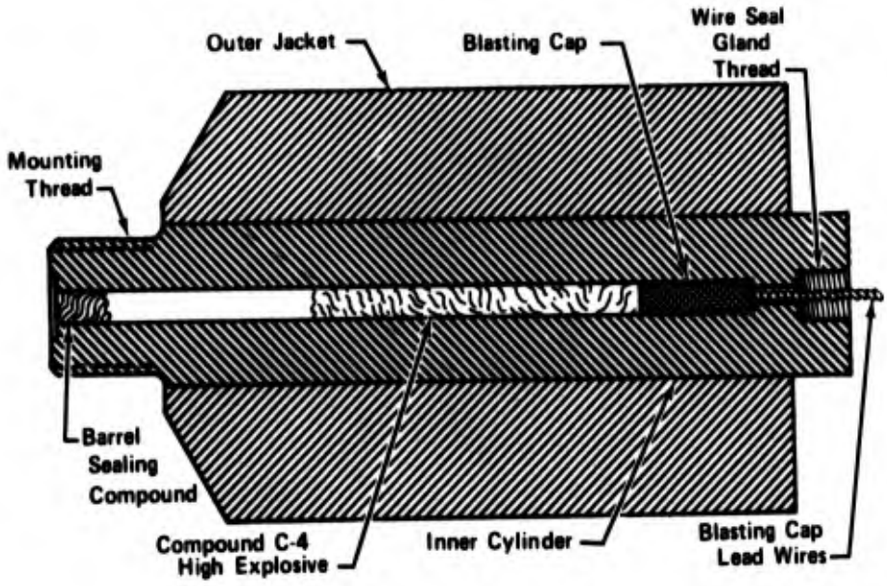

Figure 14. Pulse Gun FD 45490

Liners fabricated for the uncooled motor tests are described in table VI. All of the acoustic liners were designed to conform to the data of table II, and for installation only in the injector end of the chamber. The solid liners listed in the table were necessary to permit determination of the baseline stability characteristics of the motor, for use with partial length liners to maintain a consistent chamber inside diameter, and as backup hardware. A half-chamber length acoustic liner is shown in figure 15.

Exhaust nozzles with two different contours were fabricated for the uncooled tests; figure 16 compares the two. The original short contour was selected tc facilitate acoustic liner installation and removal. However, it was feared that the steep convergence profile might cause excessive heat fluxes in this region; therefore, a second nozzle with a longer (smooth) contour was fabricated. A short contour stainless nozzle only was used for the uncooled acoustic liner tests; however, copper nozzles of both contours were used in the heat transfer tests to aid in selecting the proper contour for the regeneratively cooled flightweight chamber.

The nickel acoustic liner was instrumented with thermocouples on the outside wall. The thermocouples were set into slots on the back wall and covered with an insulating coating of Sauerisen cement to prevent heat transfer from the hot gases in the acoustic cavity. These thermocouples were placed in 10 circumferential locations at each of 3 axial planes, 1.747, 4.347, and 7.851 in. from the injector face. In several locations, copper plugs containing a single aperture with a thermocouple at the downstream side of the aperture were inserted in the liner wall to obtain data that would permit determination of the effect of apertures on the heat transfer rate in the liner.

Table VI. Liners Fabricated for Uncooled Test Series

Liner	Ratio of Liner Length to Chamber Length	No. Apertures	Material	Refractory Coating
Acoustic	1/2	772	SS347	Mg Zn O_2 0.010 to 0.015 in. thick
Acoustic	1/4	390	SS347	Mg Zn O_2 0.010 to 0.015 in. thick
Acoustic (for heat transfer measurements	1	1544	Ni 200	None
Solid (2)	1/2	0	SS347	Mg Zn O_2 0.010 to 0.015 in. thick
Solid (2)	1/4	0	SS347	Mg Zn O_2 0.010 to 0.015 in. thick
Solid	Full	0	Ni 200	None
Solid (2)	Full	0	SS347	Mg Zn O_2 0.010 to 0.015 in.
Solid	1/2	0	SS347	None
Solid	1/4	0	SS347	None

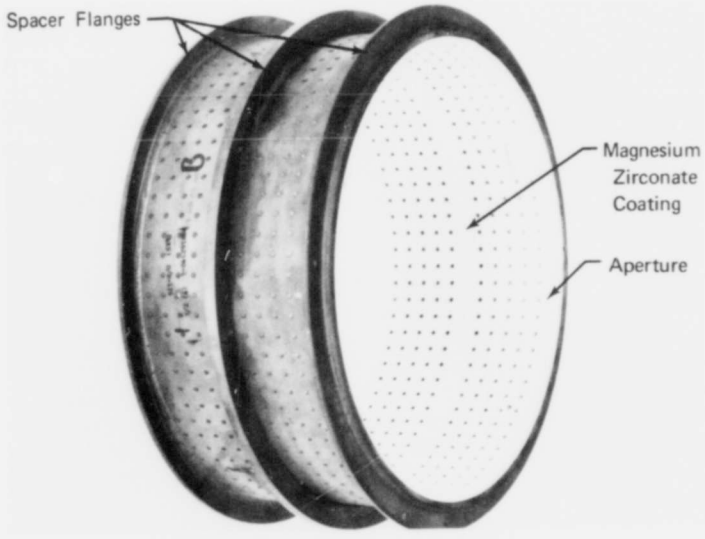

Figure 15. Half Chamber Length Acoustic Liner for Uncooled Motor FE 83720A

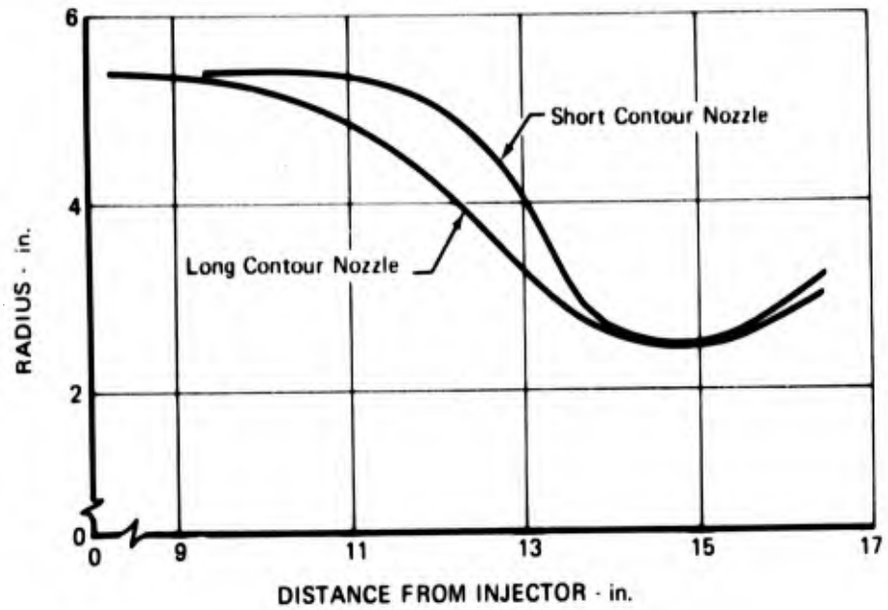

Figure 16. Comparison of Nozzle Contours FD 53718

The copper nozzles were instrumented by embedding thermocouples near the hot wall at 3 axial locations 12.1, 13.51, and 14.93 (throat) in. from the injector. The thermocouples were inserted through holes drilled from the back wall to within 0.4 in. of the hot surface. A circular groove was eloxed from the inside wall concentric with each thermocouple hole and extending beyond the thermocouple to 0.5 in. from the outside wall. These circular grooves were filled with an insulating material to inhibit heat flow parallel to the nozzle wall, thereby allowing the use of a one-dimensional analysis for the data reduction. Figure 17 illustrates the instrumentation techniques used for the aperture copper plugs and the one-dimensional nozzle thermocouples.

2. Test Program

Before fabrication of the flightweight chamber was initiated, the baseline stability characteristics of the motor and the instability suppression characteristics of the potential liner design were investigated in short duration tests of the uncooled hardware described in the previous section. Included in the uncooled test series were firings during which both the baseline heat transfer rates and the effects of liner apertures on heat transfer were measured. Additional uncooled tests were conducted with inserted acoustic liner segments to measure the dynamic stability characteristics of the potential flightweight liner design and to determine the minimum required liner length. For several of these tests, the fuel supplied to the injector was preheated so that the operating conditions of the regeneratively cooled motor would be more closely simulated.

Figure 18 shows the uncooled motor mounted on the B-5 test facility used for all firings under the program. For the uncooled tests the facility was as described in Reference 1 with the exception of the fuel preheater system described in Appendix IV, herein. A summary of each test is presented in table VII; a discussion of the test program follows.

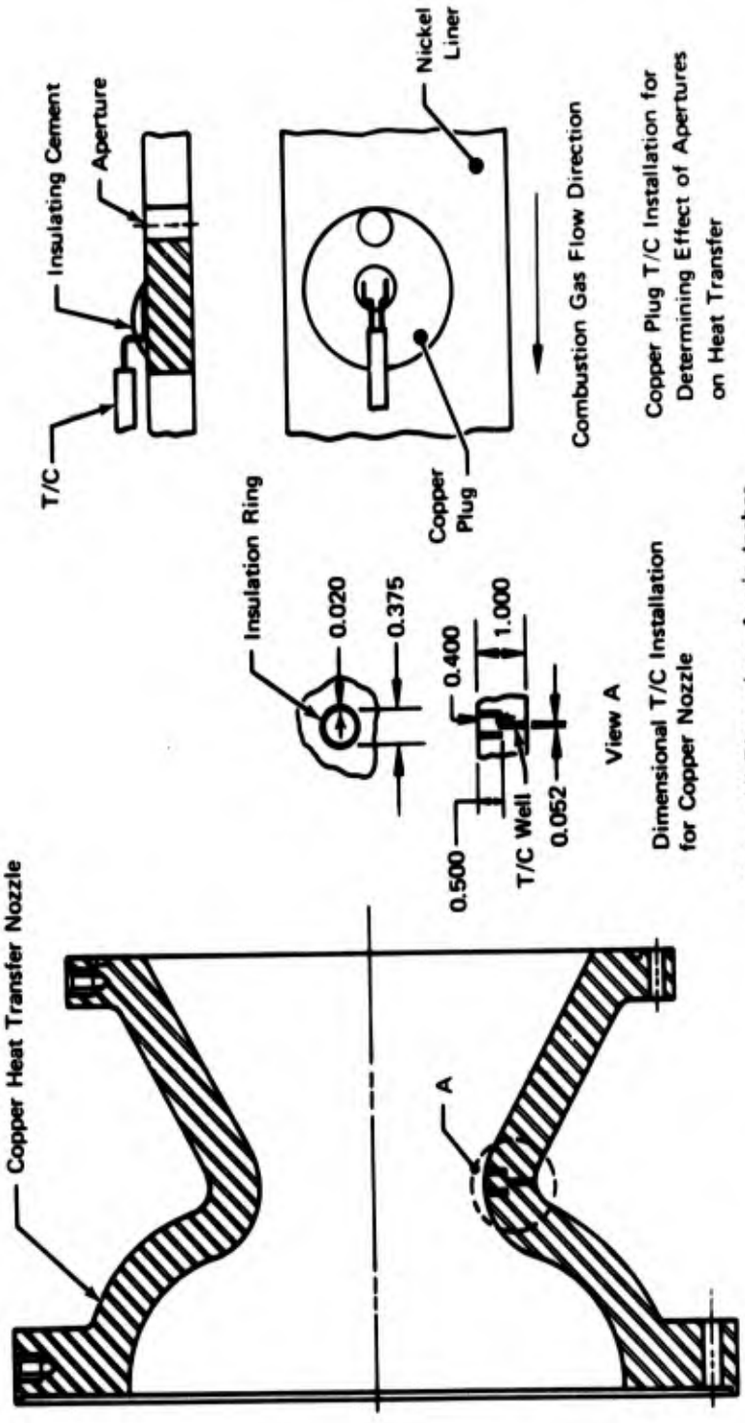

FD 51850

Figure 17. Thermocouple Installation Techniques for Copper Nozzle and Liner Copper Plugs

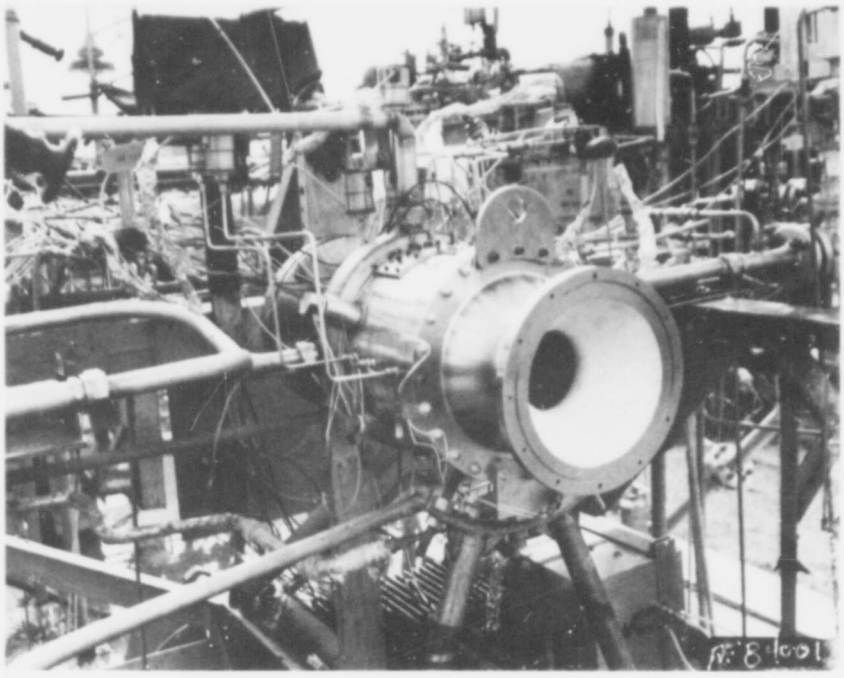

Figure 18. Uncooled Motor Mounted on B-5 Test Facility FE 84001

The first series of eight firings was made with a solid liner to determine the baseline stability characteristics of the motor. Data from the first five firings were not considered valid because of failure to reach the nominal operating conditions of table I, and/or problems associated with sealing the Kistler probes into the uncooled adaptors. Several of the Kistler adaptors were damaged from overheating during the first five tests; therefore, the test duration was shortened from 2.0 sec to 1.5 sec for test 6. Oscillograph traces from test 6 showed the motor was stable for the entire test, i.e., peak-to-peak pressure amplitudes were less than 25 psi.

Prior to the next firing, test 7, a 50-grain tangential pulse gun, timed to fire at +0.7 sec, i.e., 0.7 sec after ignition, and a 50-grain radial gun, timed to fire at +1.2 sec, were installed. The motor was stable until the tangential gun fired, causing an overpressure in excess of 500 psi, which did not damp. The pressure oscillations produced were primarily of the first tangential mode, i.e., 2600 Hz, with peak-to-peak amplitudes of approximately 400 psi. The test was aborted at +0.82 sec by the rough combustion cutoff (RCC) device.

The radial gun was fired during test 8; an overpressure in excess of 700 psi resulted, and initiated high amplitude instability similar to that of the previous test. The test was aborted at +1.32 sec by the RCC device. From these results it was concluded that the motor with no liner is dynamically unstable with resulting pressure oscillations at frequencies near that of the theoretical 1T mode and that no further baseline testing was required.

Table VII. Phase I – Uncooled Motor Test Summary

Test No.	Duration, sec	Chamber Pressure, psia	Mixture Ratio	C* Efficiency(1)	Disturbance Device(s)	Abort	Comments
1	0.75	398	2.42	-	None	RCC(2)	Test not valid, high mixture ratio and low chamber pressure due to low fuel flow.
2	2.00	482	1.99	96.6	None	None, Stable Test	Poor start transient - no Kistler data due to leaks in adaptors - adaptors damaged.
3	2.00	486	1.99	98.1	None	None, Stable Test	Kistler data invalid due to seal problems on adaptors.
4	2.00	488	1.98	98.7	None	None, Stable Test	Kistler data invalid due to dampness in connectors.
5	0.50	479	1.89	-	None	LCT(3)	Noise spike in system caused high T C malfunction abort.
6	1.50	494	1.97	98.8	None	None, Stable Test	Full duration test - P P amplitudes approximately 15 psi throughout test.
7	.82	480	2.03	95.9	Pulse Gun	RCC	Pulsed with 50 gr. tangential pulse at +.70 sec - initiated P P amplitudes approximately 400 psi that did not damp.
8	1.32	490	2.04	98.6	Pulse Gun	RCC	Pulsed with 50 gr. radial pulse at +1.20 sec - initiated P/P amplitude approximately 400 psi that did not damp.
9	1.31	484	2.01	97.4	None	LCT	1/2 length acoustic liner, stable test. LCT approximately 2600°R
10	.73	474	2.00	96.9	Pulse guns, tang. 50 gr. and radial 50g r. at +.7 sec.	False LCT Signal	1/2 length acoustic liner, stable test. Both pulsers fired simultaneously, apparently by problem in LCT circuit. Overpressure spikes as follows: 12:00"A" 3:00"A" 4:30"A" 4:46"A" 12:00"B"(4) Spike, psi 420 400 560 320 420 All spikes damped within .010 sec.
11	1.46	489	2.00	98.0	Pulse guns, tang. 50 gr. at +.7 sec. and radial 50 gr. at +1.2 sec.	None, Stable Test	1/2 length acoustic liner. Spikes 12:00"A" 3:00"A" 4:30"A" 4:46"A" 12:00"B" Tang., psi 480 350 430 370 420 Radial, psi 475 500 630 380 440 All spikes damped within .010 sec.

(1) Based on chamber pressure
(2) Rough combustion cutoff (unstable test)
(3) Liner cavity gas temperature
(4) Transducer locations, see table 5.

Table VII. Phase I – Uncooled Motor Test Summary (Continued)

Test No.	Duration sec.	Chamber Pressure, psia	Mixture Ratio	C* Efficiency (1)	Disturbance Device(s)	Abort	Comments
12	.61	476	1.97	84.5	Bomb, 10 gr. sched. for -.7 sec. Pulse gun, radial 50 gr. sched. for -1.2 sec.	RCC	1/4 length acoustic liner, unstable test. Bomb burned during start-up. No Spike, but peak-to-peak (P-P) as follows: 12:00"A" 3:00"A" 4:30"A" 4:46"A" 12:00"C" P/P, psi 240 240 200 100 180
13	1.30	488	2.00	98.0	Pulse gun, radial 50 gr. at -1.2 sec.	RCC	1 4 length acoustic liner, unstable after pulse gun fired. 12:00"A" 3:00"A" 4:30"A" 4:46"A" 12:00"C" Spike, psi 275 360 370 250 320 P/P, psi 220 220 200 120 120
14	.63	458	1.99	92.7	Pulse gun, tang. 50 gr. sched. for +.7 sec.	RCC	1/4 length liner, unstable. Pulse gun charge apparently burned during start causing instability. No Spike, but P/P as follows: 12:00"A" 3:00"A" 4:30"A" 4:46"A" 12:00"C" P/P, psi 280 280 300 120 250
15	1.46	488	1.98	98.8	Bomb, 36 gr. at +.7 sec.	None, Stable Test	1/2 length acoustic liner. 12:00"A" 3:00"A" 4:30"A" 4:46"A" 12:00"C" Spike, psi 600 600 650 450 630 All spikes damped within .015 sec.
16	1.46	488	1.98	98.3	Bomb, 36 gr. at -1.2 sec.	None, Stable Test	1/2 length acoustic liner. 12:00"A" 3:00"A" 4:30"A" 4:46"A" 12:00"C" Spike, psi 500- 590 575 415 450 All spikes damped within .015 sec.
17	1.46	488	2.00	98.5	Bomb, 71 gr. at -1.0 sec.	None, Stable Test	1/2 length acoustic liner. Bomb apparently burned during start but cap remained intact until fired producing 50 psi spike that damped within .010 sec.
18	1.46	474	2.02	95.7	None	None, Stable Test	1/2 length acoustic liner. Heated fuel used inlet temperature at injector 200°F at 1.3 sec., reached maximum of 220°F at shutdown.
19	1.75	474	2.01	95.8	None	None, Stable Test	1/2 length acoustic liner. Run duration extended. Heated fuel used, inlet temperature at injector 200°F at 1.3 sec., reached maximum of 228°F at shutdown.

(1) Based on chamber pressure

Table VII. Phase I - Uncooled Motor Test Summary (Continued)

Test No.	Duration, sec.	Chamber Pressure, psia	Mixture Ratio	C* Efficiency (1)	Disturbance Device(s)	Abort	Comments
20	1.96	474	2.00	95.7	Pulse guns, tang. 50 gr. at 1.5 sec. radial 50 gr. at -1.8 sec	None, Stable Test	1/2 length acoustic liner. Heated fuel used - max. temperature 225°F. Oxidizer control valve oscillated throughout run. Fuel control valve oscillated in response to above. Spikes,psi 12:00"A" 3:00"A" 4:30"A" 4:46"A" 12:00"A" Tang. 480 440 275 390 250 Radial 425 480 400 410 315 All spikes damped within .010 sec.
21	1.96	481	2.01	96.5	Bomb, 36 gr. at -.8 sec. Pulse guns, tang. 50 gr. at -1.5 sec. and radial 50 gr. at -1.8 sec.	None, Stable Test	1/2 length acoustic liner. Heated fuel used, maximum temperature 228°F. 12:00"A" 3:00"A" 4:30"A" 4:46"A" 12:00"C" Spike(Bomb)psi 450 440 450 410 220 Spike(Tang)psi 480 460 450 340 280 Spike(Radial)psi 410 475 370 425 325 All spikes damped within .010 sec.
22	1.27	469	2.02	95.1	None	False LCT Signal	Full length acoustic Heat Transfer liner, stable test. Heated fuel used maximum temperature 220°F.
23	1.77	467	1.99	94.7	None	None, Stable Test	Full length acoustic Heat Transfer liner. Heated fuel used, maximum temperature 225°F.
24	1.75	470	2.00	95.0	None	None, Stable Test	Full length acoustic Heat Transfer liner. Heated fuel used, maximum temperature 225°F.
25	1.77	471	2.02	96.0	None	None, Stable Test	Full length acoustic Heat Transfer liner. Heated fuel used, maximum temperature 225°F.
26	1.75	444	1.98	90.2	None	None, Stable Test	1.2 length acoustic liner; heat transfer nozzle (long contour); heated fuel, 220°F max.
27	1.76	475	1.98	96.8	None	None, Stable Test	1/2 length acoustic liner; heat transfer nozzle (long contour); ambient fuel temp.
28	1.75	474	1.98	95.6	None	None, Stable Test	1/2 length acoustic liner; heat transfer nozzle, (long contour); ambient fuel temp.
29	(Data not valid because of control valve malfunction)				Bomb 45 grain at -1.0 sec.	None, Stable Test	1/2 length acoustic liner; heat transfer nozzle, (long contour); heated fuel 240°F max. Spikes (psi): 12:00A 3:00A 4:30A 4:46A 590 500 420 220 All spikes damped within .015 sec.
30	1.75	459	1.98	93.1	Bomb, 45 grain at -0.8 sec	None, Stable Test	1/2 length acoustic liner; heat transfer nozzle, (long contour); heated fuel 240°F max. Spikes (psi) 12:00A 3:00A 4:30A 4:46A 500 510 405 350 All spikes damped within .015 sec.

(1) Based on chamber pressure

The second series of firings (tests 9 through 11) was made with a 1/2 chamber length acoustic liner to determine the liner's suppression characteristics. Test 9 was conducted without a disturbance device; tests 10 and 11 were each disturbed with 50-grain pulse gun charges. For each firing, motor operation was stable with peak-to-peak amplitudes less than 25 psia. The spike overpressures caused by the 50-grain charges were found to vary from 320 to 630 psia; all were reduced to less than 25 psi peak-to-peak within 10 milliseconds.

A series of firings (tests 12 through 14) was then conducted to determine the minimum acoustic liner length required for stable motor operation; for these tests a 1/4-chamber-length liner was used. Before test 12, a 10-grain nondirectional, injector face-mounted bomb was installed; 50-grain pulse guns were installed for tests 13 and 14. Combustion during tests 12 and 14 became spontaneously unstable during the start transient, and the tests were aborted. Test 13 was stable during the start transient and up to the time that the radial pulse charge was fired; overpressures of up to 370 psia resulted and initiated high amplitude instability. The pressure oscillations were primarily of the first tangential mode with peak-to-peak pressure amplitudes up to 220 psi.

Typical dynamic pressure data from the first three series of tests are shown in figure 19. From the results obtained, it was concluded that the 1/4 length liner did not provide sufficient total absorption to cause the motor to be dynamically stable; therefore, the minimum acoustic liner length for the flightweight chamber was set at 1/2 chamber length.

The next series of firings (15 through 17) was conducted to determine the size of nondirectional bombs necessary to produce overpressures in excess of 500 psia. The 1/2 chamber length acoustic liner was again used. A 36-grain bomb was installed on the injector face for each of the first two firings; the bomb was timed to detonate at +0.7 sec for test 15 and at +1.20 sec for test 16. Overpressures of up to 650 psia resulted during test 15 and spikes of up to 590 psia were produced during test 16. In each firing the overpressures damped to less than 25 psi within 15 millisec. A 71-grain bomb was installed for test 17. The bomb casing apparently burned off during the start transient because an overpressure of only 50 psi was recorded at detonation time.

The fourth series of firings (18 through 21) was conducted to determine the effects of heated fuel on the stability characteristics of the motor with the 1/2-length acoustic liner installed. Tests 18 and 19 were conducted without pulse guns or bombs; test 20 was disturbed at +1.5 sec with a 50-grain tangential pulse gun charge and at +1.8 sec with a 50-grain radial pulse gun charge. The firings were all stable and the spikes produced by the charges damped to less than 25 psi within 0.01 sec. Figure 20 is a typical plot of injector fuel inlet temperature vs time recorded during this series of tests. It was concluded from the results of these firings that the motor could be operated with heated fuel without adversely affecting stability.

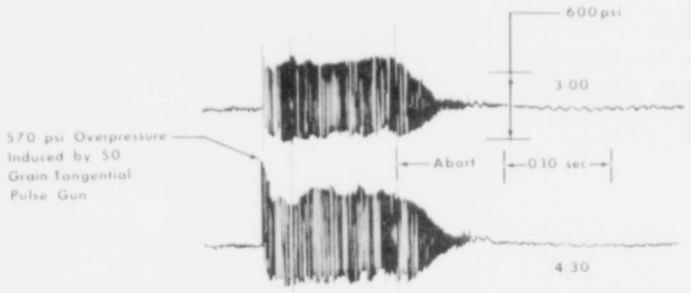

Baseline Firing, Solid Liner Insert

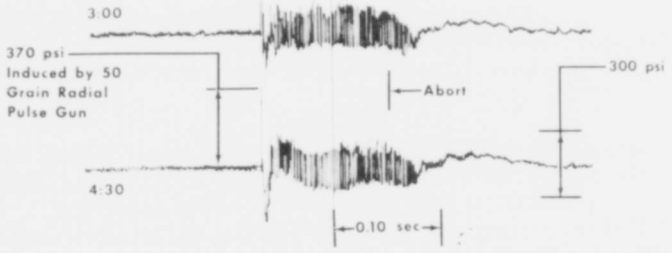

6% Open Area Liner, 1/4 Chamber Length

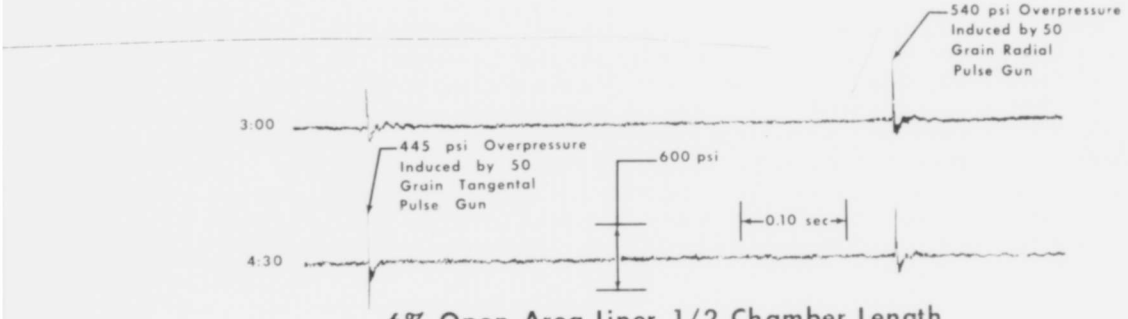

6% Open Area Liner, 1/2 Chamber Length

Figure 19. Typical Dynamic Pressure Data from First Three Series of Uncooled Motor Firings GS 12454

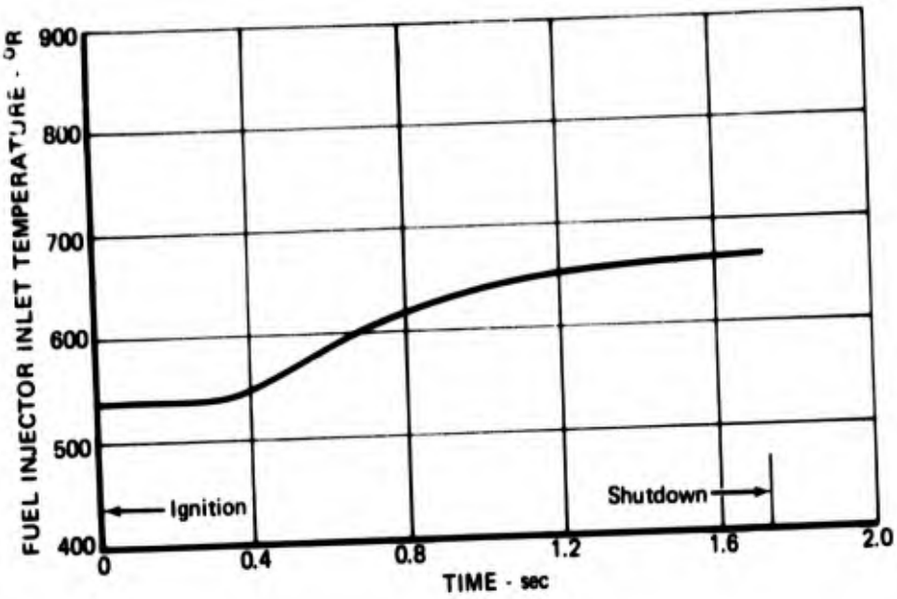

Figure 20. Injector Fuel Inlet Temperature Recorded During Fourth Series of Uncooled Motor Tests FD 53719

A series of four firings (22 through 25) was then conducted with a copper nozzle and the full-length nickel acoustic liner; both the nozzle and the liner were instrumented with thermocouples for recording transient temperature data. No disturbance devices were installed, and heated fuel was used to more closely simulate actual regenerative conditions. Test 22 was aborted at +1.27 sec by a false liner cavity temperature abort signal. Tests 23, 24 and 25 were full-duration firings; however, no nozzle thermal data were obtained, apparently due to the installation technique that had been employed.

The last six uncooled motor firings (tests 26 through 30) were conducted to obtain nozzle heat transfer data. A smoothed-contour copper nozzle reinstrumented for improved thermocouple response and a 1/2-chamber-length acoustic liner were installed. To expedite testing, heated fuel was used only during tests 26, 29, and 30. During the last two firings, the fuel was heated to 240°F and 45-grain, nondirectional bombs were detonated.

During the last two tests the highest overpressure caused by either of the 45-grain bombs was 590 psi, slightly lower than the high of 650 psi reached in a previous test with a 37-grain bomb. The lower overpressure with a larger bomb was attributed to two factors. First, it was necessary to use an oversized bomb casing because a properly sized casing was not available. (The explosive power of a bomb is a strong function of the density to which the explosive is packed.) Second, it had been noticed previously that for some unknown reason, overpressures in the motor were slightly lower when heated fuel was used. In both pulsed tests the chamber pressure stabilized within 0.010 sec.

3. Analysis of Data

a. Combustion Stability

Spectrum analysis of dynamic pressure data from the baseline test series, i.e., with no acoustic liner, were performed; typical results are shown in figures 21 and 22. Although modes of instability with peak-to-peak amplitudes greater than 25 psi (5% of chamber pressure) were not expected at frequencies higher than 5500 Hz, they were evidently present. Nevertheless, similar analysis of data from tests with the half chamber length acoustic liner revealed that, in every instance, pressure amplitudes at all frequencies were reduced by the liner to approximately 2 psi or less.

A summary of cavity gas temperature data from the 1/2-length acoustic liner is shown in figure 23. The maximum temperatures are approximately the same as the highest value (2000°R) assumed for the original liner design analysis. If the actual cavity gas temperatures had been very different from those assumed, redesign of the liner would have been warranted. However, in view of the above results and considering the demonstrated success of the half chamber length liner in suppressing the dynamic instability of the uncooled motor, it was concluded that no redesign of the liner for the flightweight chamber was necessary.

b. Performance

A summary of averaged performance data from the uncooled motor firings is given in figure 24. From these data, it was observed that within the limits of experimental uncertainty (approximately 2%) the use of an acoustic liner did not affect the specific impulse, thrust coefficient, or combustion efficiency when using ambient temperature fuel. The use of heated fuel caused a slight decrease in each of the above performance parameters probably because of the effect the heated, and therefore less dense, fuel had on the injection momentum ratios. No attempts were made during the heated fuel test series to vary the injector mixture ratios and thus possibly improve performance because of the transient nature of the tests (as shown in figure 20, the fuel inlet temperature varied throughout the firings). Also, the primary purpose of the tests was to determine the effects of heated fuel on stability; performance results were of only secondary interest. It was known that more valid performance data would be obtained from tests of the flightweight chamber. (See Section II-D-4.)

c. Heat Transfer

The data reduction technique used the same transient temperature analysis program that was used in the design of the uncooled chambers. By assuming a range of heat transfer coefficients a family of thermal response curves was prepared for each different instrumentation location. The experimental heat transfer coefficient at a particular point was determined by selecting the coefficient that produced a thermal response curve that matched the actual thermocouple response at that point. The resulting coefficients are given in figures 25 through 27. Although it was found that the coefficients in the chamber varied from 400 Btu/hr ft^2R (the Bartz theoretical value) to a maximum value of 600 Btu/hr ft^2R, thermal response data from thermocouples on the liner and from the copper aperture plugs (figure 28) indicated that the heat flux in the vicinity downstream of an aperture was not significantly different from that at a comparable location without an aperture.

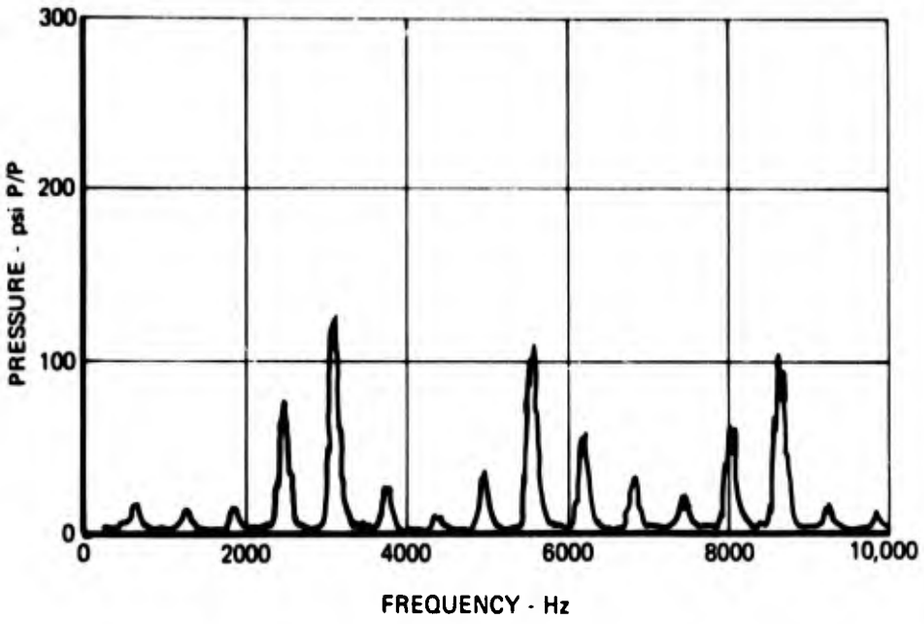

Figure 21. Results of Spectrum Analysis of Dynamic Pressure Data from Test 8, 4:30 "A" Transducer FD 53720

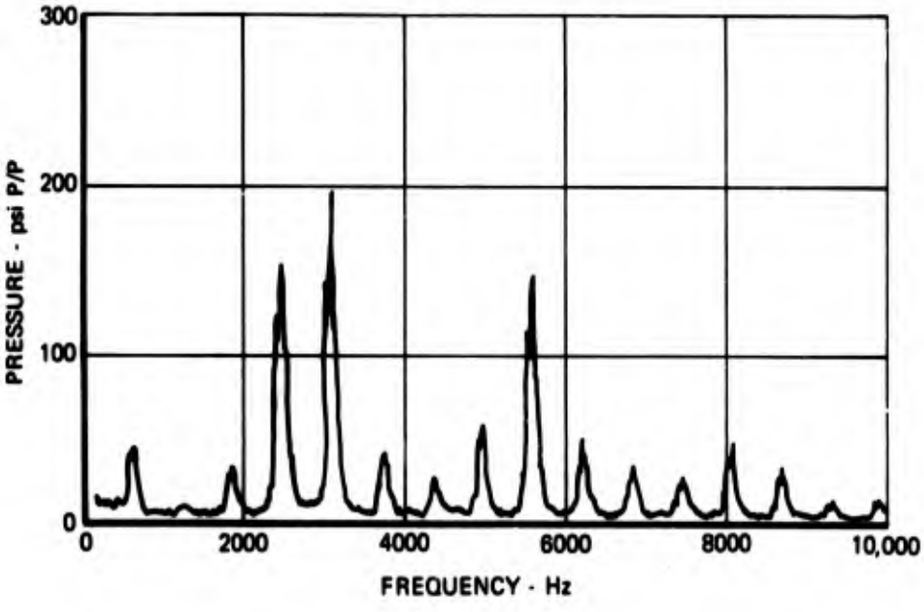

Figure 22. Results of Spectrum Analysis of Dynamic Pressure Data from Test 8, 12:00 "A" Transducer FD 53721

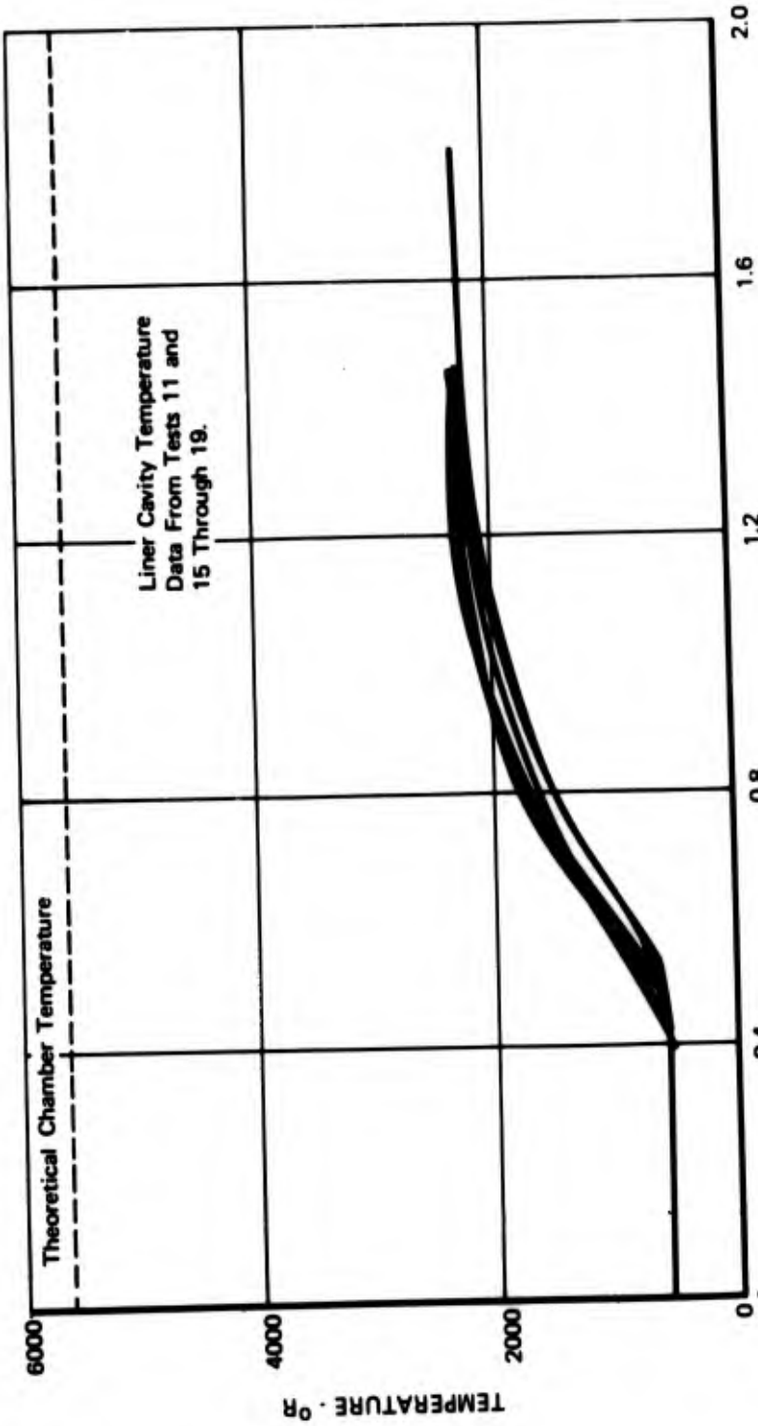

FD 53722

Figure 23. Summary of Acoustic Cavity Temperature Data for Half Chamber Length Acoustic Liner

FD 53723

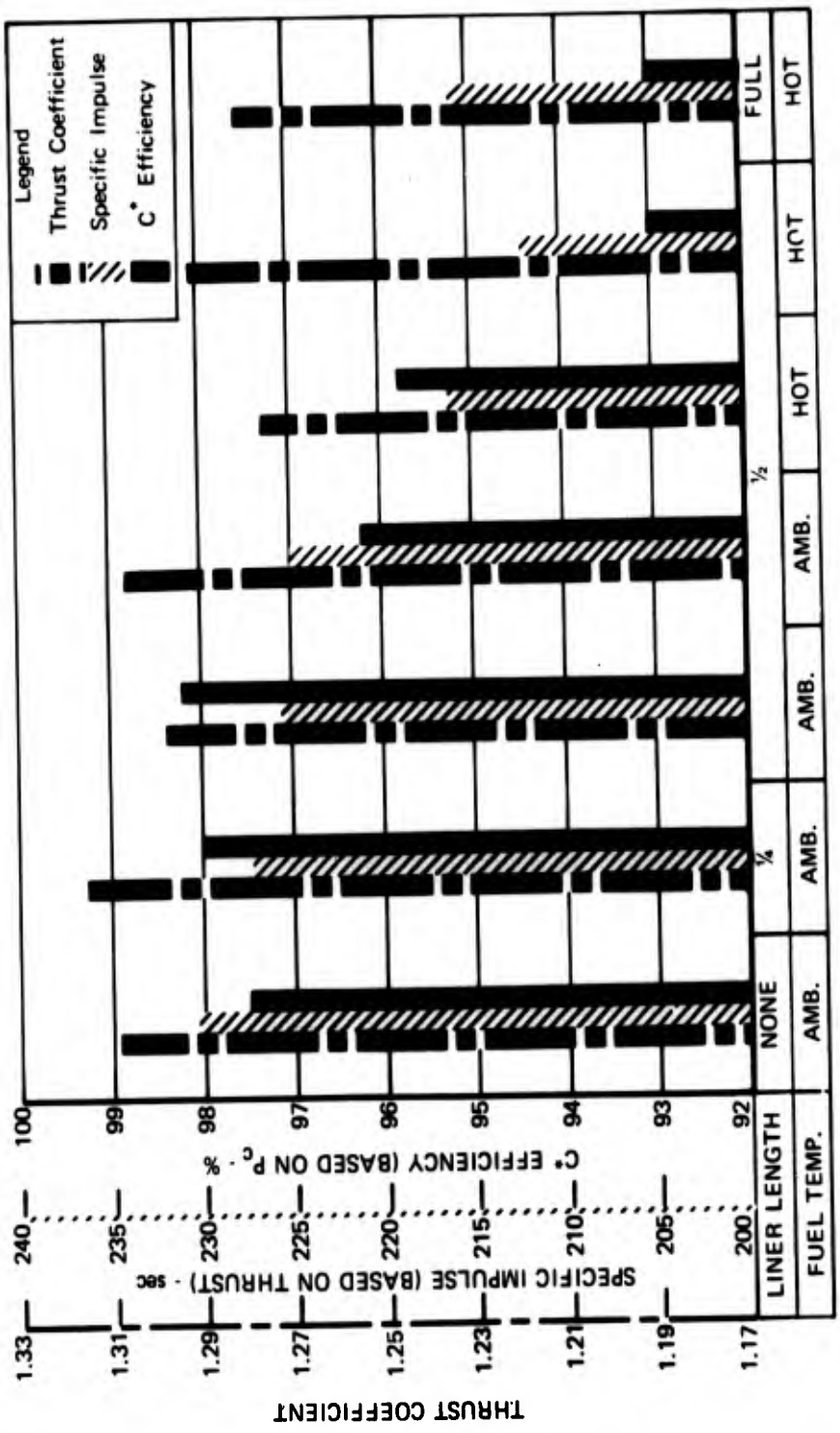

Figure 24. Summary of Uncooled Motor Performance Data

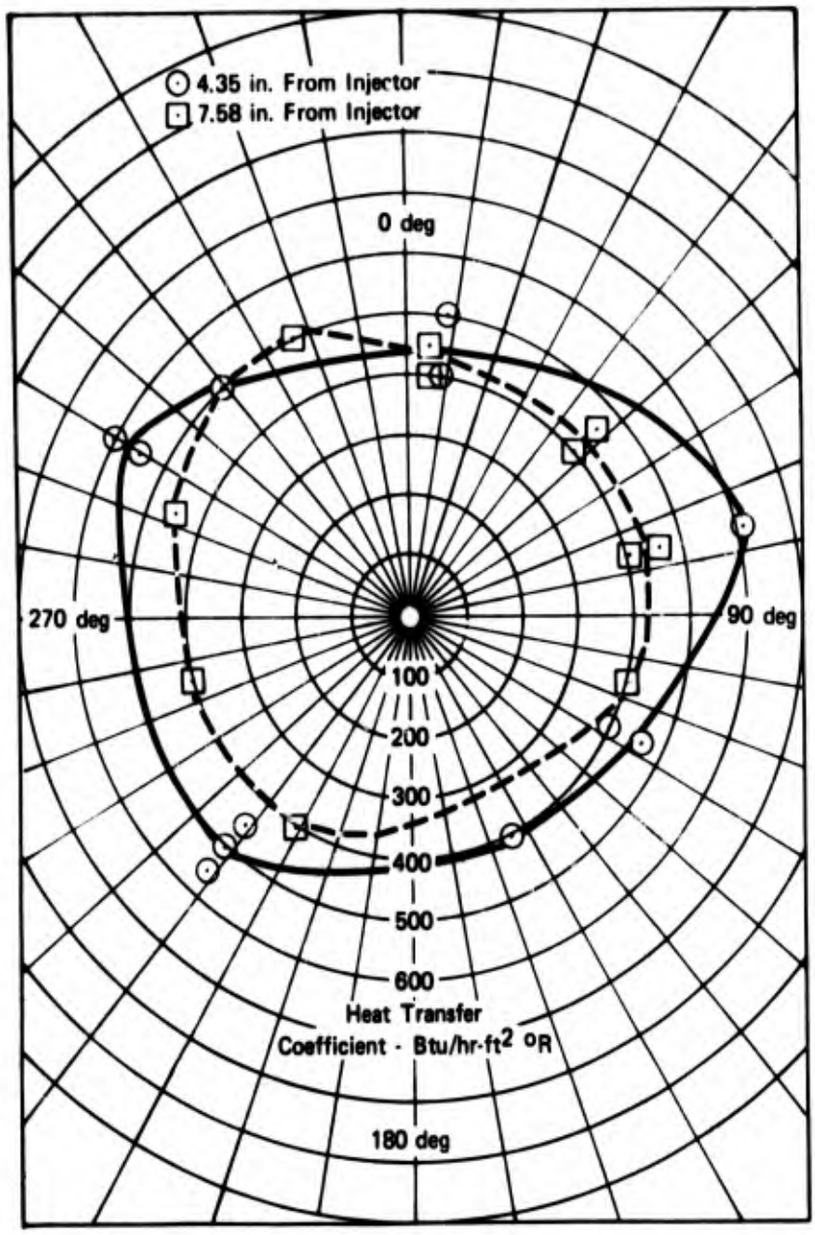

Figure 25. Azimuthal Distribution of Heat Transfer Coefficients in Chamber FD 53724

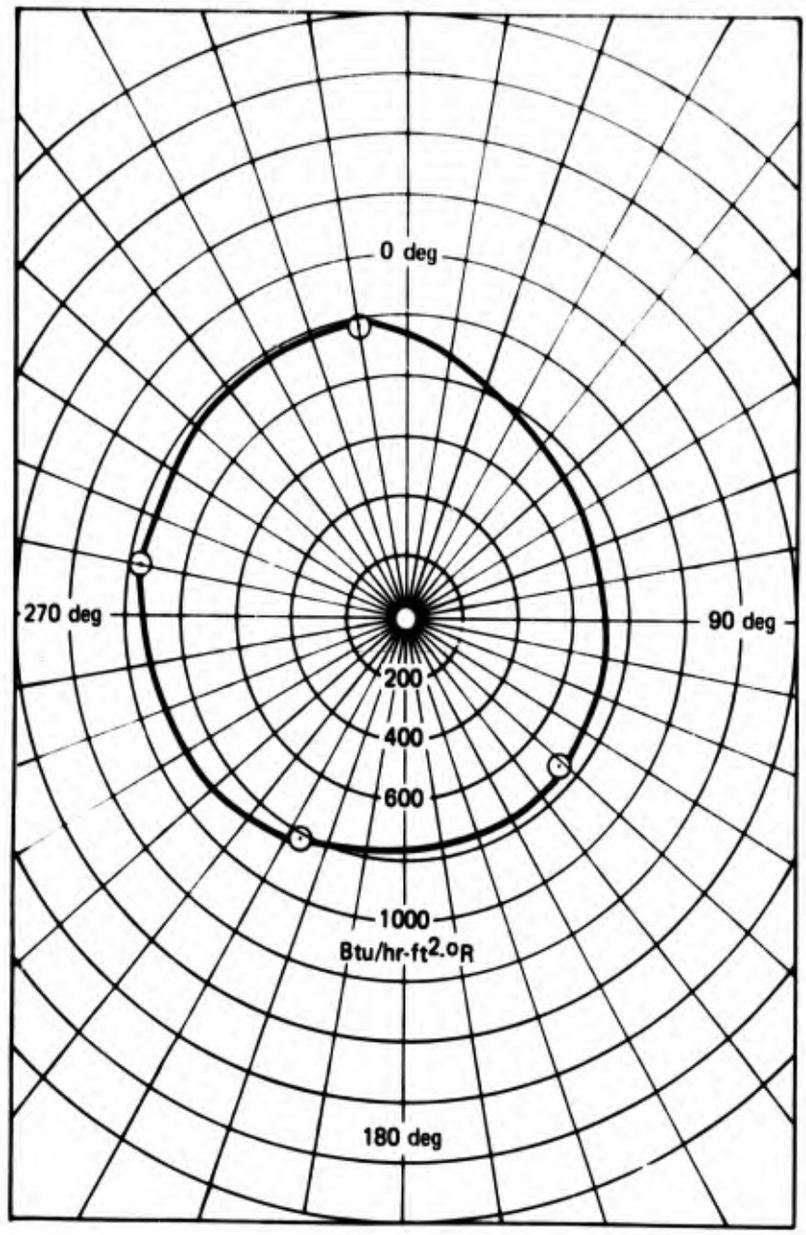

Figure 26. Azimuthal Distribution of Heat Transfer Coefficients 13.51 in. from Injector, Converging Section of Nozzle FD 53725

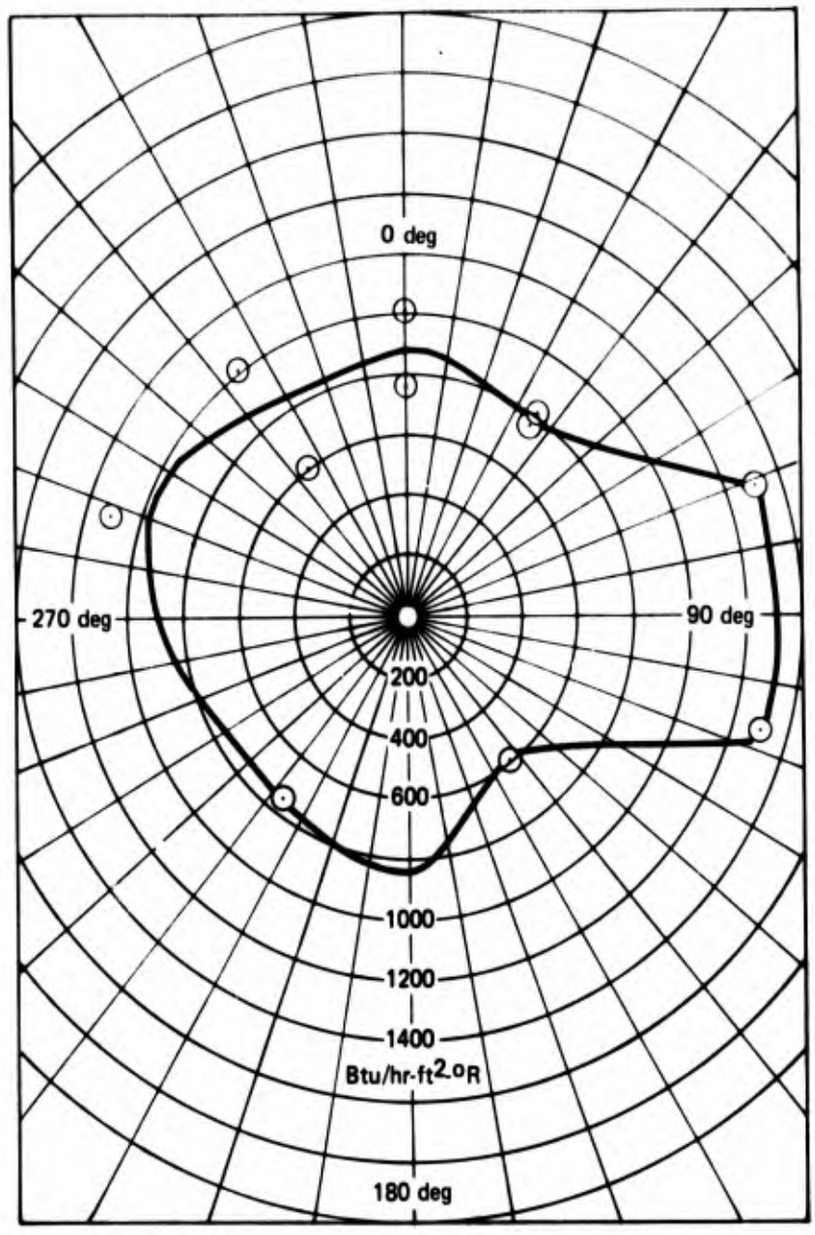

Figure 27. Azimuthal Distribution of Heat Transfer Coefficients at Throat FD 53726

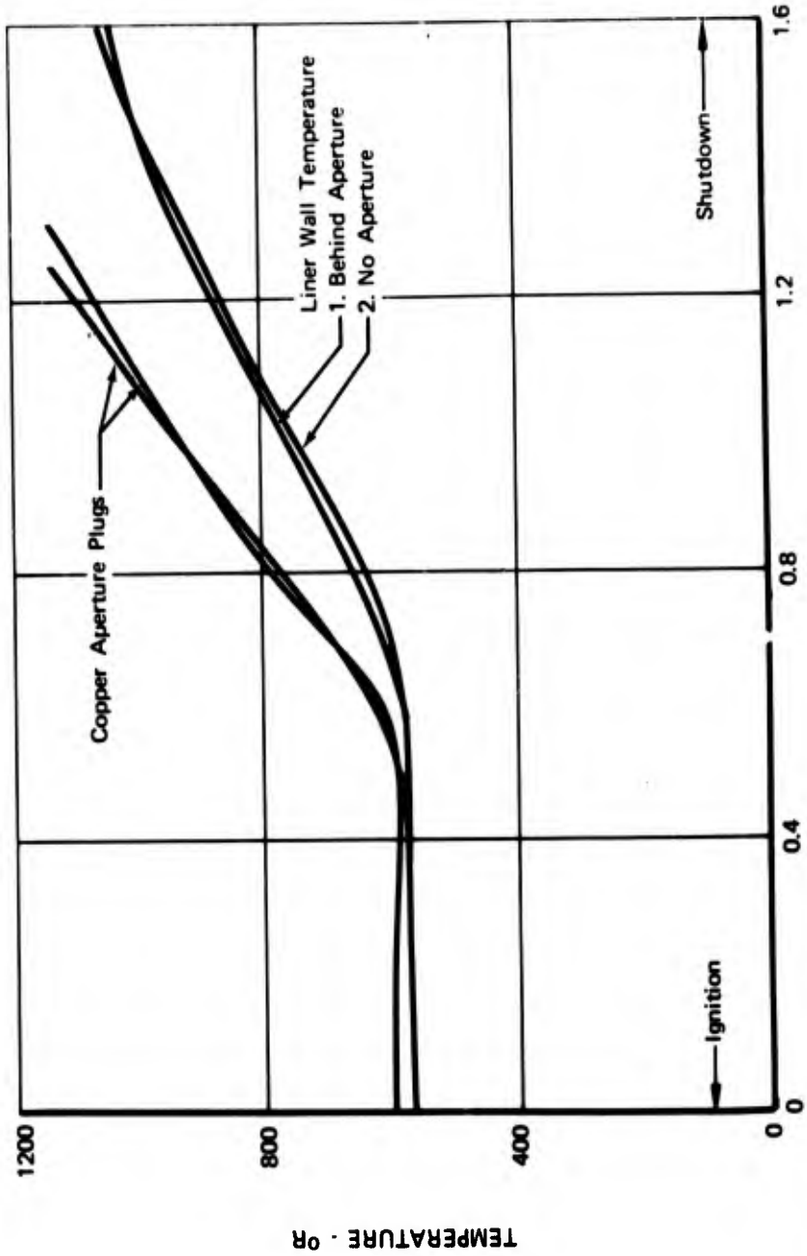

FD 53727

Figure 28. Thermal Response Data from Liner Thermocouples and from Copper Aperture Plugs

A comparison of all experimental data with theories is shown in figure 29; from these results the coefficient profile predicted by the Bartz Boundary Layer Analysis, Reference 9, was selected for use in the final design of the flightweight chamber because (1) the theoretical coefficients in the chamber agreed more closely with experiment and, (2) the nozzle throat coefficients were always higher than experiment thereby providing a safety margin in the region of highest heat flux.

D. FLIGHTWEIGHT THRUST CHAMBER

1. Design

To demonstrate the durability and effectiveness of a regeneratively cooled acoustic liner installed in flightweight-type hardware an electroformed thrust chamber incorporating an integral 1/2-chamber-length flightweight acoustic liner was designed to mate with the Agena injector. As shown in figure 30, the chamber was cooled by counterflowing fuel that entered through an inlet manifold at the nozzle exit and passed through the chamber coolant passages to a turnaround manifold at the injector end. The coolant exited from the chamber and reversed direction through coolant passages in the pressure shell to the exit manifold at the downstream end of the shell. From the exit manifold the fuel entered an external tubular manifold which lead to the injector fuel inlet.

The acoustic liner design used was, with one exception, the same as that determined from the acoustic analysis described in Section II-B. The configuration was a one-half chamber length, 6% open area liner, having a thickness of 0.20 in. and a backing cavity depth of 0.6 in.; however, the aperture diameter was reduced from the original liner specifications (0.120 to 0.094 in.) to facilitate incorporation of a desirable coolant passage geometry.

An existing digital computer program was modified for use in sizing the coolant passages. The program makes use of the Dipprey and Saversky equation (Reference 10) for calculating coolant side heat transfer coefficients, a one-dimensional fin equation developed by Kraus (Reference 11) for calculating heat conduction in the lands between the coolant passages, and the Bartz analysis (Reference 9) for determining the combustion side heat transfer coefficients.

Three revisions were necessary to adapt the program for the design of the flightweight chamber:

1. Functional relationships describing the physical and transport properties of 50-50 blend fuel were added.

2. The calculations were modified to include the capability for assuming a refractory coating on the hot wall.

3. The program was modified to allow nucleate boiling and to use the ultimate nucleate boiling heat flux data of Reference 7.

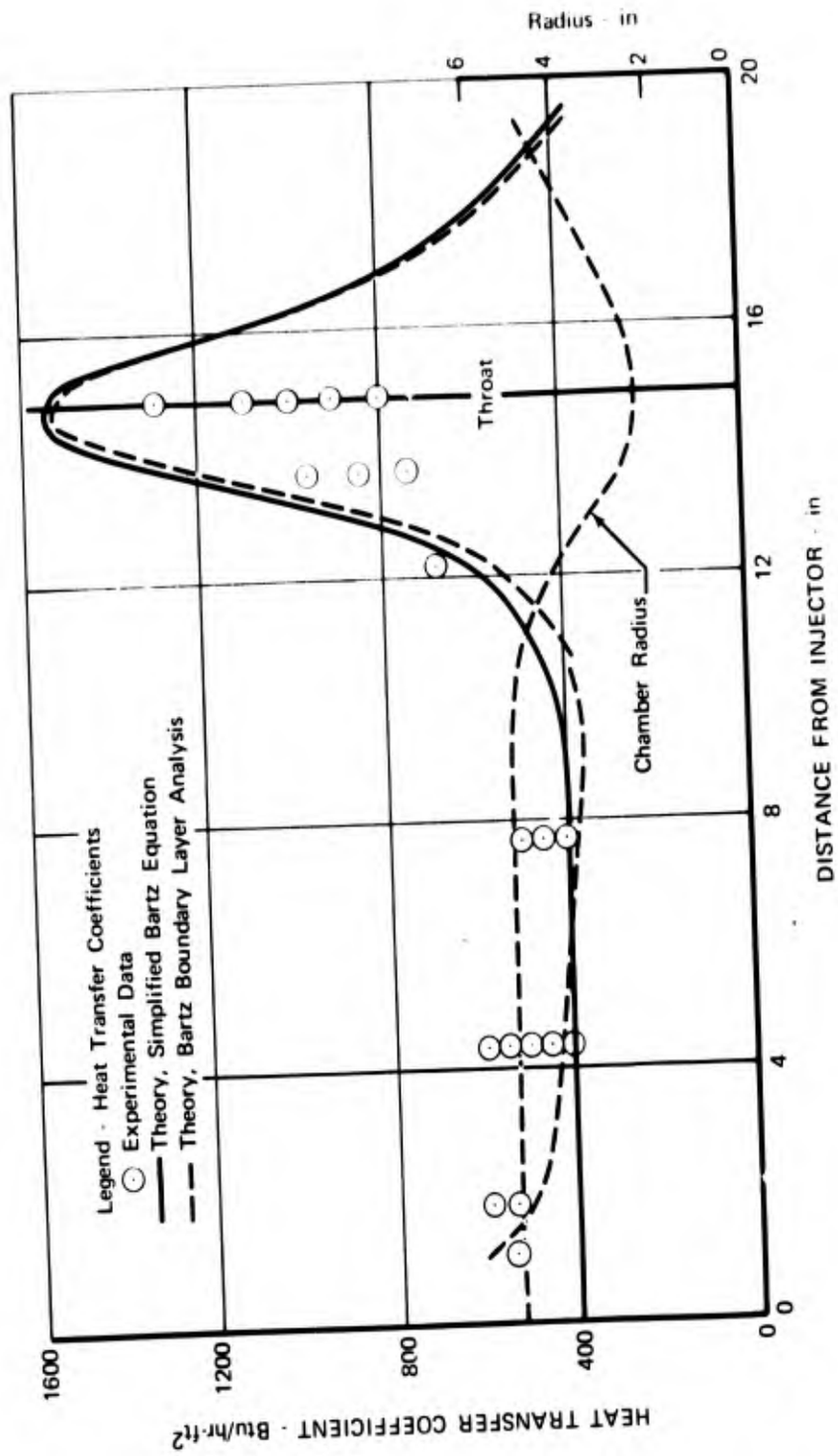

FD 53728

Figure 29. Axial Heat Transfer Coefficient Profiles

AD 517 006

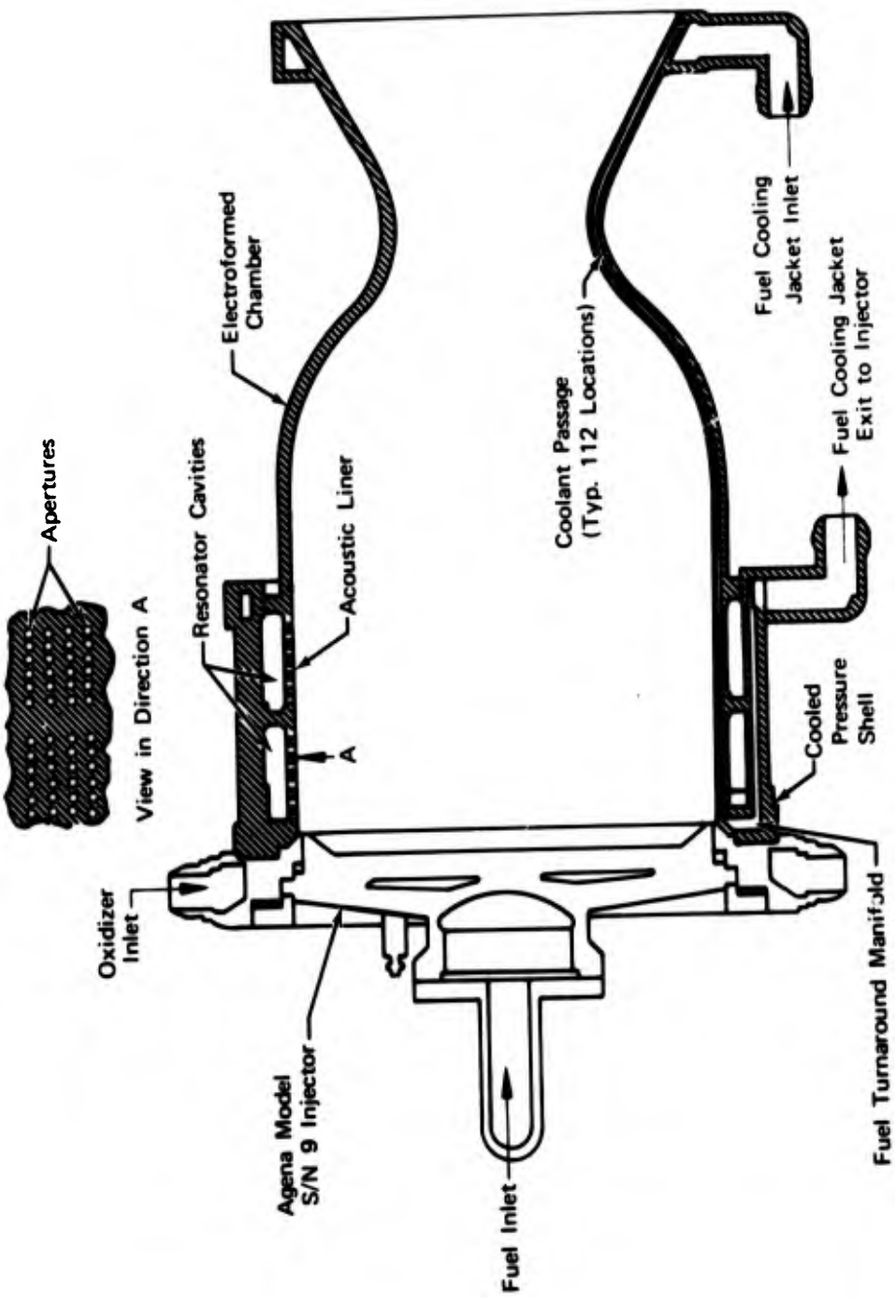

FD 53729

Figure 30. Regeneratively Cooled Motor with Integral Absorbing Liner

The cooling passage geometry was restricted by the following:

1. Land width in the chamber was held to a minimum of 0.2 in. to provide space for the installation of acoustic apertures.

2. Only passages of constant width and variable depth were considered to facilitate fabrication by electroforming.

3. The wall thickness between the coolant passages and the combustion chamber was a constant 0.035 in.

4. The minimum back wall thickness was 0.025 in.

5. Overall liner thickness was a constant 0.20 in.

The resulting liner configuration incorporated 112 constant passages with a constant width of 0.085 in., with the depth varying to meet the cross-sectional area requirements imposed by the heat transfer analysis. However, it was found that the predicted ratio of ultimate heat flux to actual heat flux was not great enough to provide a sufficient margin of safety. A refractory coating of 0.010 in. magnesium zirconate was therefore added to the hot wall to reduce the actual heat flux, thereby raising the ratio of actual to ultimate heat flux to a satisfactory level. Figure 31 shows the heat flux ratio versus axial location for coatings of 0.005 and 0.010 in. as well as for the case with no coating. A summary of final results from the flightweight chamber cooling analysis is given in table VIII.

The heat transfer analysis also indicated that it probably would not be necessary to cool the acoustic liner pressure shell; however, it was decided to flow the fuel leaving the acoustic liner section through the pressure shell to provide an extra margin of safety. The cooled pressure shell contained 48, 0.188-in. diameter drilled coolant passages.

The major parts of the flightweight motor assembly are the electroformed chamber with integral flightweight acoustic liner, the cooled pressure shell, the oxidizer manifold, and the Agena Model S/N 9 injector. The electroformed chamber was made of nickel; all other parts were made of AISI 347 stainless steel. To minimize program costs, only the liner section was of flightweight design; however, all remaining parts were designed to be easily adaptable to a flightweight configuration.

The chamber was provided with adapter bosses for mounting two 615A and two 614A Kistler dynamic pressure transducers to measure the liner backing cavity and chamber pressure oscillations, respectively. The cavity pressure transducers were mounted directly in the cooled pressure shell; however, it was necessary to design water-cooled adapters for the chamber pressure transducers because they extended through the backing cavity and were exposed to the combustion chamber environment at the transducer tip. Figure 32 shows the Kistler mounting scheme and a sketch of the water-cooled adapters for the cooled chamber.

Additional instrumentation included thermocouples at the fuel inlet manifold, turn around manifold, fuel exit manifold, injector fuel inlet, injector oxidizer inlet, and in the liner backing cavity. (See figure 33.) Pressure transducers were provided for all these locations along with two chamber pressure taps in the injector face.

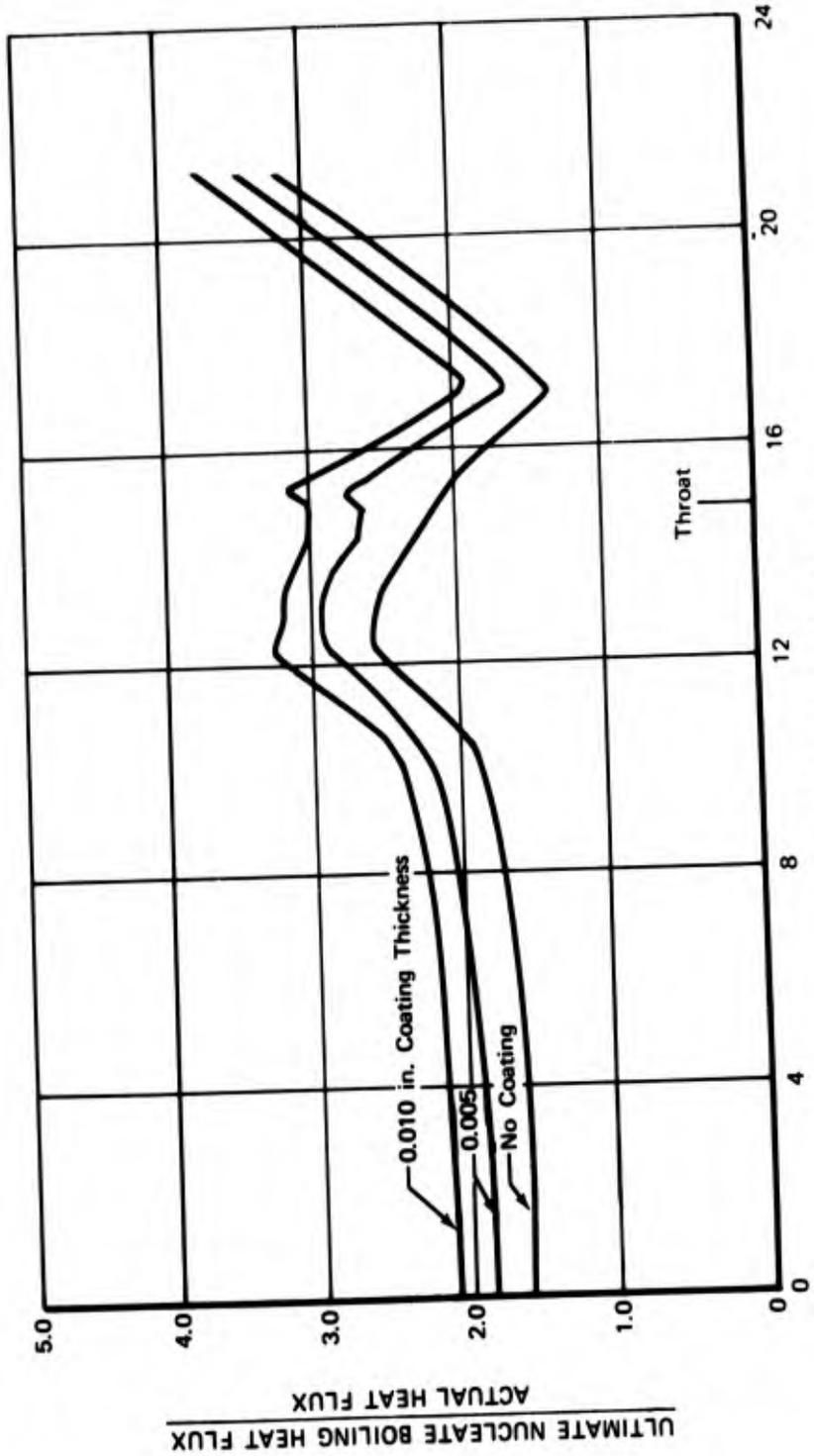

FD 53730

Figure 31. Effect of Magnesium Zirconate Coating Thickness on Chamber Heat Flux Ratio

Table VIII. Results of Flightweight Chamber Cooling Analysis

(Magnesium Zirconate Coating 0.010-in. Thick)

	Chamber	Throat	Nozzle
Passage Depth, in.	0.140	0.059	0.140
Passage Width, in.	0.085	0.085	0.085
Hot Wall Thickness, in.	0.035	0.035	0.035
Chamber Radius, in.	5.40	2.46	3.95
Distance from Injector, in.	0.0	14.93	18.0
Heat Transfer Coefficient, Btu/hr-ft^2-°F	600	1310	560
Coolant Temperature, °R	768	610	559
Coolant Pressure, psia	587	606	696
Heat Flux Ratio	2.08	2.89	2.68
Coating Temperature, °R	2045	2743	1960
Coolant Side Wall Temperature, °R	991	996	1012
Temperature Drop Across Coating, °R	848	1389	759

Chamber pressure perturbation was provided by an injector face mounted nondirectional bomb as described in Section II-C.

2. Fabrication

The regeneratively cooled chamber wall with integral 1/2-length acoustic liner was fabricated using an electroforming process by Camin Laboratories, Inc., Brooklyn, N. Y. All other parts were fabricated by conventional machining processes.

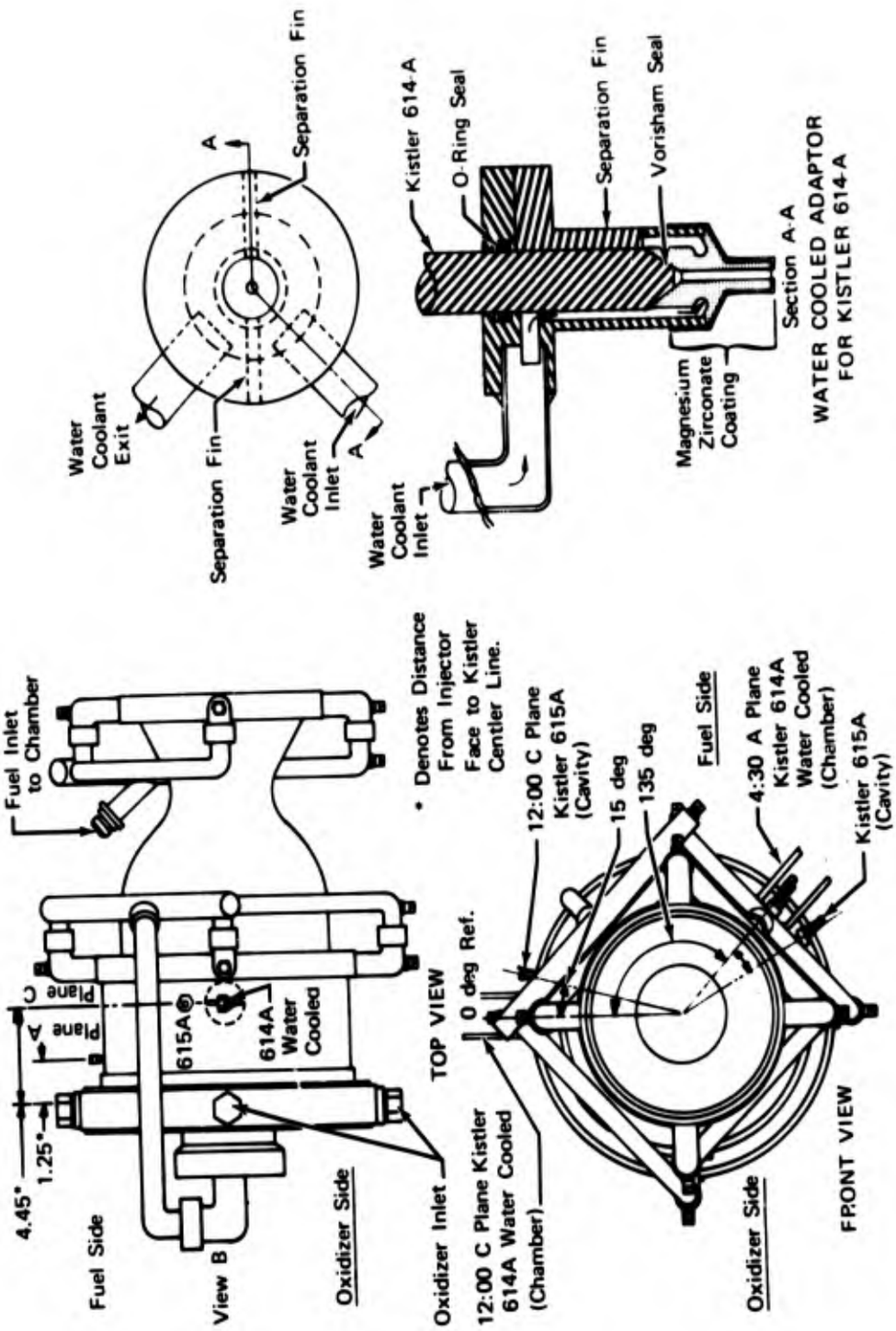

FD 53731

Figure 32. Flightweight Liner, Kistler Pressure Transducer Adapter and Mount Locations

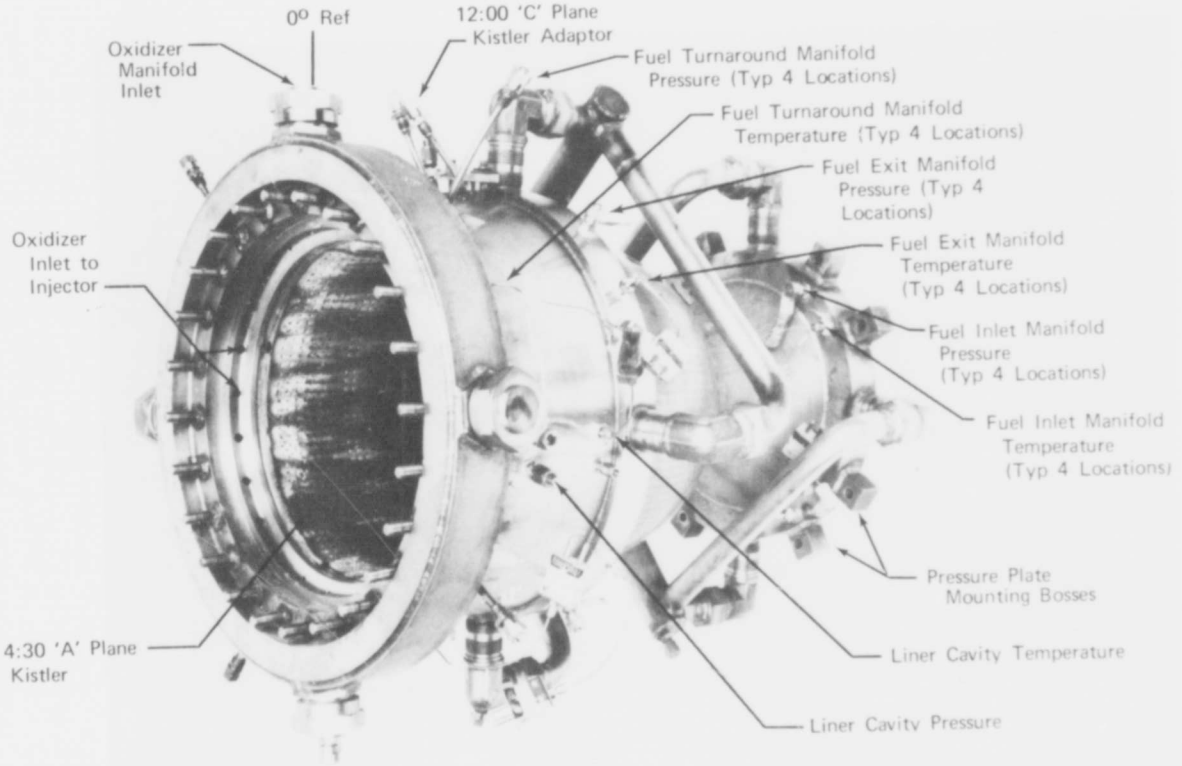

FE 107224A

Figure 33. Flightweight Chamber Instrumentation Locations

Figure 34 illustrates the steps in the electroforming process, which included:

1. Nickel was electrodeposited over a shaped mandel to form the chamber inner wall, the mandrel having been machined to produce the desired chamber contour.

2. The deposited nickel was machined to a thickness equal to the coolant passage hot-side wall thickness plus the passage depth. This distance corresponds to the dimension from the liner hot wall to the cold side (outer side) of the coolant passage.

3. The coolant slots were machined into the deposited nickel.

4. The slots were filled with conductive wax.

5. The outer liner wall was electrodeposited to form the coolant passage closure. This nickel was deposited to the lands and bridged the passage slots.

6. The liner outer dimensions including bosses, etc., were machined.

7. The conductive wax was removed by flushing.

After the electroforming process was completed the liner apertures were drilled into the lands between the coolant passages, and the remaining conventional fabrication was completed. Figures 35 through 37 are photographs of the flightweight chamber showing the front and back of the liner section and an overall view of the chamber.

The chamber was assembled by the vendor and pressure-checked at 1180 psig with gaseous nitrogen; however, before the motor could be fired, several preparations and tests were completed, including: X-raying, applying the magnesium zirconate coating, installing external fuel manifolding and instrumentation adapters, final assembly, leak checking, cleaning, and water flowing.

The liner was X-rayed to determine if any foreign material was located in the coolant passages, and two indications of foreign matter were noted. One was at the throat section and the other in a passage 0.25 in. from the coolant inlet manifold. It was decided to continue with the other preparations as scheduled before attempting to remove the objects since additional foreign material could have been deposited in the passages during the installation of the external plumbing and instrumentation adapters. The X-rays also revealed that the holes drilled through the cooled liner for the Kistler dynamic pressure transducers were not centered between the coolant passages as per design. The holes were located 0.020 in. from one coolant passage and 0.040 in. from the other; however, stress calculations indicated that the mislocation would not cause a structural problem.

The magnesium zirconate coating was applied to the inner chamber wall and the motor was assembled using the S/N 9 injector and the oxidizer manifold. The external plumbing was fabricated and installed and the instrumentation adapters were mounted.

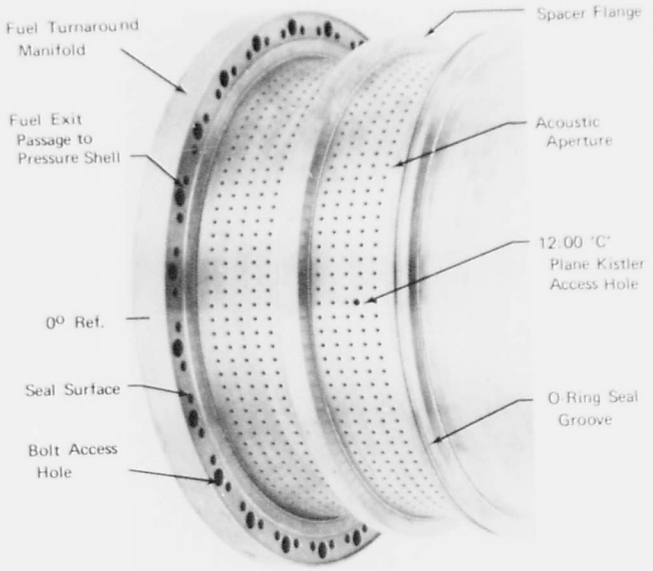

Figure 35. Flightweight Chamber with Acoustic Liner Pressure Shell Removed FE 97367A

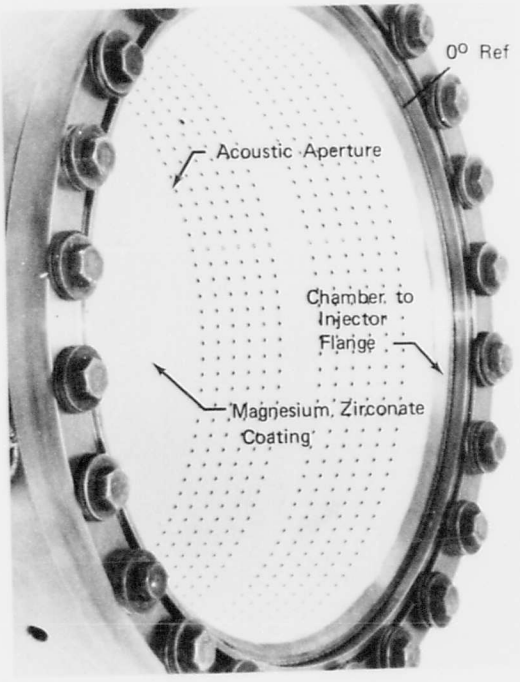

Figure 36. Integral Acoustic Liner in Cooled Flightweight Chamber FE 97366A

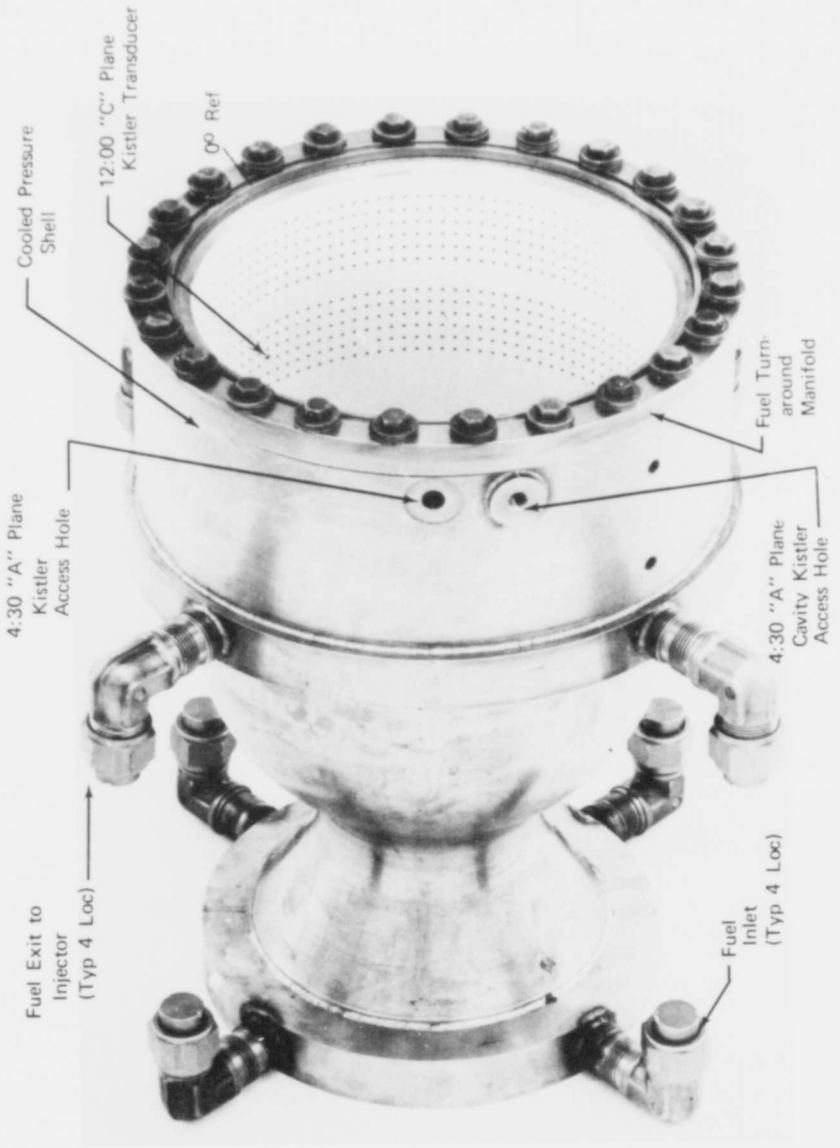

Figure 37. Flightweight Chamber Assembly

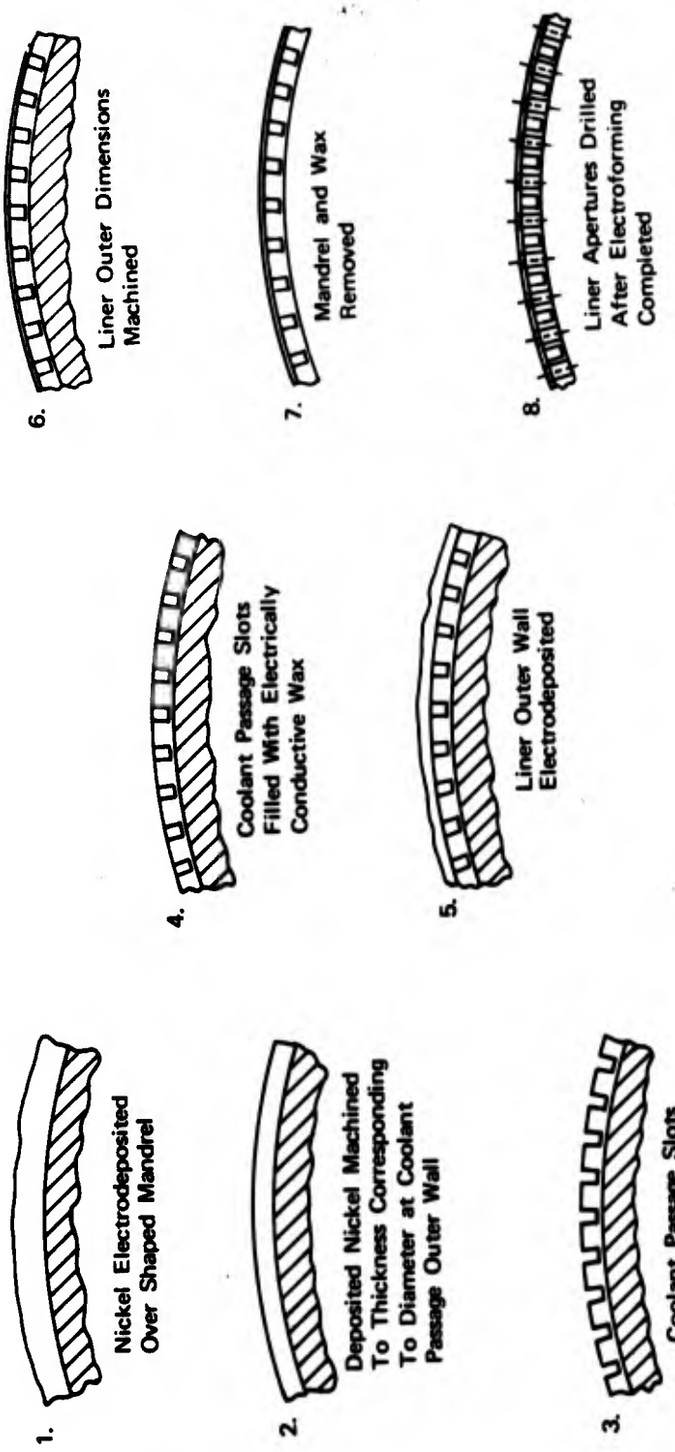

FD 53732

Figure 34. Fabrication Technique Used for Regeneratively Cooled Flightweight Chamber

The pressure leak check of the motor assembly revealed an inadequate seal between the pressure shell and the cooled liner. The problem was corrected by building up the seal surface with weld and remachining to the proper specification. The motor was reassembled and again leak-checked; no leaks were detected. The motor was then flushed with hot degrease fluid and with steam in an attempt to remove the foreign objects in the coolant passages.

The liner was X-rayed again; the indications of material in the flow passages were still present, in the same locations. Several additional X-rays were made from various angles to locate exactly the suspected material in the passages, and a representative of Camin Laboratories, Inc., was shown the X-ray film. After close examination of the film he suggested that the indications were probably caused by nickel, electrodeposited before the final layer of nickel was deposited, in tiny impressions made in the wax used to fill the passages. An end view X-ray of the material in the throat passage indicated that the impression was approximately 0.002 to 0.005 in. in depth. It was concluded that this blockage should not be sufficient to cause coolant flow disruption; and, therefore, no further attempt should be made to correct the condition. Nevertheless, it was decided to apply a temperature-indicating paint to the outside wall of the liner so that the areas of concern could be monitored for hot spots.

Water-flow calibration tests were conducted on the assembly to determine the coolant passage pressure drop and the time required to fill the fuel side of the motor. A fill time of approximately 1.1 sec was established for use as a first approximation for the sequencing of the stand control valves during the start transient. The results of flow tests showed the pressure drop across the liner at design flowrate (143 gpm) with water was 235 psid, with a total pressure drop for the liner, cooled pressure shell, and the manifold lines of 337 psid. Previous results of water-flow tests compared to firing data for pressure drop across the injector alone indicated that, for the design flowrate, the fuel pressure differential would be approximately 68% of that measured with water. Using this relationship, the pressure drop across the manifold, cooled pressure shell, and liner was predicted to be 230 psid with fuel with a pressure drop across the liner section alone expected to be 162 psid. The total pressure drop was used to establish the fuel run tank pressure for the first firing.

3. Test Program

The motor was mounted on the B-5 test stand and after final instrumentation of the assembly and controls setup were completed, three overcooled, i.e., at low mixture ratios, firings were made. (See Test Summary, table IX.)

The first firing was made to check out the control system and to verify operating parameters. The test duration was 2.0 sec and the mixture ratio was 1.4 with a nominal chamber pressure of 363 psia. The start transient was rough, primarily because the oxidizer side of the injector was not full at ignition. The oxidizer flowrate was approximately 11 gpm higher than the intended flow, which resulted in a higher than planned mixture ratio. The coolant temperatures in the liner exit manifold did not reach steady state before the end of the firing.

Table IX. Flightweight Chamber Test Summary

Test No.	Duration, sec	Chamber Pressure, psia	Bomb	Mixture Ratio	C* Efficiency, %(1)	Liner Coolant Exit Temperature Actual/Predicted, °R	Comments
1	2.0	363	None	1.4	95.6	628/732	System checkout test. 90 Hz chamber pressure oscillations occurred, due to mixture ratio below design value.
2	5.0	365	None	1.2	99.0	657/732	Cooling data test. 90 Hz oscillations more pronounced. Test aborted by hot gas leak at one Kistler seal.
3	4.99	420	None	1.5	98.7	672/758	Cooling data test. Increased injector ΔP's (higher mixture ratio) eliminated 90 Hz oscillations.
4	3.81	481	None	1.98	95.9	693/768	Cooling data test. Test terminated by hot gas leak due to pressure shell-to-fuel turnaround manifold gasket failure.
5	1.36	370	None	1.50	74.4	537/768	Run was aborted by burn-wire at +1.36 sec. No rig damage.
6	10.00	479	None	1.97	97.2	724/768	
7	4.99	483	10 gr.	2.00	97.4	717/768	Bomb fired at +2.0 sec producing a 230 psi pressure spike that damped in 0.005 sec.

(1) Based on chamber pressure.

Table IX. Flightweight Chamber Test Summary (Continued)

Test No.	Duration, sec	Chamber Pressure, psia	Bomb	Mixture Ratio	C* Efficiency, %(1)	Liner Coolant Exit Temperature Actual/Predicted, °R	Comments
8	5.01	481	30 gr.	1.97	97.6	727/768	Bomb was set to fire at +2.3 sec, but was thermally destroyed before firing.
9	4.99	479	36 gr.	1.97	97.4	729/768	Bomb was set to fire at +2.0 sec, but was thermally destroyed before firing.
10	5.00	485	45 gr.	2.01	97.3	732/768	Bomb was timed to fire at +2.0 sec, but fired spontaneously at +1.74 sec producing a pressure spike of 200 psi that damped within 0.007 sec.
11	5.00	481	36 gr.	2.00	97.1	738/768	Bomb fired at +1.55 sec, producing a pressure spike of 100 psi that damped within 0.005 sec.
12	5.15	473	40 gr.	1.99	96(2)	727/768	Bomb detonated at +1.82 sec producing a 400 psi pressure spike that damped in 0.010 sec.
13	60.07	480	None	2.00	96(2)	729/768	

(1) Based on chamber pressure.

(2) ±1% Uncertainty in efficiency because of malfunction in oxidizer temperature probe, located at flowmeter.

Prior to the second firing, minor timing and control valve position changes were made in the oxidizer system, and the test duration was extended to 5.0 sec. The objective of this firing was to obtain preliminary cooling data at a mixture ratio of 1.2. The start transient was not as rough as the previous firing, but a 90-Hz chugging was initiated with peak-to-peak amplitudes of 50 to 60 psi. The chugging continued until the test was aborted by a hot gas leak caused by a dynamic pressure transducer seal failure. The abort occurred at shutdown (+5.0 sec). The chugging was concluded to be the result of the oxidizer injector pressure differential, which was only 25 psid and therefore considerably below the design value (60 psid). Review of preliminary cooling data indicated that the bulk temperature of the fuel in the liner exit manifold was at least 75 degrees below the predicted value of 732°R. Post-test inspection of temperature-indicating paint on the outside surface of the liner revealed that the wall temperature did not exceed the cold change point of the paint (1000°R).

In an attempt to stop the 90-Hz chugging instability during the third firing, the oxidizer flowrate for the start transient was increased from 107.4 gpm to 127.0 gpm, which increased the oxidizer injector differential pressure from 25 to 45 psid. At 1.4 sec into the test, the oxidizer flowrate was increased to 133.6 gpm to reach the desired mixture ratio of 1.5.

Slight chugging (20 psi P/P) was present during the start transient; it continued until the mixture ratio of 1.5 was attained and then damped. The liner exit coolant temperature reached a maximum of 690°R, 86 degrees below the predicted value. The coolant temperature measured in the upper half of the motor was 25 degrees higher on the average than the temperatures in the lower half. The temperature-indicating paint on the outside liner surface had not changed, indicating that the wall temperature was below 1000°R. Post-test inspection of the combustion chamber revealed areas of chipped magnesium zirconate coating. The coating failed at two locations, 6:00 and 8:00, adjacent to the injector face (figure 38); each was about 1 sq in. in area. The motor was removed from the stand and disassembled for repairs; the nickel liner was inspected for hot spots and cracks, but none were located. The thickness of the coating around the chipped areas was measured and found to be 0.025 to 0.035 in., much thicker than the desired 0.010 in. It was concluded that the chipping resulted from severe thermal gradients that would be present in such a thick coating. The old coating was completely removed by vapor-blasting and the chamber was resprayed. The motor was then assembled, leak-checked and cleaned.

A leak was discovered during the cleaning operation and the motor was again disassembled and new seals fitted. A slight out-of-round condition was found in the cooled pressure shell; however, the new seal prevented any leakage. After cleaning, the motor was mounted on the test stand.

The purpose of the fourth firing was to obtain cooling data at design operating conditions. The average steady-state chamber pressure was 481 psia, mixture ratio was 1.98, C* efficiency was 95.9% (based on chamber pressure), and liner coolant exit temperature was 693°R (predicted value is 768°R). The test was aborted at +3.81 sec into the scheduled 5.0-sec run when a hot gas leak occurred. Post-run inspection of the rig revealed that the pressure shell-to-fuel turnaround manifold gasket had failed, allowing hot chamber gases to leak outside the chamber. Also, one injector-to-pressure shell bolt was stripped and blown out, apparently the result of liquid fuel leaking from the pressure shell coolant

passages into the bolt hole and then detonating. The rig was dismounted and disassembled for further inspection and repair. The only damage found (other than to the Teflon gasket that failed) was some chipping of the magnesium zirconate coating at the injector end of the chamber. Because of the high temperatures, the failed gasket had begun to flow and was slightly charred in several places along the inside edge. It was decided that the gasket should not be replaced and that the rig would be reassembled using weld seals instead.

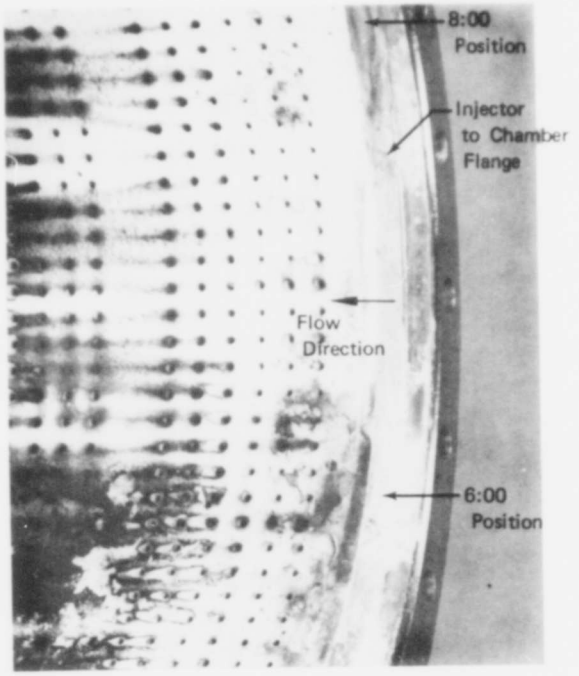

Figure 38. Damaged Area of Magnesium Zirconate Coating After Test 3 FE 99038A

Figures 39 through 41 describe the revisions to the injector-to-chamber attachment and sealing scheme. The original configuration is shown in figure 39. Figure 40 shows how the pressure shell-to-turnaround manifold seal was accomplished by welding. It was necessary to seal at "C" to prevent the fuel from leaking into the acoustic cavity from the pressure shell coolant passages. However, to gain access to "C" it was necessary to remove the turnaround manifold by cutting as shown. After the seal weld at "C" was completed, the turnaround manifold was replaced and welded at "A" and "B".

The complete repair scheme is shown in figure 41; the injector-to-pressure shell bolts were replaced by studs that were threaded into the pressure shell and sealed with selds at "D" and "E". The oxidizer manifold was then welded to the turnaround manifold at "F". Prior to attachment of the oxidizer manifold the inside chamber wall was recoated. The new coating was held to approximately 0.010 in. thick.

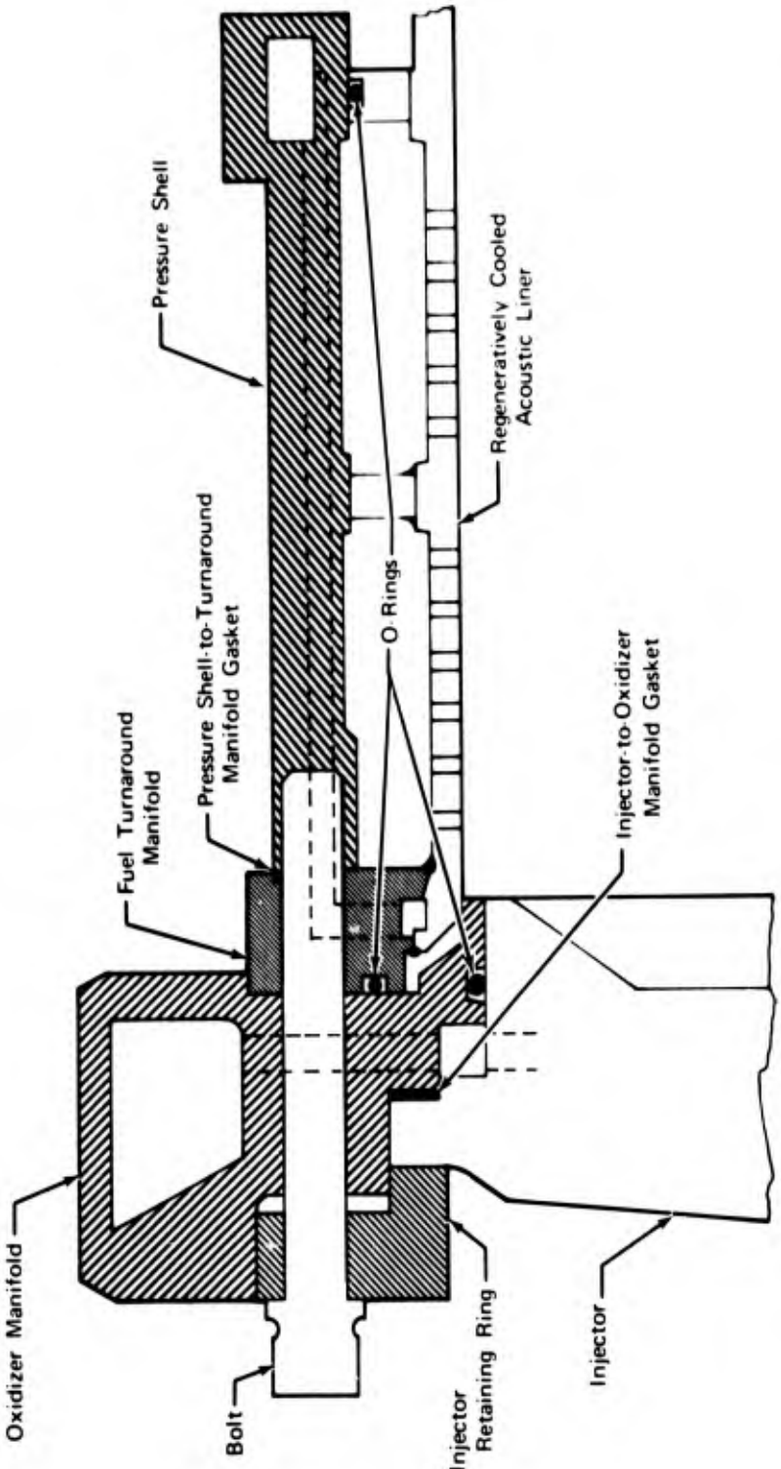

FD 53750

Figure 39. Original Injector-to-Chamber Attachment and Sealing Scheme

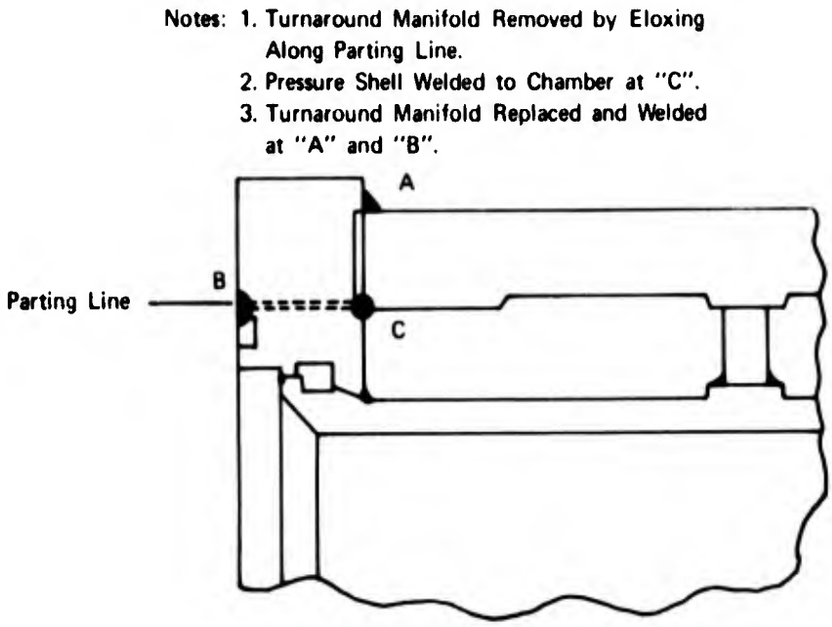

Figure 40. Method of Removal and Rewelding of Fuel Turnaround Manifold FD 53751

The motor was checked, cleaned and mounted to the test stand. The next firing, test 5, was scheduled for 10 sec duration but was terminated prematurely at +1.4 sec by the burnwire abort system. Review of the data indicated that the burnwire sample time was marginal, and post-test visual inspection of the motor revealed no hardware damage; therefore, the oxidizer control valve was re-scheduled to open 0.15 sec earlier and the burnwire sampling time was increased from +1.4 to +1.8 sec in preparation for the next test.

Test 6 was conducted for a scheduled duration of 10.0 sec to demonstrate durability and to obtain cooling data. The steady-state mixture ratio was 1.97 at a nominal chamber pressure of 478 psia. The flightweight chamber was in excellent condition following the test; there were no indications of hot spots or chipping on the magnesium zirconate coating.

Notes: 1. Studs Welded in Place at "D" and "E".
2. Oxidizer Manifold Welded to Turnaround Manifold at "F".

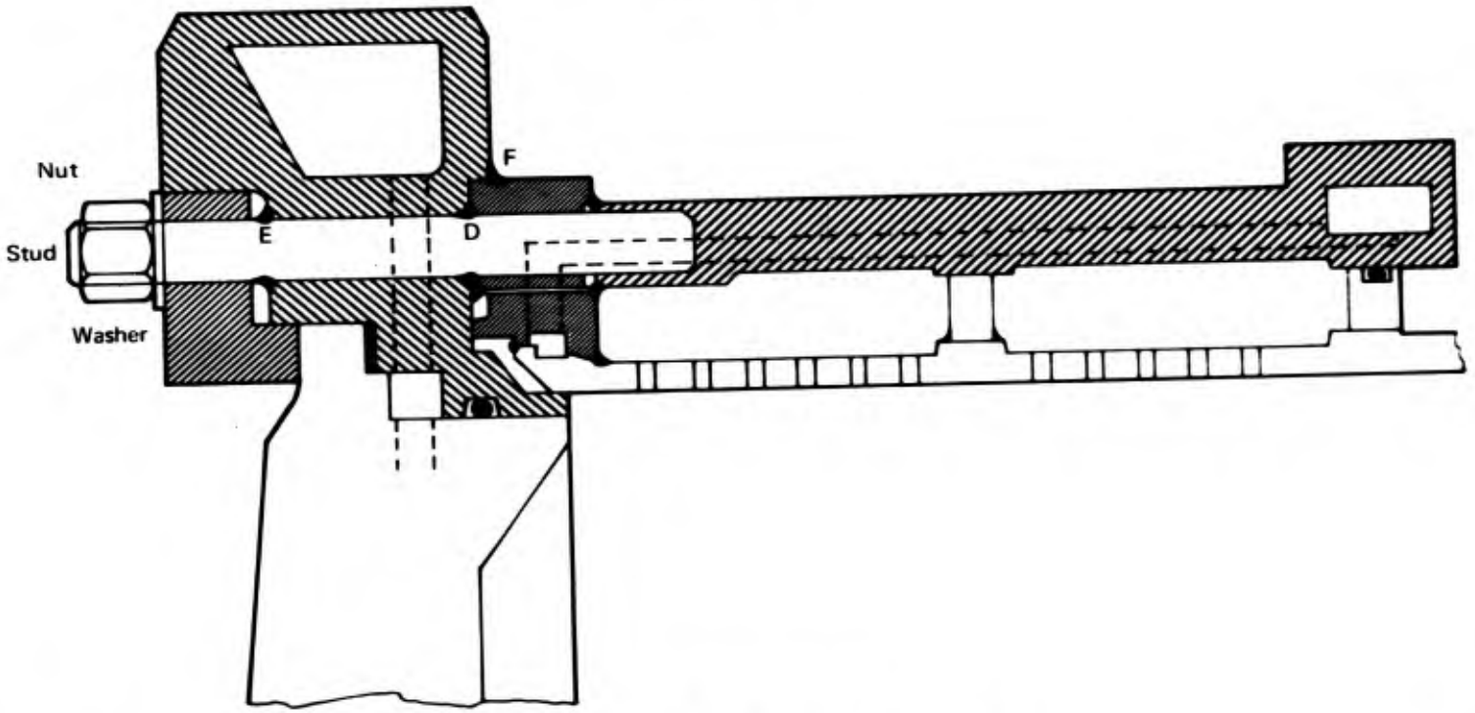

FD 53752

Figure 41. Repaired Injector-to-Chamber Attachment and Sealing Scheme

Temperature data recorded during test 6 are shown in figure 42. The coolant exit temperature reached a maximum of 720°R, 48 degrees lower than the design value. The coolant temperature increase from the chamber inlet to exit was 160°R. At the end of the firing the cavity temperature recorded by the No. 2 probe was 1120°R, 400 degrees higher than that recorded by the No. 1 probe. The difference in cavity probe readings is attributed to radiation heating of the No. 2 probe; it was located directly behind an aperture where it could "see" the combustion zone. The No. 1 probe is located behind the liner wall midway between two apertures.

Test 7 was conducted to verify the dynamic stability characteristics of the flightweight chamber. The test duration was 5.0 sec and the mixture ratio was 2 with a nominal chamber pressure of 483 psia. A nondirectional, 10-grain bomb was detonated at +2.0 sec producing a pressure spike of 230 psi which damped in 5 millisec. Post-test inspection of the chamber revealed that several small fragments of the Teflon bomb casing were stuck to the chamber wall near the bomb mount; however, no damage or deformation of the liner was apparent. The threaded tip of the bomb mount was approximately 50% eroded.

Test 8 was conducted to further verify the chamber dynamic stability. A larger bomb, 30 grains, was timed to detonate at +2.3 sec. This particular time was selected to ensure that the perturbation would occur well after full chamber pressure was obtained. The test stand dynamic pressure data indicated that the bomb did not produce an overpressure when triggered. A post-test visual inspection of the chamber showed that the bomb had been destroyed, but it could not be determined if it had been detonated or burned.

A larger bomb, 36 grains, was installed for test 9. The time of detonation was scheduled earlier in the test (at +2.0 sec) to determine if the suspected thermal failure could be eliminated. As in the previous test, no perturbation was obtained when the bomb was triggered. Again the visual inspection verified the bomb had been destroyed.

Before test 10 additional thermal insulation in the form of a room temperature vulcanizing compound approximately 0.05 in. thick was applied to the bomb casing. The bomb had been set to detonate at +2.0 sec, but dynamic pressure data traces showed an overpressure spike of 230 psi occurred at +1.75 sec and damped to stable operation in 7 millisec. Because the bomb had not been triggered it was assumed to have been thermally detonated.

In an attempt to reduce the occurrence of bomb thermal failure, test 11 was conducted using a bomb coated with approximately 0.10 in. of insulation and timed to detonate earlier in the test, at +1.55 sec. The 36-grain bomb detonated as scheduled, but the Kistler traces indicated that an overpressure spike of only 100 psi occurred.

The bomb casing was then redesigned to provide longer life in the hot flow stream. The walls were made 0.14 in. thick, double the original thickness.

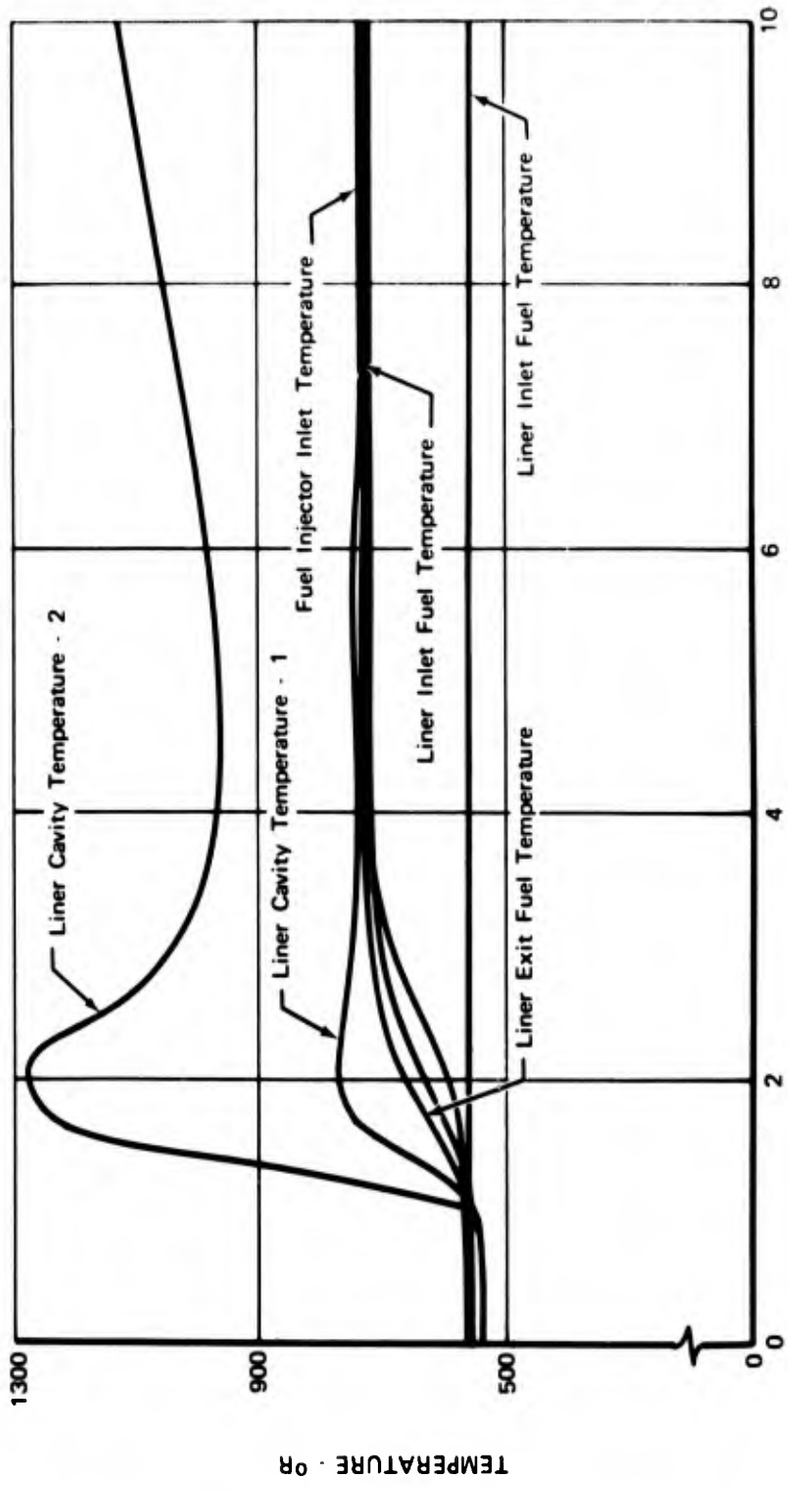

FD 53753

Figure 42. Temperature Data from Test 6

During preparation for the final series of tests, a static pressure test of the motor revealed a small leak from a coolant passage to the outside of the motor in the converging section of the nozzle. The leak was not noted during the post-test pressure check of test 11. No reason for the leak could be determined. There were no visible cracks; therefore the failure, a tiny pinhole, did not appear to be the result of thermal fatigue. The leak was repaired by welding at the test stand.

Test 12 was conducted using a bomb loaded with a 40-grain charge timed to detonate at +1.8 sec. A spike of 400 psi was recorded by one of the Kistler probes. The overpressure damped to stable operation in 10 millisec. The post-test inspection of the chamber revealed that several fragments of the Teflon bomb casing were stuck to the chamber wall near the location of the bomb mount; however no deformation of the liner was apparent and no chipping of the magnesium zirconate coating was found.

Test 13 was conducted without a bomb for the scheduled duration of 60 sec. The test was extremely stable; no change in performance was noted during the test. A post-test inspection of the chamber showed that the bomb mount plug had eroded approximately 40%; a slight discoloration was noted in the nozzle throat section on the magnesium zirconate coating in the downstream area corresponding to angular location of the bomb mount. No damage had occurred to the liner portion of the chamber from either aperture erosion or liner deformation. The post-test static pressure check of the motor revealed three additional pin-hole leaks in the area of the throat convergent section. (See figure 43.) A close inspection of the area using X-ray and zyglo techniques revealed no visible cracks in the chamber wall. The pin-holes were so small that X-ray film could not detect their source. The chamber after disassembly is shown in figures 44 through 47.

4. Analysis of Data

a. Performance and Stability

Comparison of the performance data from the flightweight chamber firings with data from the uncooled motor (figure 48) shows that the performance of the cooled chamber was approximately the same as that of the uncooled motor with no acoustic liner. Although the cooled chamber specific impulse and C^* efficiency, based on P_c, were 3 seconds and 0.6% lower, respectively, than that of the uncooled motor, these deviations are well within the limits of experimental error for the test and thus cannot be considered significant.

Combustion was stable for every test of the flightweight liner; no spontaneous combustion pops occurred. The dynamic stability of the motor was demonstrated during six tests that were disturbed with nondirectional bombs of various charges. In all cases the resulting overpressures damped in less than 10 millisec. The highest overpressure, 400 psi, was recorded during test 12.

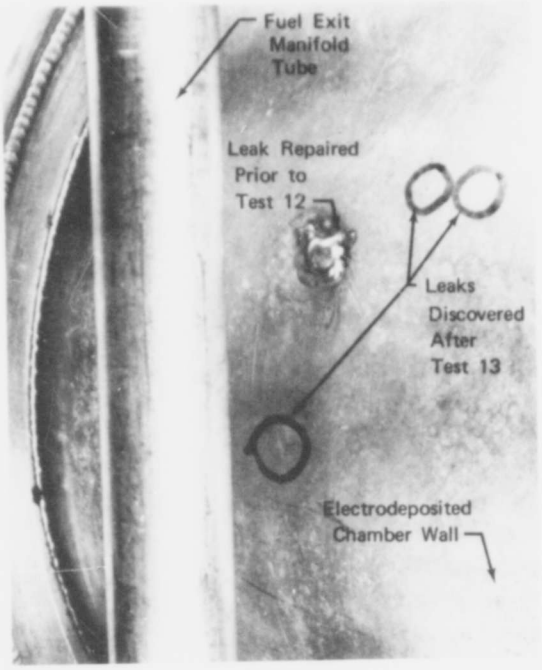

Figure 43. Leak Areas on Electrodeposited Chamber Wall FE 107227A

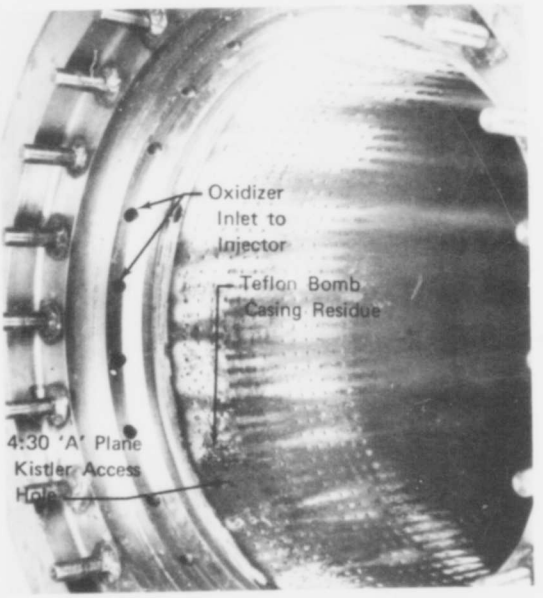

Figure 44. Flightweight Chamber After Test 13 FE 107223A

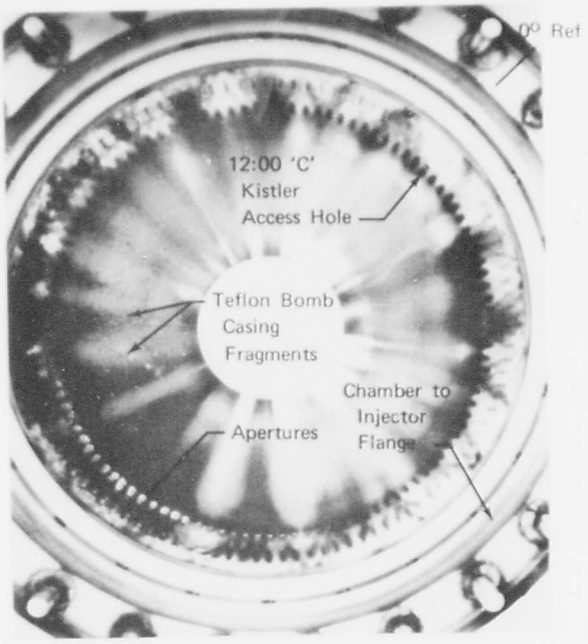

Figure 45. Flightweight Liner Looking Downstream from Injector Flange FE 107225A

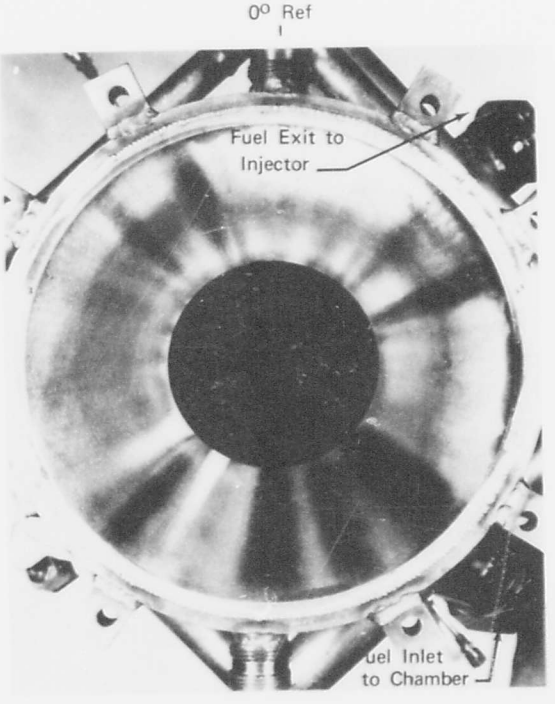

Figure 46. Flightweight Liner Looking Toward Flow Direction After Test 13 FE 107226A

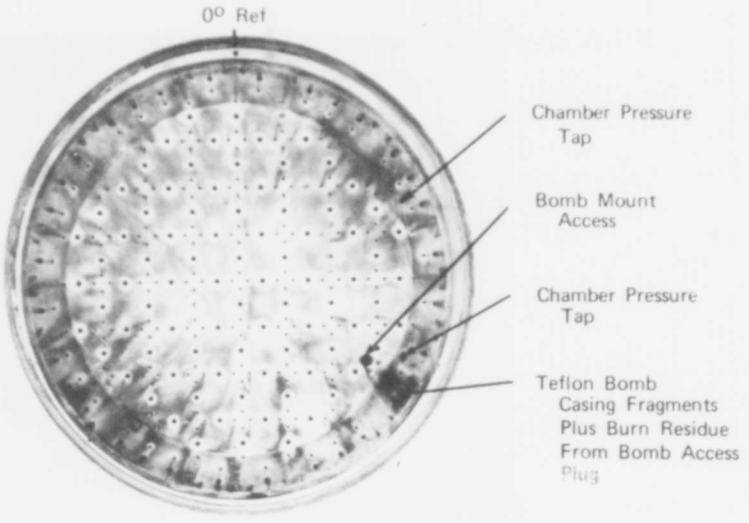

Figure 47. Agena Model S/N 9 Injector After Test 13 FE 107228A

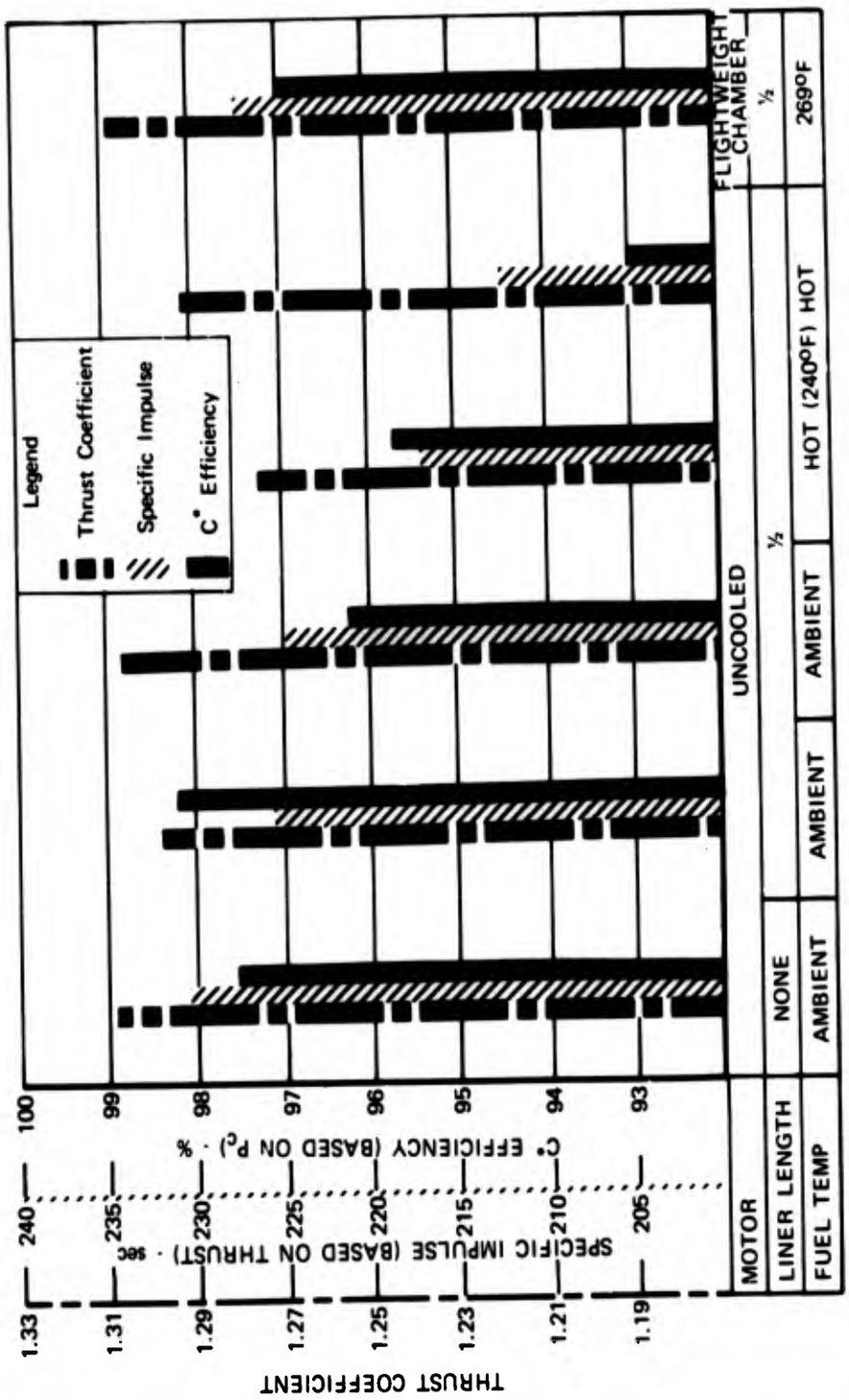

FD 53754

Figure 48. Summary of Performance Data

b. Heat Transfer

The temperature rise and pressure drop for the coolant between the inlet and turnaround manifolds for the flight weight chamber tests are shown in table X. The actual temperature rise is consistently 75% of the predicted value. The difference is most probably caused by uncertainty in both the thermal conductivity and thickness of the magnesium zirconate coating on the chamber wall; e.g., a variation of only 0.005 in. in thickness can cause a 15% change in the theoretical temperature rise. The difference between predicted and measured pressure drop values is caused by the difficulty in accurately predicting the pressure losses of boiling fluids.

Table X. Coolant Temperature Rise and Pressure Drop Between Inlet and Turnaround Manifolds

Test	Mixture Ratio	Temperature Rise (°F) Measured	Temperature Rise (°F) Predicted	Pressure Drop (psid) Measured	Pressure Drop (psid) Predicted
2	1.2	119	192	146	99
3	1.5	132	218	156	99
6	2.0	171	228	169	114
7	2.0	170	228	162	114
10	2.0	166	228	167	114
11	2.0	171	228	161	114
12	2.0	168	228	164	114
13	2.0	169	228	166	114

The effectiveness of the chamber cooling scheme was evident after the final series of firings. Inspection showed that no damage of any kind had occurred to the acoustic liner or the chamber wall, and, in addition, the nozzle showed no signs of erosion.

The preliminary analysis of heat transfer to the pressure shell indicated that the total heat flux to that section would be small. As predicted, the temperature rise in the pressure shell was small, averaging less than 5°F.

The temperature in the liner cavity was found to be considerably lower for the cooled liner (820°R) than for the uncooled liner (2250°R). Figure 49 shows a typical cavity gas temperature rise with time for the cooled and the uncooled motor; the cavity temperatures were lower for the cooled motor because the gases in the cavity were forced through the cooled apertures of the liner. The effect of the cavity temperature difference on the theoretical absorption characteristics of the motor are shown in figure 50.

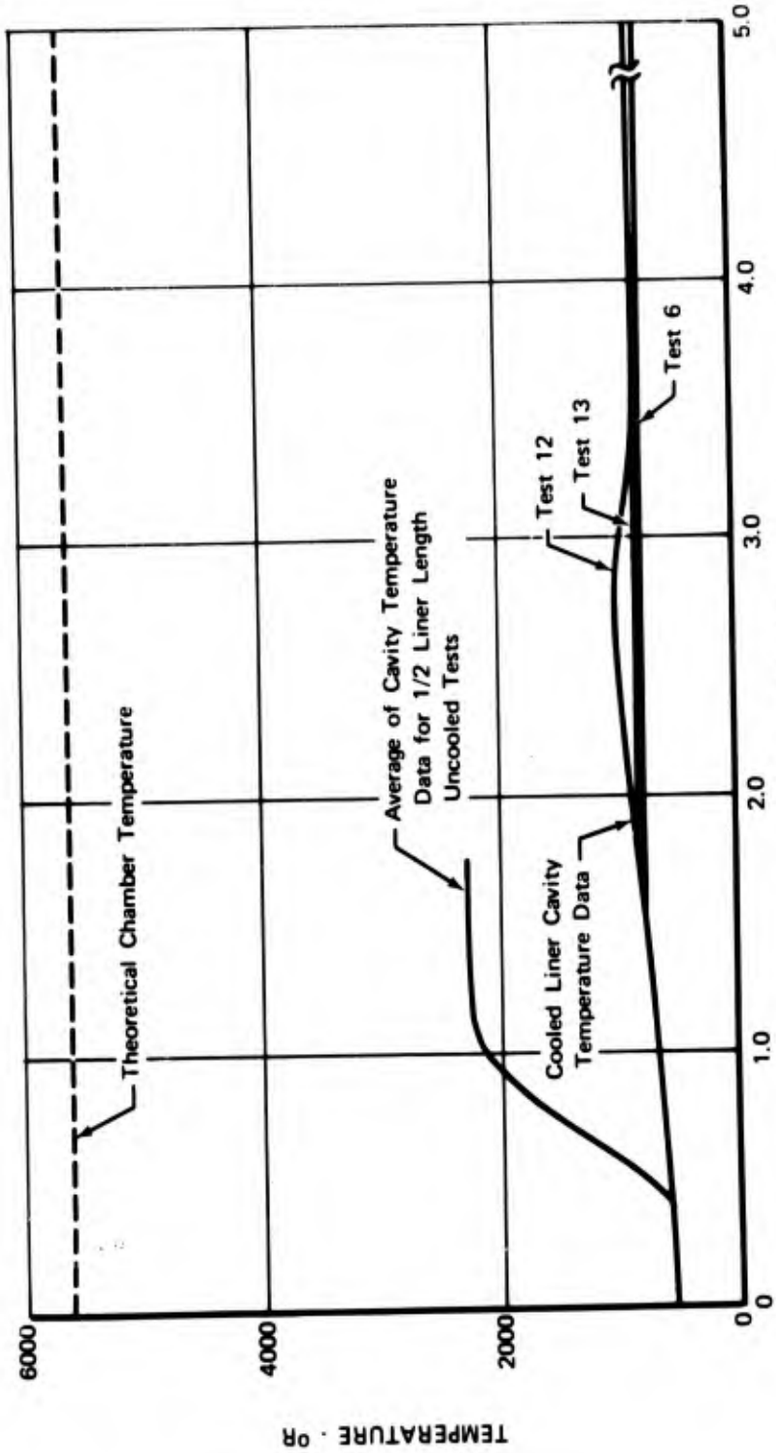

FD 53755

Figure 49. Comparison of Cooled and Uncooled Liner Cavity Temperature Data

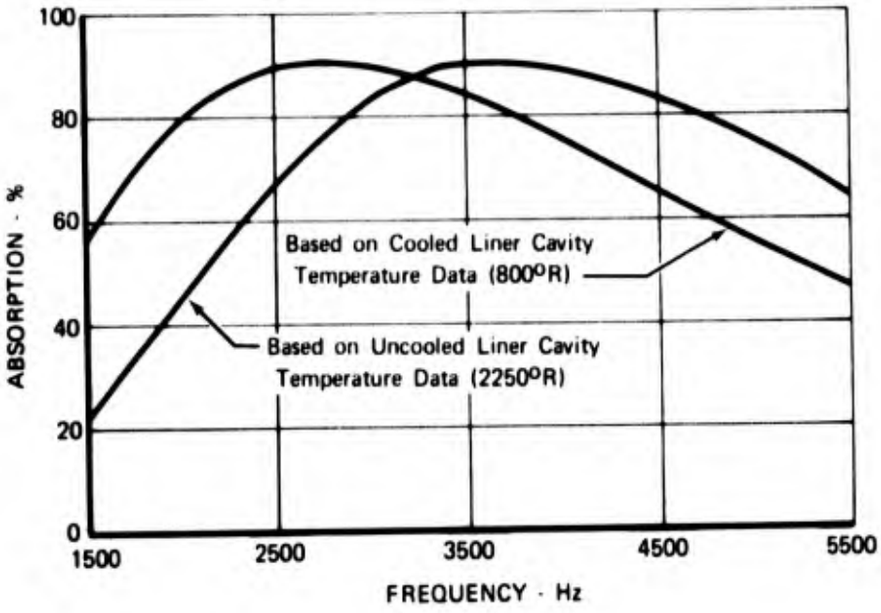

Figure 50. Comparison of Cooled and Uncooled Liner Theoretical Absorption Characteristics FD 53756

5. Conclusions

The results of the cooled chamber tests showed that (1) the performance of the motor was not adversely affected by the addition of the acoustic liner, (2) the acoustic liner dynamically stabilized combustion following overpressures of up to 83% of chamber pressure, and that (3) the acoustic liner chamber cooling scheme demonstrated durability. It was therefore recommended that regeneratively cooled acoustic liners be considered as a feasible solution to flightweight motor combustion instability problems.

This page intentionally left blank

SECTION III
PHASE II - HIGH CHAMBER VELOCITY ANALYSIS

A. BACKGROUND

The effectiveness of liners for suppressing combustion instability can be correlated with the absorption coefficient, defined as the fraction of incident wave energy (sound energy) that is dissipated by the device. Theoretically, the absorption coefficient, α, is computed from:

$$\alpha = 1 - \left(\frac{Z - 1}{Z + 1}\right)^2 \tag{1}$$

where Z is the specific acoustic impedance of the liner. The impedance has a real part, resistance, and an imaginary component, reactance. The resistance, analogous to friction in a mechanical system, directly opposes the wave motion, thereby dissipating energy from the wave. The reactance is a measure of the inertia and compressibility of the gas in the liner apertures and cavity, respectively. The magnitude of the components (resistance and ractance) are functions of the liner geometry, the media properties and flow fields, and the frequency and amplitude of the pressure oscillations. For any frequency, the absorption coefficient can be expressed in terms of the specific resistance ratio and specific reactance ratio, as

$$\alpha = \frac{4\theta}{(\theta + 1)^2 + \chi^2} \tag{2}$$

where the specific reactance ratio is computed from

$$\chi = \frac{2\pi f_o \ell_{eff}}{12 c \sigma} (f/f_o - f_o/f). \tag{3}$$

In the above equation, the frequency at which the term in parenthesis becomes zero (thus causing the reactance to vanish) is defined as the resonant frequency, f_o; it is computed from

$$f_o = \frac{c}{2\pi} \sqrt{\frac{144\sigma}{L \ell_{eff}}} \tag{4}$$

where L is the backing cavity depth and ℓ_{eff} is the effective aperture length.

Many complex factors affect the application of the above theory to the design of rocket chamber absorbers. The high gas temperatures, complex and high velocity flow situations, high pressure amplitudes, and other related effects impose serious limitations and uncertainties on the design techniques.

Since 1963, a systematic approach to the solution of these problems has been underway. The effects of each of the above factors on liner impedance have been quantitatively described and corroborated through cold flow experiments using ambient air, gaseous helium and nitrogen as test media, (References 1, 12, 13, 14 and 15). Unfortunately, extrapolation of the liner design theory, based on the results of cold flow experiments to hot firing conditions,

also can introduce significant uncertainties, primarily because the rocket chamber environment can only be simulated in cold flow experiments. In the past, it has been necessary to assume that the results from the cold flow experiments would be applicable, because no reliable experimental techniques for making similar measurements during firings were known. Therefore, a new impedance-measuring technique was recently developed (Reference 13) for use during actual rocket firings, and using a motor with low chamber gas velocities, carefully controlled hot-firing experiments were conducted (Reference 14). From analysis of the acoustic data obtained it was found that:

1. The steady-state flow coefficient (or discharge coefficient) of the liner apertures has a significant effect on impedance.

2. The specific acoustic resistance and effective aperture length with zero net parallel flow, i.e., with no flow past the liner apertures, are best computed from

$$\theta = 0.37\, u/c\sigma C_f^2 \tag{5}$$

and

$$\ell_{eff} = t + 0.7d \tag{6}$$

where the amplitude of oscillations in the apertures, u, (or particle velocity) is found by solving

$$u^4 + (2.7\sigma\ cC_f^2\ ux)^2 = \left(\frac{P_1 C_f^2 g}{0.37\rho}\right)^2 \tag{7}$$

In equation (7), P_1, the pressure amplitude at the liner facing (in units of lb_f/ft^2), is the highest amplitude permitted for combustion to be considered stable, e.g., 5% of chamber pressure.

Experiments with simultaneous flow through and past the resonator apertures (Reference 15) revealed that the past-flow had no effect on the acoustics of the liner if the Mach number of the through-flow was greater than 0.1. Other results from experiments with through-flow were (Reference 13) the effective length and particle velocity can be computed from equations (6) and (7) and resistance from

$$\theta_t = \frac{M_t}{\sigma C_f^3} \quad \text{if } M_t > u/2c \tag{8}$$

If $M_t \leq u/2c$ the effects of through-flow on absorption were negligible.

Attempts to determine the effects of parallel flows on impedance were also made (references 12 and 13.) Cold flow experiments were conducted with net velocities of up to 600 ft/sec; however, the results from the two series of experiments were inconsistent and, in addition, because of the limited range of velocities the results had to be extrapolated for most rocket chamber applications.

B. PHASE II PROGRAM RESULTS

The objective of work under Phase II was to overcome the uncertainties in the present design theory imposed by the lack of suitable functional relationships describing the effects of high-velocity parallel flows on rocket liner impedance. To obtain the necessary acoustic data, both cold flow experiments and firings of a dynamically unstable rocket motor were conducted. The cold flow experiments were conducted with net velocities of up to 1681 ft/sec; the rocket motor, which contained small sections of liner arrays instrumented to measure the impedance and the gas properties in the liner apertures and cavity, could be fired with different nozzles to vary the net velocity past the liners.

Conclusions from the results of the parallel flow experiments are:

1. Effective aperture length with flow past the apertures is best described by

$$\ell_{eff} = t + 0.375\,[0.85d\,(1-0.7\sqrt{\sigma})] \tag{9}$$

This value should then be used in the equations for zero net flow to compute the liner resonant frequency, reactance, and particle velocity, u.

2. Liner resistance, for values of the flow parameter,

$$\frac{V_p\left(\frac{\rho_a}{\rho_c}\right)^{3/2}}{u} \geq 1.5 \tag{10}$$

where V_p is the parallel net flow velocity and ρ_c is the density of the combustion chamber gas, should be calculated using

$$\theta_p = \frac{0.123}{\sigma c\, C_f^2}\left[V_p\left(\frac{\rho_a}{\rho_c}\right)^{3/2} + 1.5\,u\right] \tag{11}$$

For other values of the flow parameter, equation (10), the resistance is computed from equation (5). These equations, with the previously discussed theory, were used as the basis for a new liner design computer program, which is included herein as Appendix III. The program was then used to design two different types of resonant absorbing liners for the spontaneously unstable 5000 lb_f motor, which had been used extensively under both phases of the previous program (References 1 and 2). An existing nozzle for the motor was modified to produce a chamber contraction ratio of 1.82, which gave a mean gas velocity of 1250 ft/sec past the liners.

Five firings of the 5000 lb_f motor were conducted. With no absorption, combustion was extremely unstable with peak-to-peak amplitudes at 3300 Hz (2T mode) in excess of 60% of chamber pressure, which was nominally 100 psia. Results with both absorbing liners were similar; the high-amplitude 2T mode was suppressed to less than 10% of chamber pressure, but, amplitudes in excess of 10% occurred at frequencies greater than 6400 Hz even though both liners theoretically had enough absorption to suppress the high-frequency modes.

It is not known why the liners failed to stabilize combustion at all frequencies. Because identical results had been obtained in the previous programs with several different liners, all tested with the same 5000 lb_f motor with lower chamber gas velocities, it was concluded that the failures were not caused by the high velocities used in the latter program. To compute the theoretical absorption at frequencies greater than 3300 Hz, extrapolations of the theory were necessary. It is therefore postulated that, because of these extrapolations, the actual absorption was not as great as indicated. To overcome the uncertainty additional firings of the 5000 lb_f motor with liner elements instrumented for impedance measurements are recommended. A description of all work performed under this phase of the program follows.

C. COLD-FLOW ACOUSTIC EXPERIMENTS

1. Apparatus

The cold flow apparatus shown in figure 51 was used for the acoustic experiments. Three Ling EPT-94B air-modulated acoustic transducers were used to produce pressure amplitudes in excess of 170 db at frequencies to 1200 Hz in gaseous nitrogen and 3300 Hz in a gaseous helium environment. The system was theoretically capable of producing net flow velocities past the liner test section of 850 ft/sec (M = 0.73) in a gaseous nitrogen environment and velocities up to 2200 ft/sec (M = 0.67) in a gaseous helium environment.

The operation of the apparatus was as follows: sound waves, along with a metered supply of gaseous nitrogen (or helium), enter the tube section parallel to the perforated face of the test section and exit through a gap between the reflection plate and the end of the tube extension. A pitot tube located just upstream of the test section was used to determine the velocity profile approaching the liner test section. The sound waves moving down the tube are reflected at the end plate and a standing wave is produced.

The absorption characteristics of the test section are then determined from measurements of the sound pressures in the tube at the face of the liner and in the resonator cavity. The sound pressure data were recorded using two Atlantic Research pressure transducers. The output from each transducer was fed through a wave analyzer containing a millivolt meter from which the pressure amplitudes were read and manually recorded. The outputs of both transducers were also connected to a dual-channel synchronous filter and a digital phase meter to determine the phase difference between the incident (facing) and transmitted (cavity) sound waves. The transducers were calibrated by charting their millivolt output as a function of sound pressure level using as the reference a condenser microphone previously calibrated with a pistonphone.

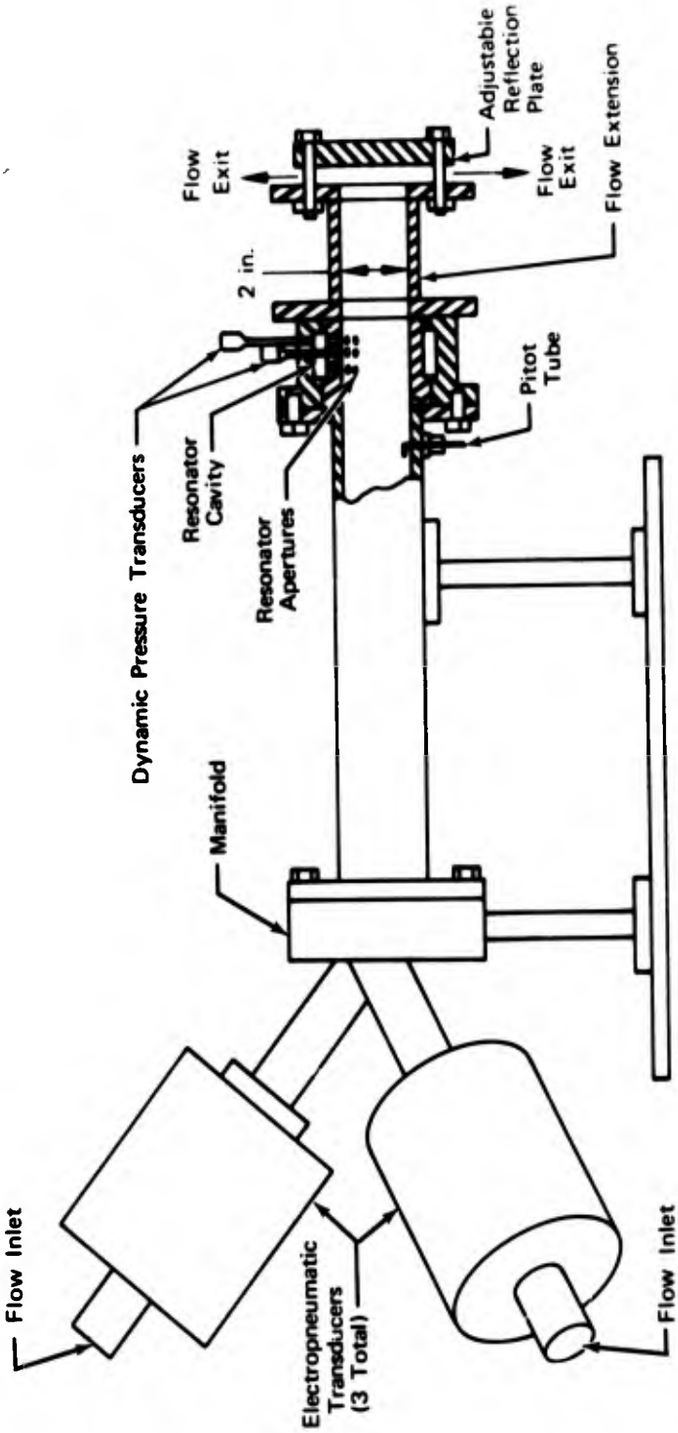

FD 53757

Figure 51. Cold Flow Apparatus

2. Test Program

The first attempts to conduct experiments with net flow velocities above 300 ft/sec and with sound pressure levels above 170 db were considered unsuccessful because of considerable inconsistency in the acoustic data obtained. An investigation was conducted and several ways to improve the data precision were discovered.

First, to vary the flow velocity past the sample, the flow exit gap at the reflection plate was varied from 0.10 to 0.75 in. It was found that changing the position of the reflection plate could cause severe acoustic pressure gradients across the sample, especially at higher frequencies. Changes in the pressure gradient across the sample produced differences in the cavity pressure reading and in the phase angle, thus causing inconsistencies in the data. The effect was reduced by testing at reflection plate distances that kept the pressure gradient at a minimum for each frequency and gas medium.

Second, the three acoustic transducers were positioned in a horn manifold to permit the flow to enter the tube in a symmetric pattern; however, for some tests the acoustic power from only one or two of the drivers was necessary. It was believed that this method of testing could have caused unsteady flow patterns in the tube, thus causing inconsistent data to be obtained. To reduce this possibility, all three transducers were used as the sound source in all further testing.

Finally, subsequent checkout testing indicated that data consistency was further improved by the addition of a gasket sealer around the dynamic pressure probes and around the outer edge of the backing cavity plate. The sealer prevented flow through the liner sample that resulted from increased pressure in the impedance tube at the higher new flow velocities.

Tests were then conducted with net flow velocity of up to 681 ft/sec (Mach number = 0.59) with nitrogen and with net flow velocity of up to 1681 ft/sec (Mach number = 0.51) with helium. The liner test section had a 0.3 in. thick facing, a 0.009-in. aperture diameter, an open area ratio of 0.027 and a backing cavity depth of 0.51 in. Data, used in the analysis of the effects of flow past the apertures (Section III-E), were obtained from 65 nitrogen experiments with a frequency of 1100 Hz and from 25 helium experiments with frequencies of 2500 and 3300 Hz, both conducted at sound pressure levels of 150 to 160 db, and from an additional five experiments, conducted with sound pressure levels varying from 152 to 176 db, at 1100 Hz, in a nitrogen medium.

To determine the impedance and other acoustical characteristics, data from each test were input to a digital computer program that used the pressure-phase data reduction equations of Appendix I. A complete list of input and reduced data is included in Appendix II.

D. HIGH VELOCITY UNCOOLED MOTOR EXPERIMENTS

1. Hardware

The uncooled motor used for the high chamber velocity firings is shown in figure 52. The uncooled motor consisted of a modified Agena S/N 7 injector,

the uncooled Phase I thrust chamber with inspection ports (Section II-C), two liners containing the test samples, a solid liner, and two exhaust nozzles.

The S/N 7 injector modifications involved trimming excess material that remained after separation from a thrust chamber and removal of weld buildup to match the chamber, the Phase I oxidizer manifold, and injector retaining ring. After machining, the injector was water-flowed. The results of the water-flow tests indicated that only slightly higher injector differential pressures would be required for the S/N 7 injector than for the S/N 9 injector used for the Phase I hot firings. Visual inspection of the water-flow tests revealed that the injection pattern was regular and that there would be negligible propellant impingement on the chamber wall.

The two exhaust nozzles were fabricated to produce mean chamber Mach numbers of 0.36 and 0.60 (table XI). Each liner design incorporated three small aperture arrays compartmented in the backing cavity so that data could be obtained from three different acoustic test sections simultaneously. Open area ratios of 2.5, 4.5, and 6.0% were used on one liner, which was fabricated from a Phase I solid liner of 0.200 in. thickness and 0.600 in. backing distance. The other three-element liner was fabricated with a facing thickness of 0.30 in.; a 0.50 in. backing cavity depth; and open area ratios of 2.5, 6.0, and 8.0%. For each aperture array the backing cavity was partitioned to produce the desired resonator volume. Figure 53 is a sketch of a typical liner test element. The chamber inspection cover plates were modified as mounts for the two Kistler pressure transducers that were used to measure the dynamic pressures at the liner element face and in the resonator cavity.

2. Test Program

The test program included tests of six different rig configurations, i.e., all combinations of three liners with two nozzles. The tests were organized in three series, one for each liner, and each series included tests with both nozzles.

The high velocity motor tests are summarized in table XII. The first two tests used the high velocity nozzle. For test 1, no pulse guns were used; combustion was stable for the full scheduled duration of 1.8 sec. For test 2, 25-grain pulse guns were mounted at both the tangential and radial locations; the tangential gun was set to fire at +0.7 sec and the radial at +1.2 sec. Combustion was stable until the first gun fired, causing instability that remained until the motor was shut down at +0.83 sec by the rough combustion cutoff (RCC) abort system.

Tests 3 and 4 were with the low velocity nozzle. No guns were used for test 3, and combustion was stable for the scheduled duration of 1.8 sec. For test 4, two 25-grain pulse guns were mounted with the locations and timing identical to that for test 2. Combustion was stable until the first (tangential) gun fired; however, the motor was not shut down because the resulting pressure amplitudes were not high enough to trigger the RCC system, which was set at 25 psi P/P. The motor was shut down by the RCC after the radial run fired.

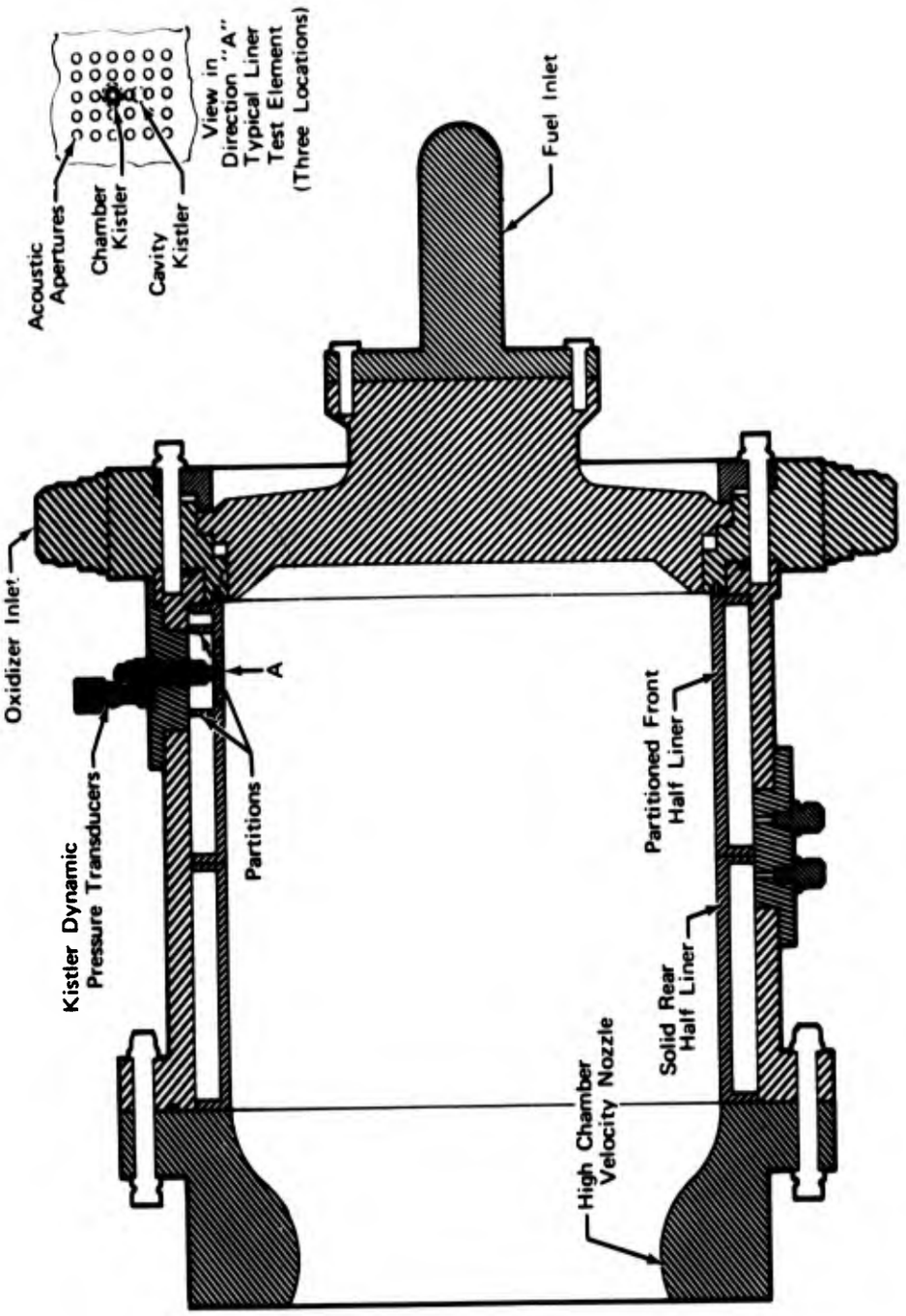

FD 53758

Figure 52. High Velocity Uncooled Test Motor

Table XI. High Velocity Chamber Characteristics
(Based on C^* = 100%)

	Low Velocity Nozzle	High Velocity Nozzle
Chamber Gas Mach number	0.36	0.60
Chamber Gas Velocity, ft/sec	1415	2345
Chamber Pressure, psia	180	122
Chamber Gas Temperature, °R	5745	5675
Propellant Flowrate, lb_m/sec	53.7	53.7
Mixture Ratio	2.0	2.0
Thrust, lb_f	11,000	10,600
Chamber Diameter, in.	10.8	10.8
Contraction Ratio	1.765	1.2
Throat Diameter, in.	8.12	9.84
Expansion Ratio	1.14	1.14
Exit Diameter, in.	8.67	10.5

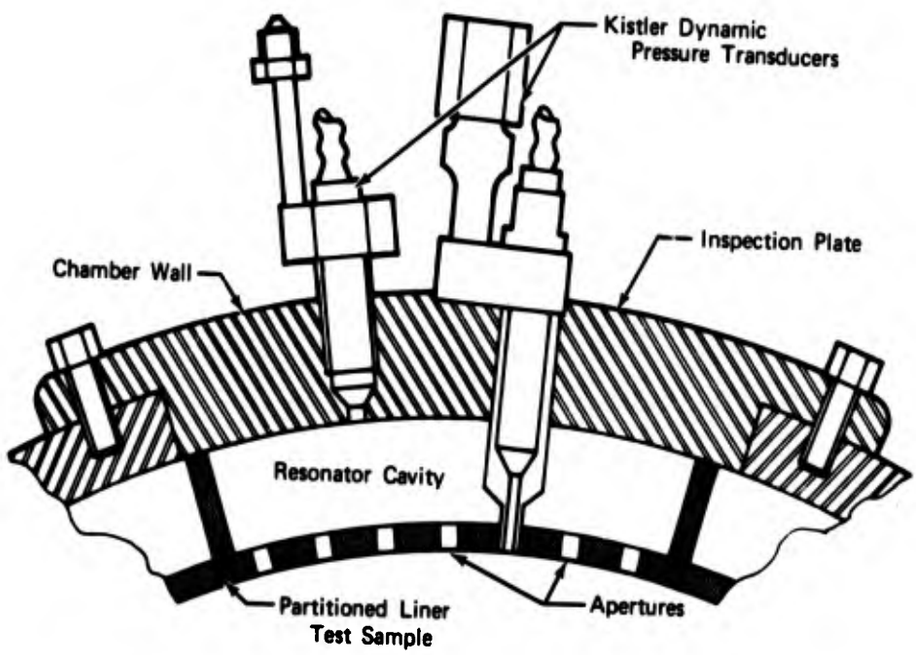

Figure 53. High Velocity Liner Test Element FD 53759

Table XII. Phase II - High Chamber Velocity Uncooled Motor Test Summary

Test No.	Duration, sec	Chamber Pressure, psia	Pulse Gun(s)	Mixture Ratio	c* Efficiency % (1)	Comments
1	1.80	128	None	2.02	99.0	Stable (Solid Liner, M = 0.6 Nozzle)
2	0.83	117	Tangential at +0.7 sec (25-grain)	1.92	96.8	RCC Abort (Solid Liner, M = 0.6 Nozzle)
3	1.80	180	None	2.00	98.6	Stable (Solid Liner, M = 0.36 Nozzle)
4	1.67	171	Tangential at +0.7 sec, Radial at +1.2 sec (25-grain each)	1.99	94.2	RCC Abort (Solid Liner, M = 0.36 Nozzle)
5	0.88	163	Tangential at +0.7 sec (25-grain)	1.98	92.8	RCC Abort (No. 1* Liner, M = 0.36 Nozzle)
6	1.80	128	Radial at +0.7 sec, Tangential at +1.2 sec (25-grain each)	2.01	99.0	Stable (No. 1* Liner, M = 0.6 Nozzle)
7	1.34	128	Tangential at +1.2 sec (50-grain)	1.99	95.4	RCC Abort (No. 1* Liner, M = 0.6 Nozzle)
8	1.80	126	Radial at +0.7 sec (25-grain) Tangential at +1.2 sec (50-grain)	2.00	99.0	Stable (No. 1* Liner, M = 0.6 Nozzle)
9	0.93	166	Radial at +0.7 sec (25-grain)	1.95	92.0	RCC Abort (No. 2** Liner, M = 0.36 Nozzle)
10	0.85	118	Radial at +0.7 sec (25-grain)	1.91	96.7	RCC Abort (No. 2** Liner, M = 0.6 Nozzle)
11	1.43	178	Radial at +0.7 sec (25-grain) Tangential at +1.2 sec (50-grain)	1.99	98.9	RCC Abort No. 2** Liner, M = 0.36 Nozzle)

*No. 1 Liner - Thickness = 2.00 inch, Backing Depth = .600 inch, Open Area Ratios 2.5, 4.5, and 6.0%.

*No. 2 Liner - Thickness = .300 inch, Backing Depth = .500 inch, Open Area Ratios 2.5, 5.0, and 8.0%.

(1) Uncorrected, based on chamber pressure.

For tests 5 through 7, the liner with open area ratios of 2.5, 4.5, and 6.0% was used. Test 5, using the low velocity nozzle, was stable until the firing of the 25-grain tangential gun at +0.7 sec. Combustion was then unstable; shutdown by the RCC occurred at +0.88. Test 6, using the other nozzle, was stable throughout the full scheduled duration of 1.8 sec even though two 25-grain pulse guns were fired. Test 7, using the same nozzle, was stable until driven unstable by a 50-grain tangential gun at +1.2 sec.

For tests 8 through 11, the liner with open area ratios of 2.5, 5.0, and 8.0% was used. Tests 8 and 10 used the high-velocity nozzle. Test 8 was stable throughout the scheduled duration of 1.8 sec despite the firing of one 25-grain pulse gun. Test 9 was stable until the 25-grain radial pulse gun fired at +0.7 sec; it was then unstable until RCC shutdown at +0.93 sec. Usable data were obtained from only one of the three liner test elements used for the test because of pressure transducer malfunctions. Test 10 was driven unstable by a 25-grain radial gun at +0.7 sec; shutdown occurred at +0.85 sec. Because insufficient data were obtained from test 9, test 11 was programed identical to 9 with a 25-grain radial pulse gun set to fire at +0.7 sec and a 50-grain tangential gun set for +1.2 sec. The firing of the 25-grain charge failed to cause combustion to be unstable, but it was driven unstable by the second gun and continued so until shutdown at +1.34 sec by the RCC.

Chamber wall static pressure and injector face total pressure data showed that the local velocity past the liner test elements, which were located 2.3 in. downstream of the injector face, was lower than the design Mach number. The velocities measured were 950 ft/sec (M = 0.25) for the tests with the M = 0.36 nozzle, and 1450 ft/sec (M = 0.38) for the tests using the M = 0.6 nozzle. The chamber Mach number increased with increasing distance from the injector until the design Mach number was obtained at approximately 7 in. from the injector face with both nozzles.

3. Pressure-Phase Data Reduction

Pressure-phase data were obtained from high-speed oscillograph traces of the Kistler transducer signals, which were recorded on magnetic tape. Before the oscillograph traces were made, a spectrum analysis of the dynamic pressure data was conducted. The analysis was used to determine the frequency of pressure oscillations above the random noise level, i.e., approximately 1 psi. To eliminate all but the high-amplitude signals the data were filtered using a tracking generator, leaving a small frequency band about the desired frequency.

The high-speed oscillograph traces were made by running the oscillograph paper at approximately 160 in./sec while the data originally recorded on magnetic tape at 30 in./sec was played back at 1.9 in./sec. By playing the data back at the reduced speed a higher resolution of the data was obtained, enabling a more accurate measurement of the phase angle to be made. All channels in the oscillograph were ac coupled to eliminate the dc drift that is caused by variations in chamber pressure (primarily a result of the shock wave produced when the pulse gun was fired).

The phase angle and pressure amplitudes were manually read from the oscillograph traces. The phase angle between two pressure traces was determined by locating the zero point of each pressure wave (as shown in figure 54), and by measuring the relative displacement between them. The phase angle was calculated from the relationship:

$$\frac{\text{Phase Angle}}{\text{Relative Displacement Between Zero Points}} = \frac{360 \text{ deg}}{\text{Wave Length}}$$

The calibration of the phase measuring system was performed prior to and after testing. Calibration involved the measurement of the system induced

phase shift (baseline phase shift) between each of the two data recording channels used to monitor the dynamic pressures in the combustion chamber and in the cavity behind the liner. If the baseline phase shift was not determined it could add to the phase angle being measured, introducing an error of unknown magnitude.

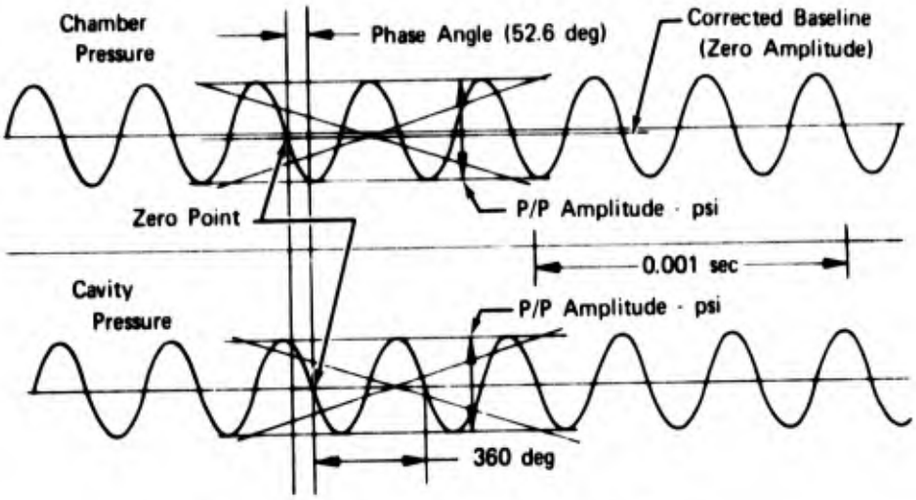

Portion of Oscillograph Trace for Hot Fire Test No. 15.01
α = 8.0% L = 0.6385 in.

Figure 54. Method of Pressure Phase Data Reduction FD 37874A

A special high-frequency, high-sound-level generating unit (see figure 55) was used for calibrating the phase-measuring system. The calibration apparatus consists of four sound drivers interconnected by a manifold and exiting into a closed-end tube. With this device sound pressure levels of 175 db can be generated up to a frequency of 3000 Hz or 160 db to a frequency of 6000 Hz. The closed end is formed by a special end plate in which the two dynamic pressure transducers being calibrated and a 1/4-in. microphone were mounted so that all three simultaneously monitored the standing wave pressure oscillations at the end of the tube. The passages leading from the end of the transducers were the same length and were identical to those used in the liner test sections. To supply data for determining the baseline phase shift between two channels, both pressure transducers were mounted in the end plate of the phase-calibrating apparatus and connected to the test stand recording system, with the same cables used for the particular transducers for actual testing.

A signal of known frequency was generated in the tube by the four sound drivers and the amplitude was monitored with the 1/4-in. microphone. The entrances to both pressure transducer passages were in the end of the tube; therefore, a known phase angle of zero deg was generated for recording by both pressure transducer channels. Calibration tests for each of the sets of dynamic pressure recording channels were conducted before and after the test series. Each set of channels was calibrated over a range of frequencies from 800 to 6500 Hz, with dynamic pressure amplitudes up to 3-psi peak-to-peak. Comparison of pretest and post-test calibration data indicated that the baseline phase shift was the same before and after the test program.

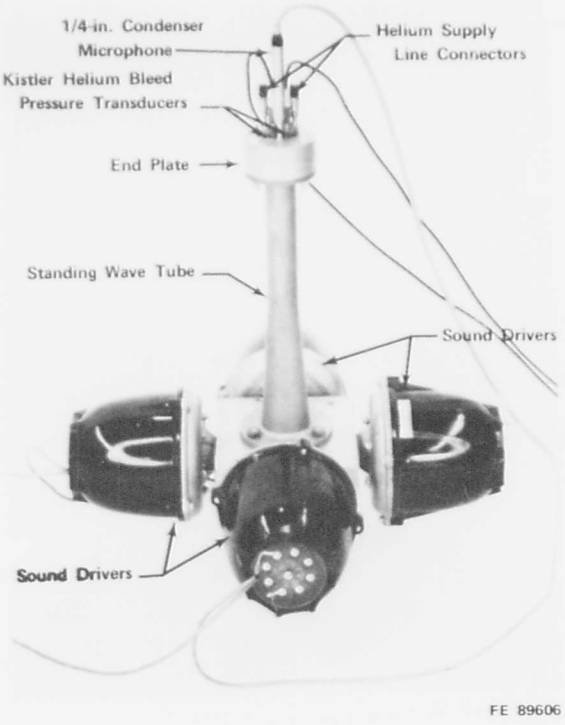

Figure 55. Phase Calibration Apparatus FD 33724

Using the impedance relations of Appendix I the impedance and other acoustic characteristics of each liner test section were computed from pressure-phase data obtained during each unstable firing. The data, and the computed results are listed in Appendix II.

E. ANALYSIS OF ACOUSTIC DATA

To determine the absorption characteristics of the test samples for both the cold flow and high velocity rocket experiments, the impedance relations derived in Appendix I were used to determine the components of impedance, orifice particle velocity, absorption coefficient, and incident sound levels for each data point. The absorption characteristics were then correlated with the theory for no flow to determine the effects of flow on the performance of the liners.

Results of attempts to correlate specific resistance data from cold flow experiments with Mach number are shown in figure 56, the data are represented as the ratio of acoustic resistance with flow past the apertures, θ_p, to that with no flow, θ_n, and correlated with the Mach number of the past flow. From these results it was noted that for a given Mach number increasing the sound level caused the effect of flow on resistance to be less pronounced. Further analysis revealed that below a certain critical Mach number, which appeared to be a function of sound level, the effects of flow on resistance were negligible.

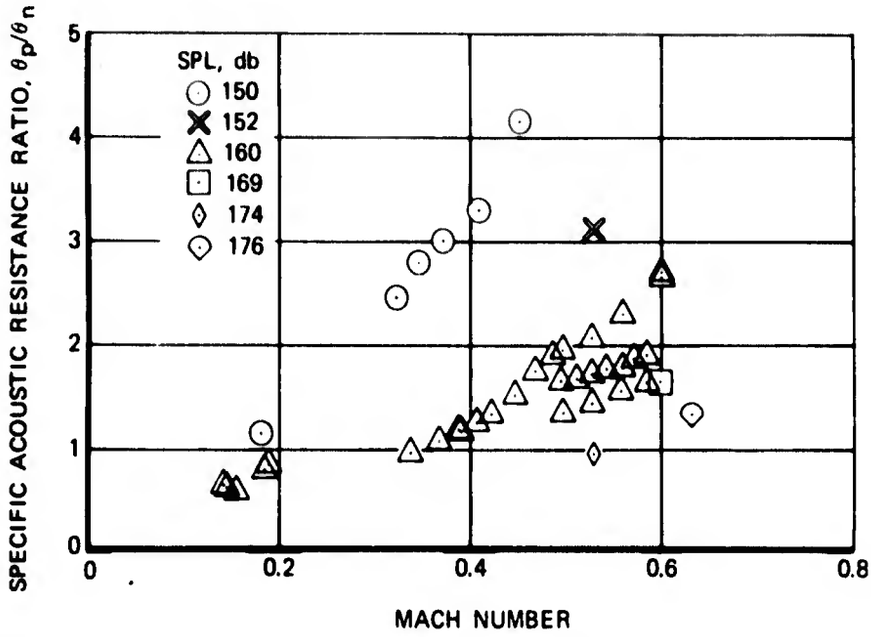

Figure 56. Correlation of Acoustic Resistance Ratio With Mach Number of Net Flow Past Apertures: Data From Cold Flow Experiments With Nitrogen at 1100 Hz FD 53760

Based on the above observations, the following empirical equation was determined from the cold flow data sample:

$$M_C = (0.0035\ SPL)^{0.5} \tag{12}$$

where M_C is the critical Mach number and SPL is the sound pressure level in lb/ft^2.

A similar correlation of the rocket data was attempted. It was found, as shown in figure 57, that for a chamber Mach number of 0.25, the resistance ratio was approximately unity, indicating that the effect of flow at this Mach number was small. For a Mach number of 0.38 at low SPL there was an increase in the resistance ratio over that obtained at M = 0.25, but the apparent effect of velocity decreased as total sound pressure level increases. This trend agreed with the cold flow results; however, quantitatively there was discrepancy. The data of figure 57 indicated that the critical Mach number for the sound pressure levels shown must lie between 0.25 and 0.38, which was lower than the critical Mach number of 0.55 predicted by equation (12).

A second correlation of the rocket data was attempted (figure 58), using the resistance ratio as a function of the flow past velocity divided by the experimental particle velocity in the apertures. The resistance data for both flow velocities follow approximately the same trend with velocity ratio.

An accurate prediction of particle velocity would be necessary if correlations of the above type are to be used in liner design. Therefore, an evaluation was made of the accuracy in predicting particle velocity with flow past the apertures using the present theory. Results are shown in figure 59 where the ratio of experimental particle velocity to theoretical particle velocity with no flow as a function of the ratio of the local velocity past the liner apertures to the experimental particle velocity. Although the experimental and theoretical particle velocities were different, a satisfactory correlation for the particle velocity ratio as a function of the ratio of past flow velocity to particle velocity was obtained. For low past-flow velocity-to-particle velocity ratios the theory was fairly accurate, but for ratios above 0.8, the experimental orifice velocity was only 0.6 times the theoretical.

The results of attempts to improve the correlation of the resistance ratio with past-flow are shown in figures 60 through 63. In the figures, the dependent variable was the ratio of the acoustic resistance with flow to that with no flow; the cold flow results were included as a band because of the large number of data points.

In figure 60 the results of attempts to correlate the resistance data using the flow velocity to particle velocity ratio are shown. The correlation was not satisfactory because of the lack of agreement between the two samples of data, and because all the data points at small values of velocity ratio were less than unity while the slope at higher ratios was too steep for satisfactory agreement with the cold flow data. A comparison of the resistance data using the ratio of past flow Mach number to particle Mach number is shown in figure 61; this correlation was also unsatisfactory for the same reasons.

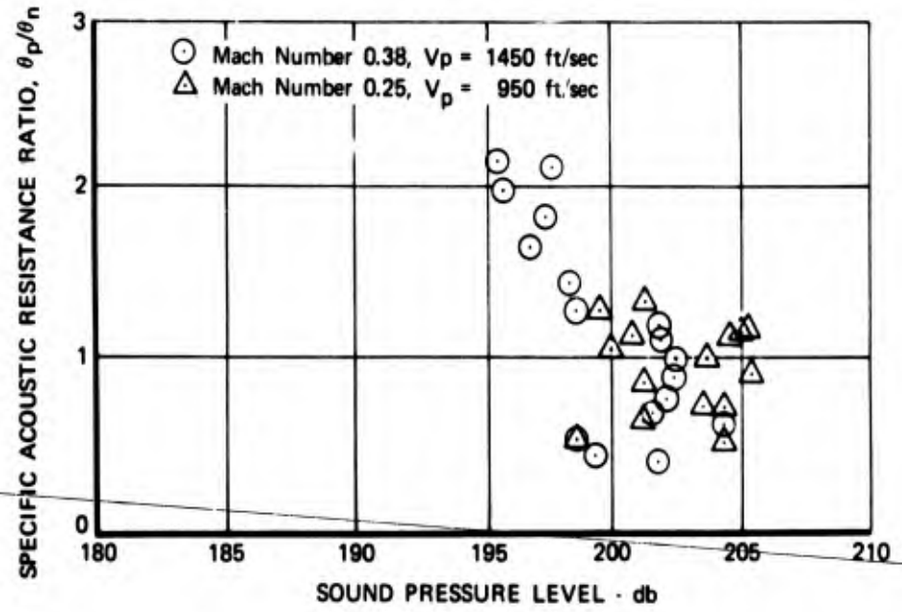

Figure 57. Specific Acoustic Resistance Ratio Data From High Chamber Velocity Test Program FD 53761

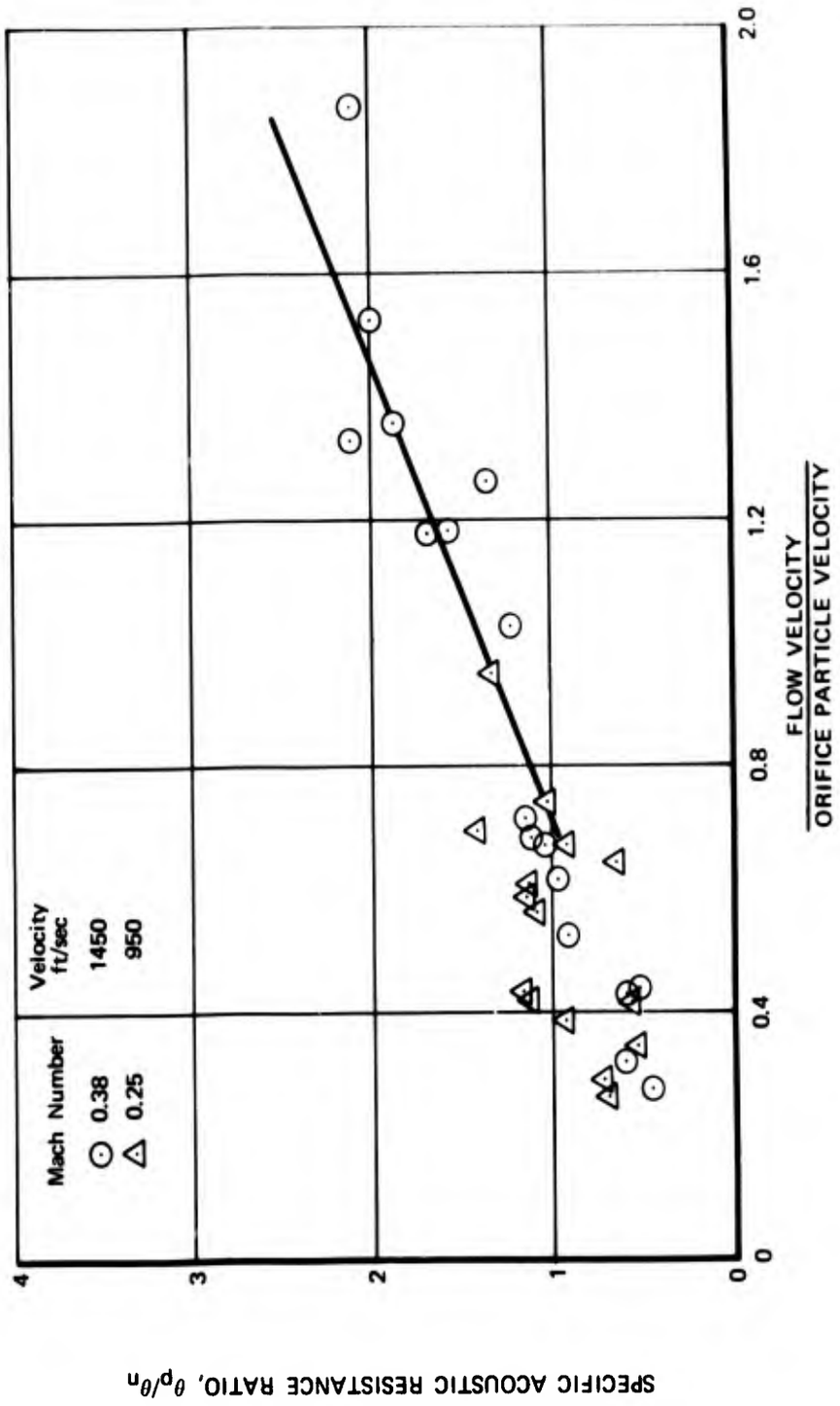

FD 53762

Figure 58. Correlation of Resistance Data From High Chamber Velocity Rocket Tests

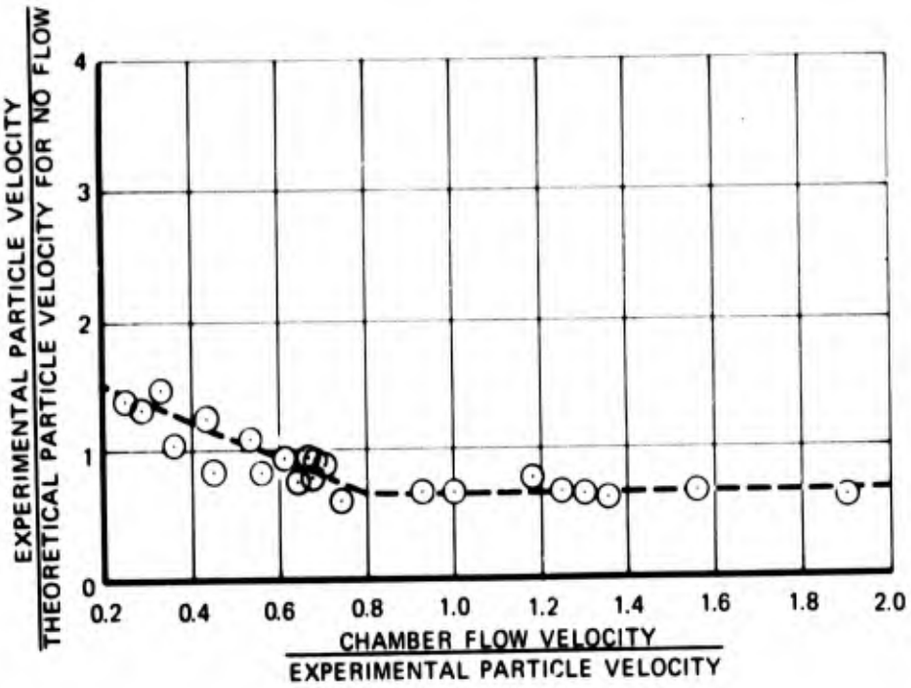

Figure 59. Correlation of Particle Velocity Data From High Chamber Velocity Test Program FD 53763

Further analysis led to the conclusion that the ratio of flow velocity to particle velocity was the best parameter for correlating resistance data from the rocket tests and cold flow experiments, separately; however, an additional parameter was needed to obtain agrerment between both samples of data. The ratio of aperture gas density to chamber gas density was a reasonable choice because the primary difference between rocket and cold flow experiments was in the gas properties; they were uniform for cold flow conditions, but there was an appreciable difference, caused by temperature gradients, between chamber, aperture, and cavity gases in the rocket experiments. The use of the density ratio effectively accounted for this difference and, as shown in figure 62, by including it in the independent variable, agreement between the data samples was considerably improved.

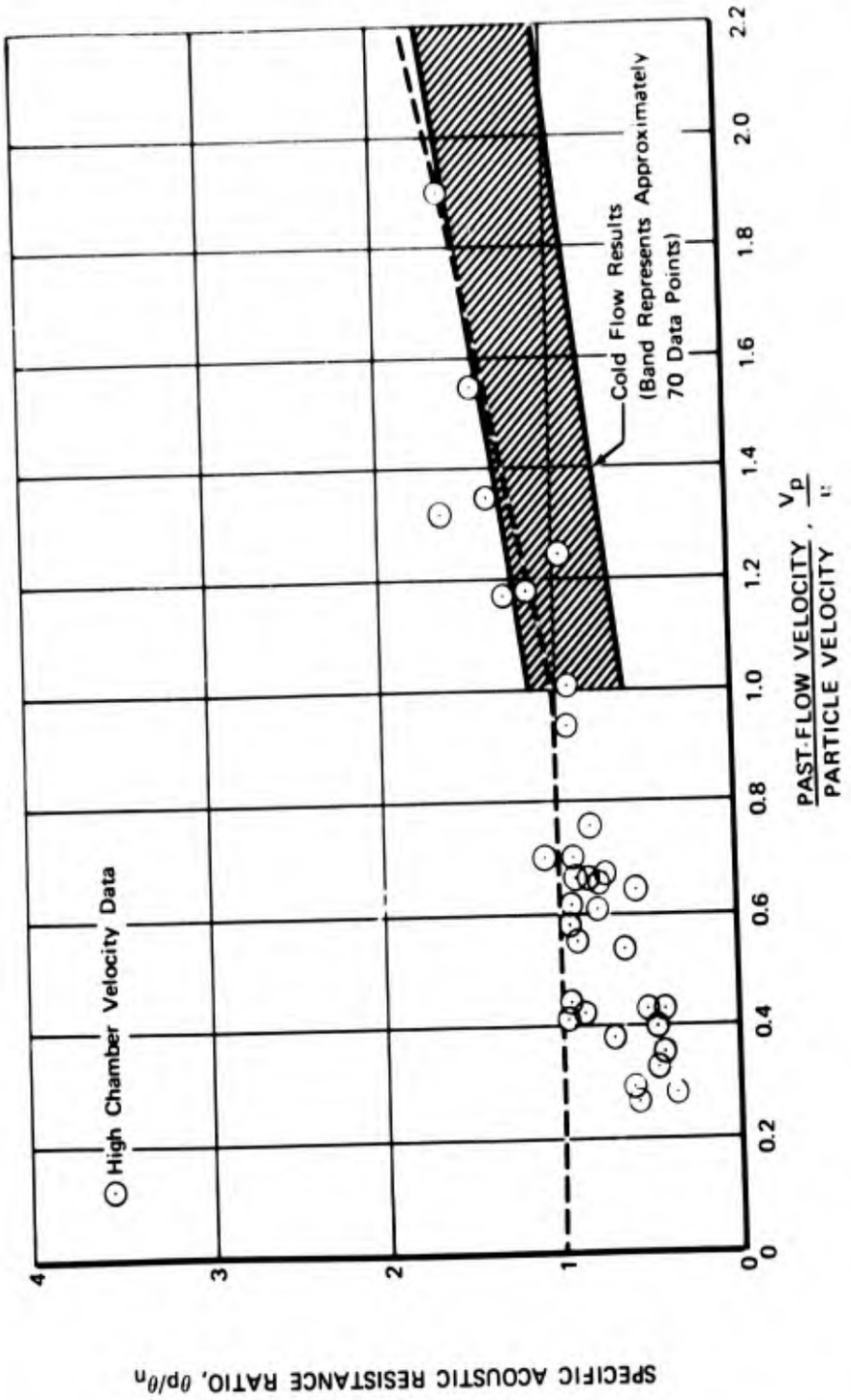

FD 53764

Figure 60. Correlation for Resistance Ratio Using Velocity Ratio

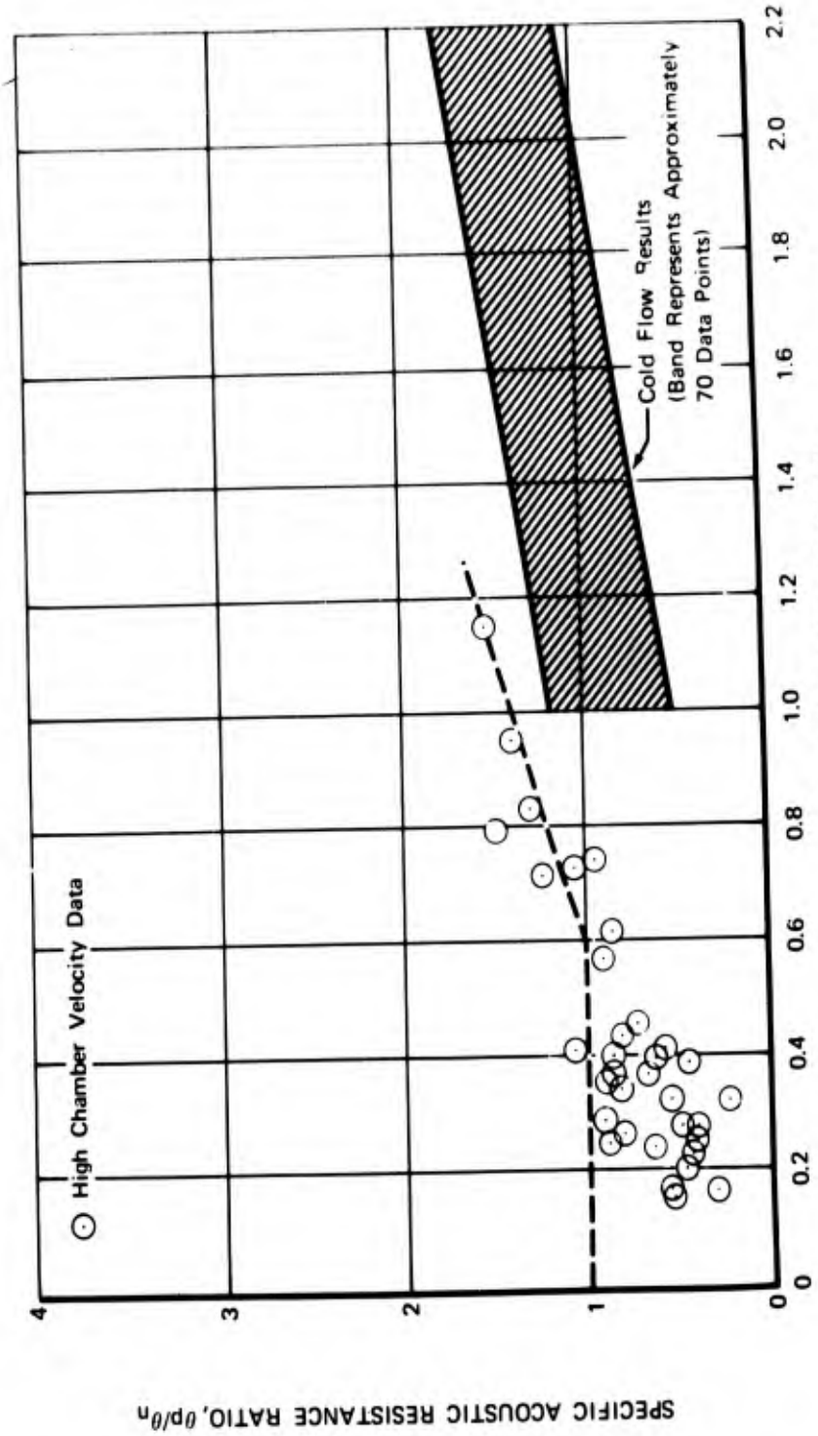

FD 53765

Figure 61. Correlation for Resistance Ratio Using Mach Number Ratio

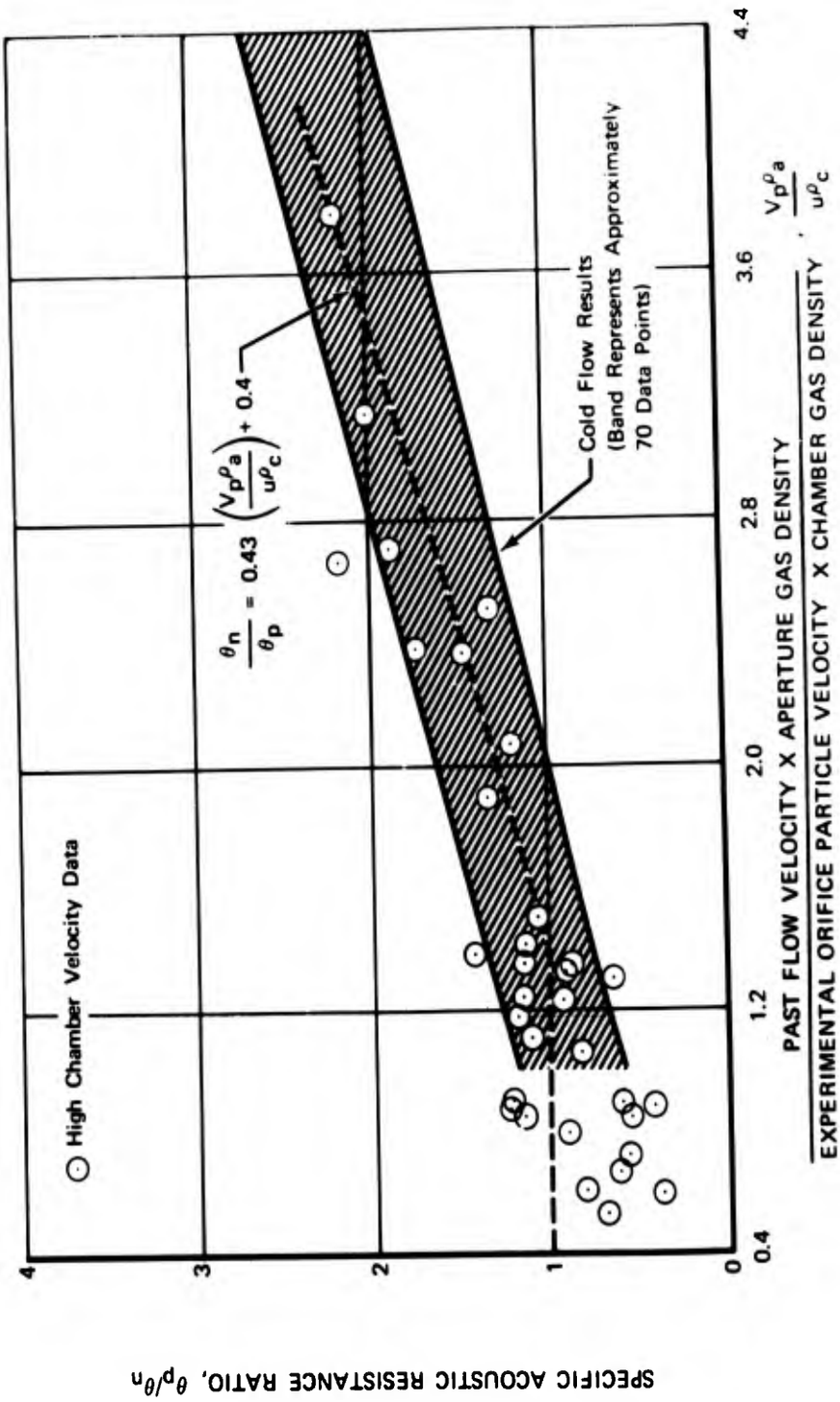

FD 53766

Figure 62. Correlation for Resistance Ratio Using Velocity Ratio and Density Ratio

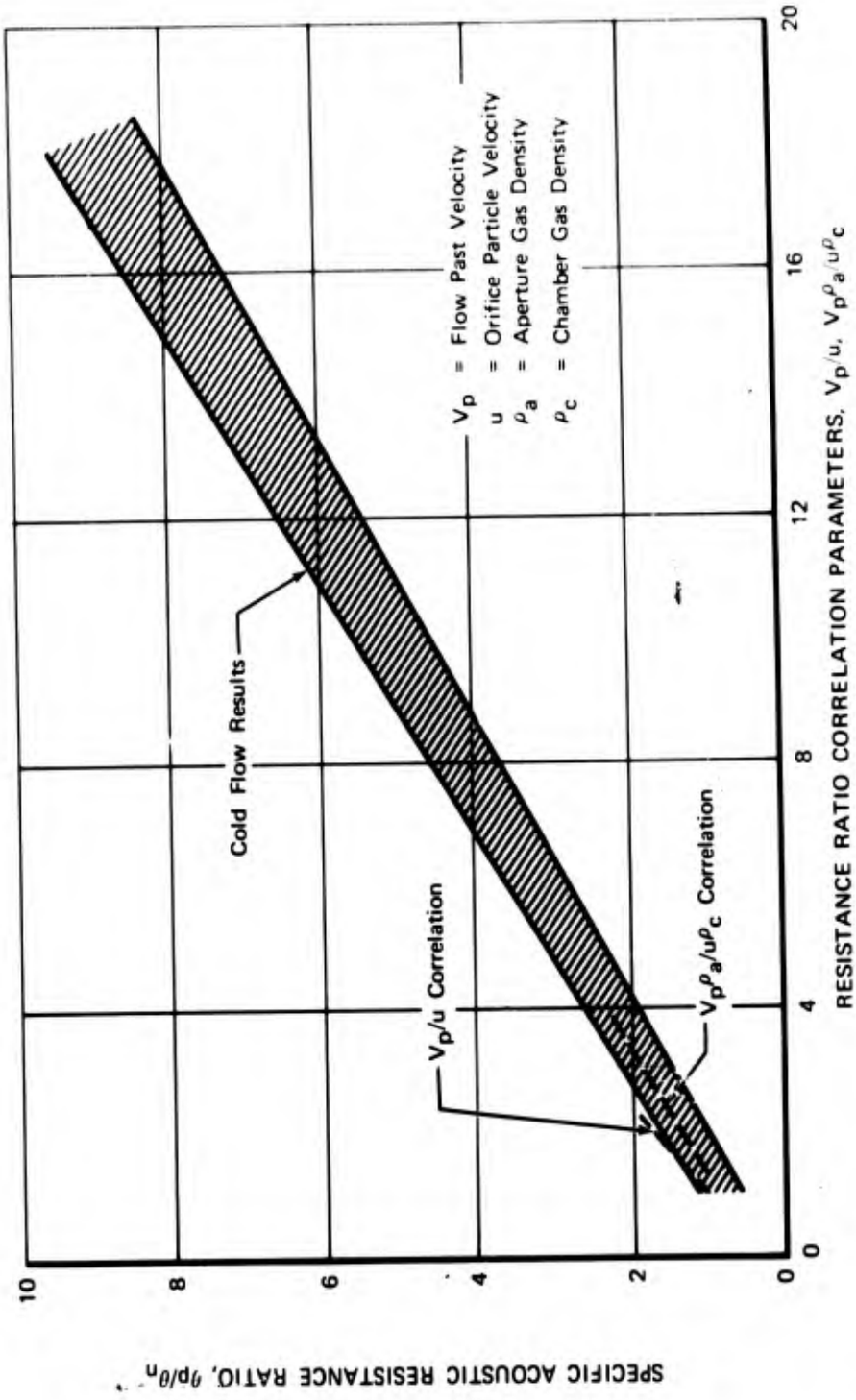

FD 53767

Figure 63. Comparison of Resistance Ratio Correlations

In figure 63 the above correlation and that from figure 60 are shown together for comparison on a plot including the entire range of the cold flow data. It was apparent that the correlation using the density ratio is better; the equation best representing this correlation is

$$\frac{\theta_p}{\theta_n} = 1 \text{ when } \frac{V_p \rho_a}{u \rho_c} \leq 1.0 \tag{13}$$

when

$$\frac{V_p \rho_a}{u \rho_c} > 1.0$$

$$\frac{\theta_p}{\theta_n} = 0.43 \left(\frac{V_p \rho_a}{u \rho_c} \right) + 0.4 \tag{14}$$

Attempts were then made to determine the effects of flow on effective aperture length, liner resonant frequency, and acoustic reactance. Figure 64 shows the ratio of experimental effective aperture length to theoretical vs chamber gas velocity divided by particle velocity. Two equations for the theoretical effective length were used:

$$\ell_{eff_T} = t + \delta \tag{15}$$

and

$$\ell_{eff_T} = t + 0.375\ \delta \tag{16}$$

where

$$\delta = 0.85d\ (1 - \sqrt{0.707\sigma}) \tag{17}$$

Equation (15) is the theoretical effective length with no flow past the apertures and the relationship expressed by (16) and (17) is the Phillips equation (Reference 16) for effective aperture length with flow past the apertures. For the cold-flow results the Phillips equation, as anticipated, represented the data sample better than equation (15). Neither equation was completely satisfactory for use with the high chamber velocity data because of the considerable amount of scatter in the data; however, the Phillips equation represented the results reasonably well.

Figures 65 through 67 show the ratio of experimental to theoretical value for reactance, particle velocity, and liner resonant frequency as functions of the ratio of chamber gas velocity to particle velocity. Both equation (15) and the Phillips equation were used to compute the theoretical values of effective length. In each instance it was found that the Phillips equation produced better agreement between the theory and experimental data.

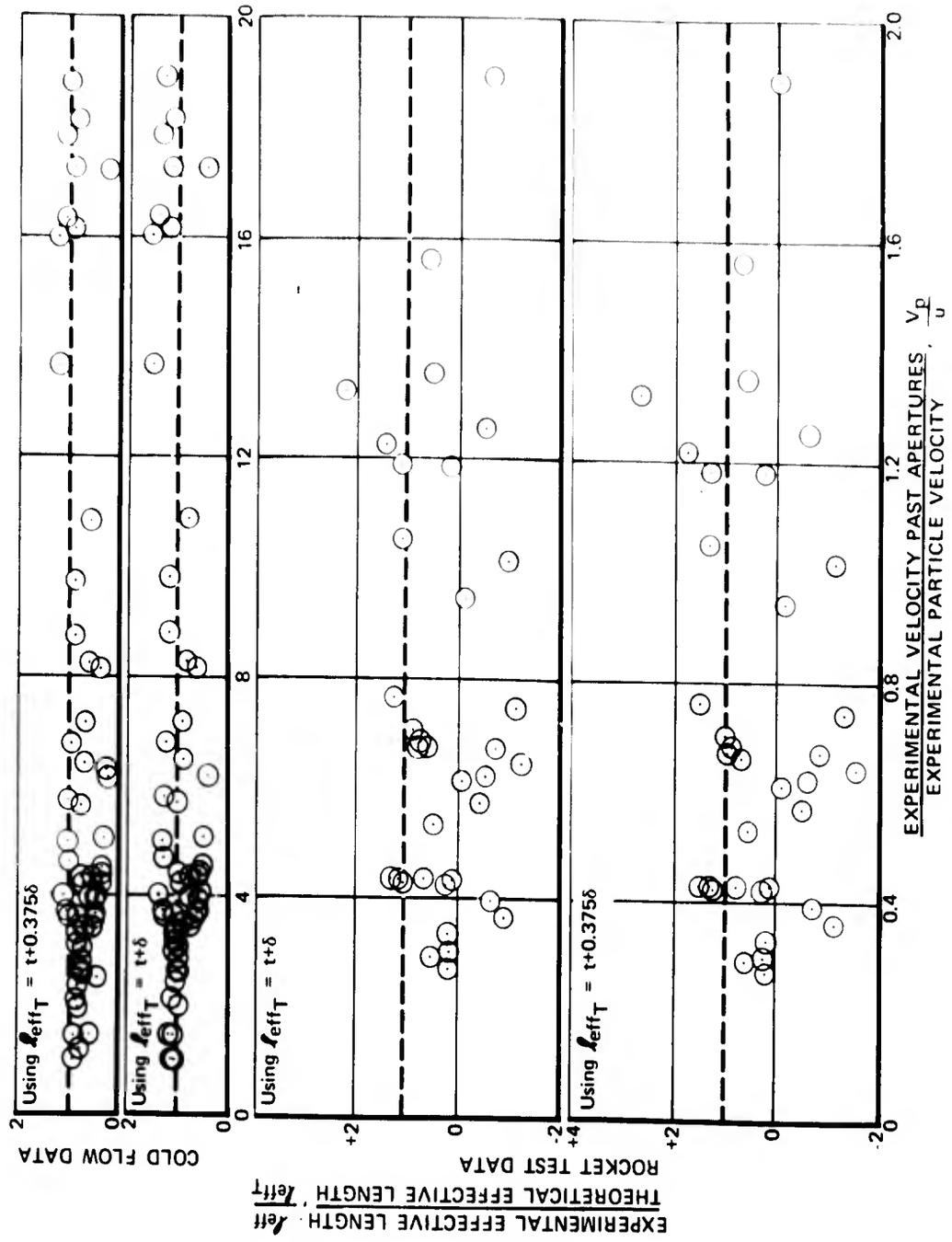

FD 53768

Figure 64. Correlation of Effective Length Data With Flow Ratio

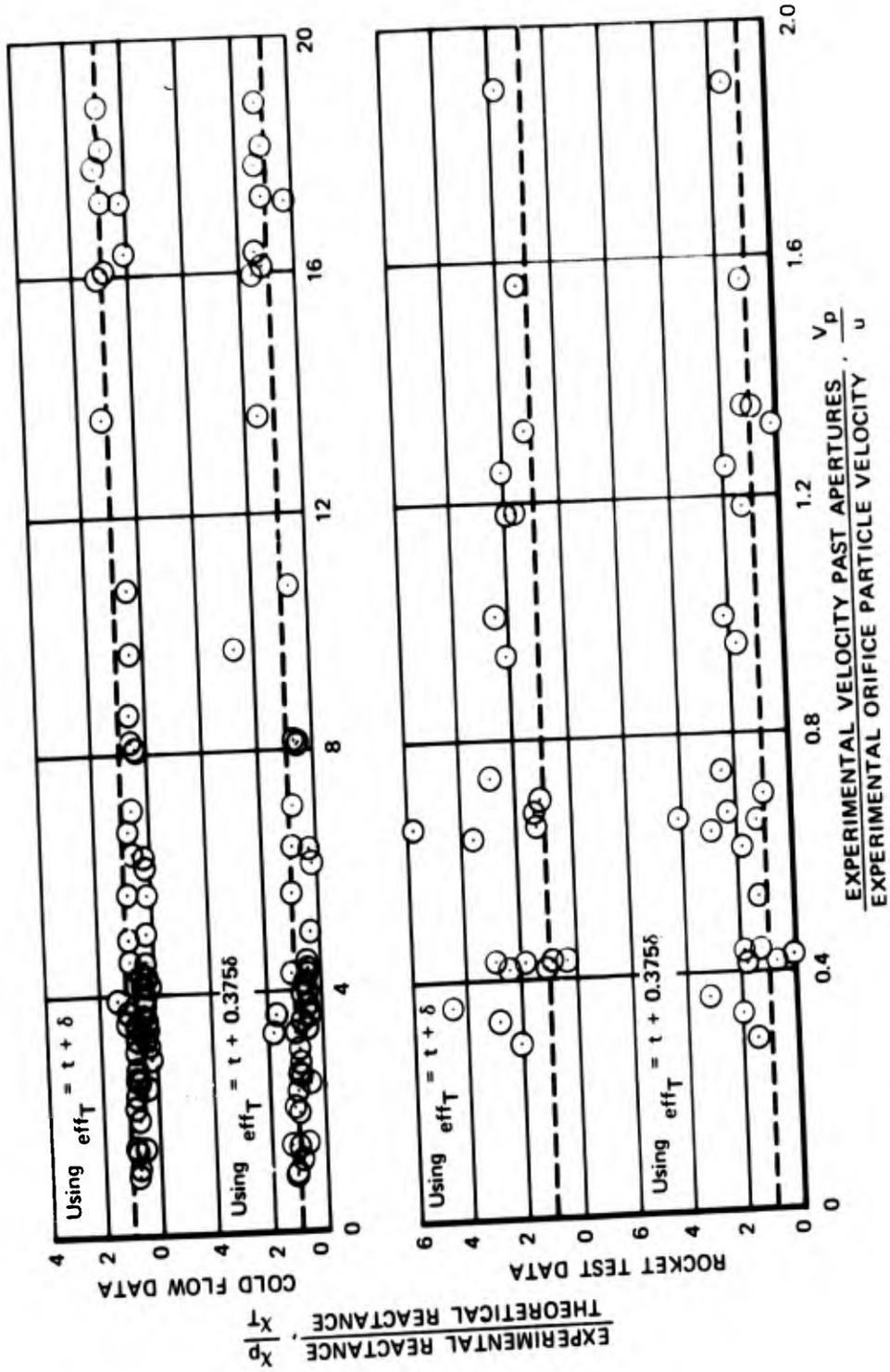

FD 53769

Figure 65. Correlation of Reactance Ratio With Flow Ratio

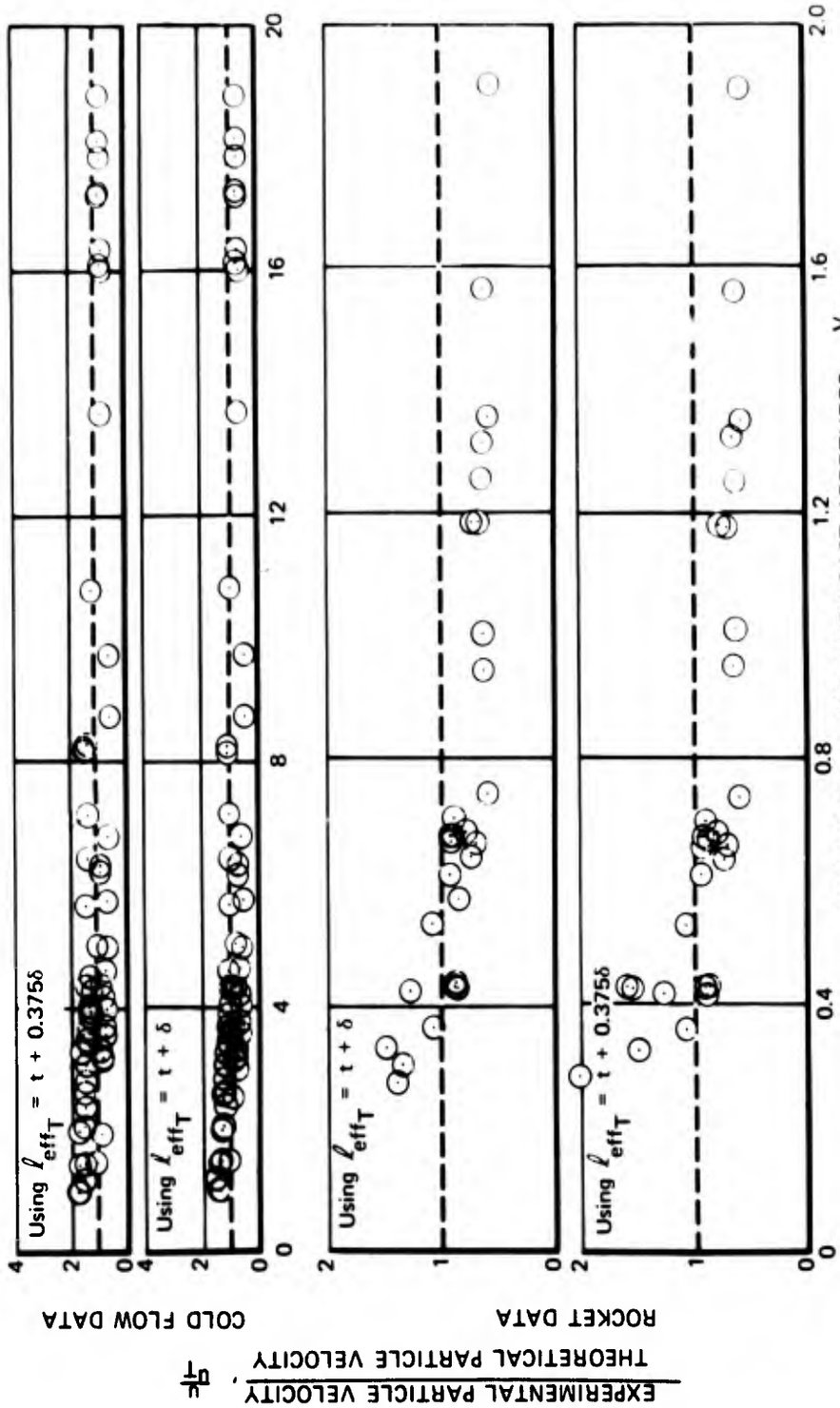

FD 53770

Figure 66. Correlation of Particle Velocity With Flow Ratio

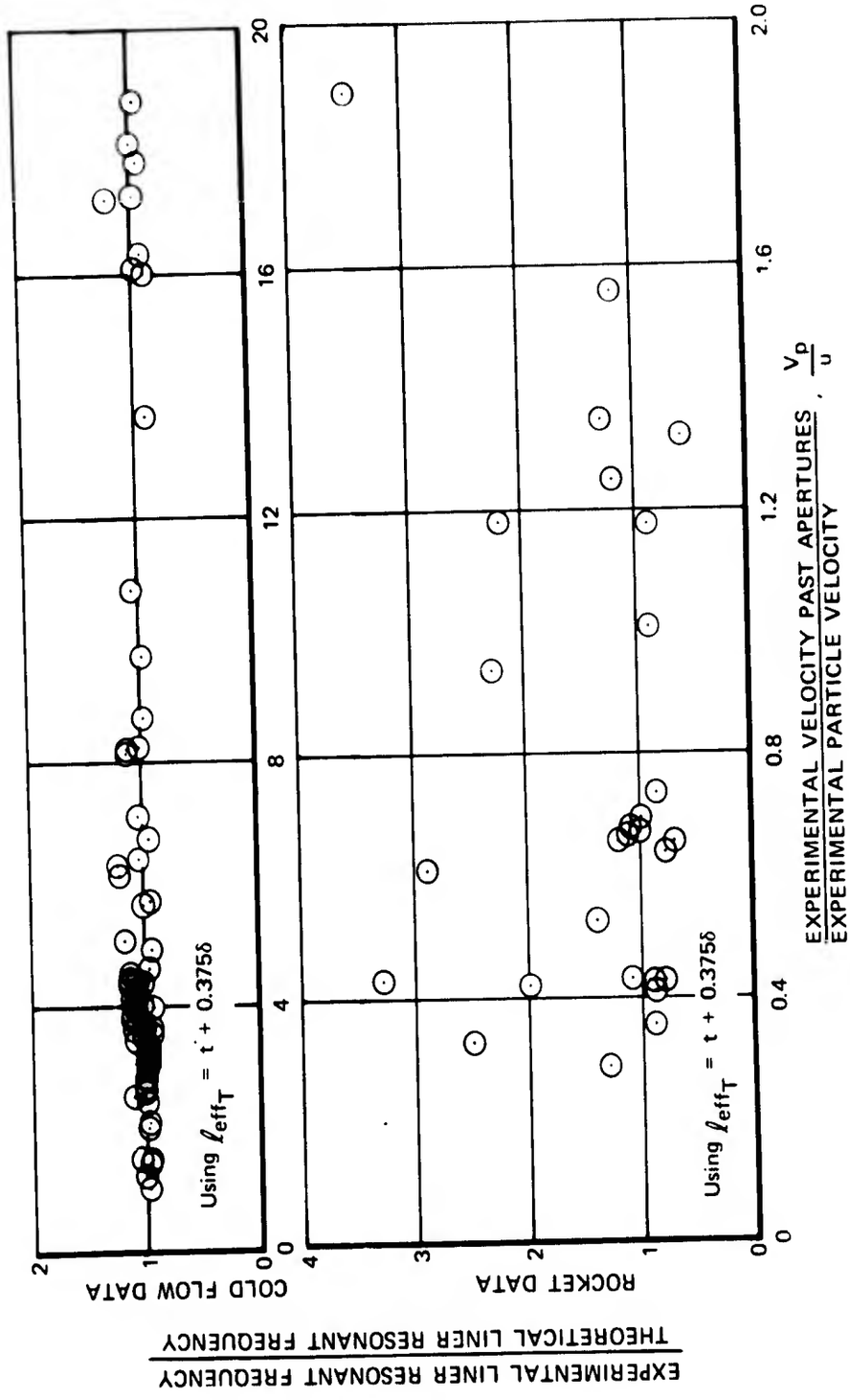

FD 53771

Figure 67. Correlation of Resonant Frequency Data With Flow Ratio

In addition, it was found that the correlation of acoustic resistance ratio with velocity ratio multiplied by density ratio, equations (13) and (14), was further improved by using the Phillips equation for calculating the effective aperture length, which is used in the theoretical particle velocity and in θ_n. The improved correlation that best represented both can be described by

$$\frac{\theta_p}{\theta_n} = 1 \quad \text{when} \quad \frac{V_p}{u}\left(\frac{\rho_a}{\rho_c}\right)^{3/2} \leq 1.5 \tag{18}$$

$$\frac{\theta_p}{\theta_n} = \frac{V_p}{3u}\left(\frac{\rho_a}{\rho_c}\right)^{3/2} + 0.5 \qquad \text{when} \quad \frac{V_p}{u}\left(\frac{\rho_a}{\rho_c}\right)^{3/2} > 1.5 \tag{19}$$

Comparison of equation (19) with both rocket and cold-flow resistance data are shown in figures 68 and 69.

The ratio of experimental absorption coefficient to theoretical is shown in figure 70. Using the Phillips effective length equation and the above resistance correlation produces satisfactory agreement between the theory and experimental data.

Recommendations from the analysis of the acoustic data may be summarized as follows:

1. The effective aperture length, reactance, particle velocity, and liner resonant frequency with flow past the apertures should be determined using the Phillips effective length equation in the existing equations for no flow

2. Resistance should be computed using equations (18) and (19), where the Phillips effective length is used in calculating θ_n and particle velocity.

Using the above recommendations and the theory as outlined in Section III-A, an absorbing liner design computer program was formulated. The program is valid for no flow, past-flow, or through-flow situations. A source program listing and a test case are contained in Appendix III.

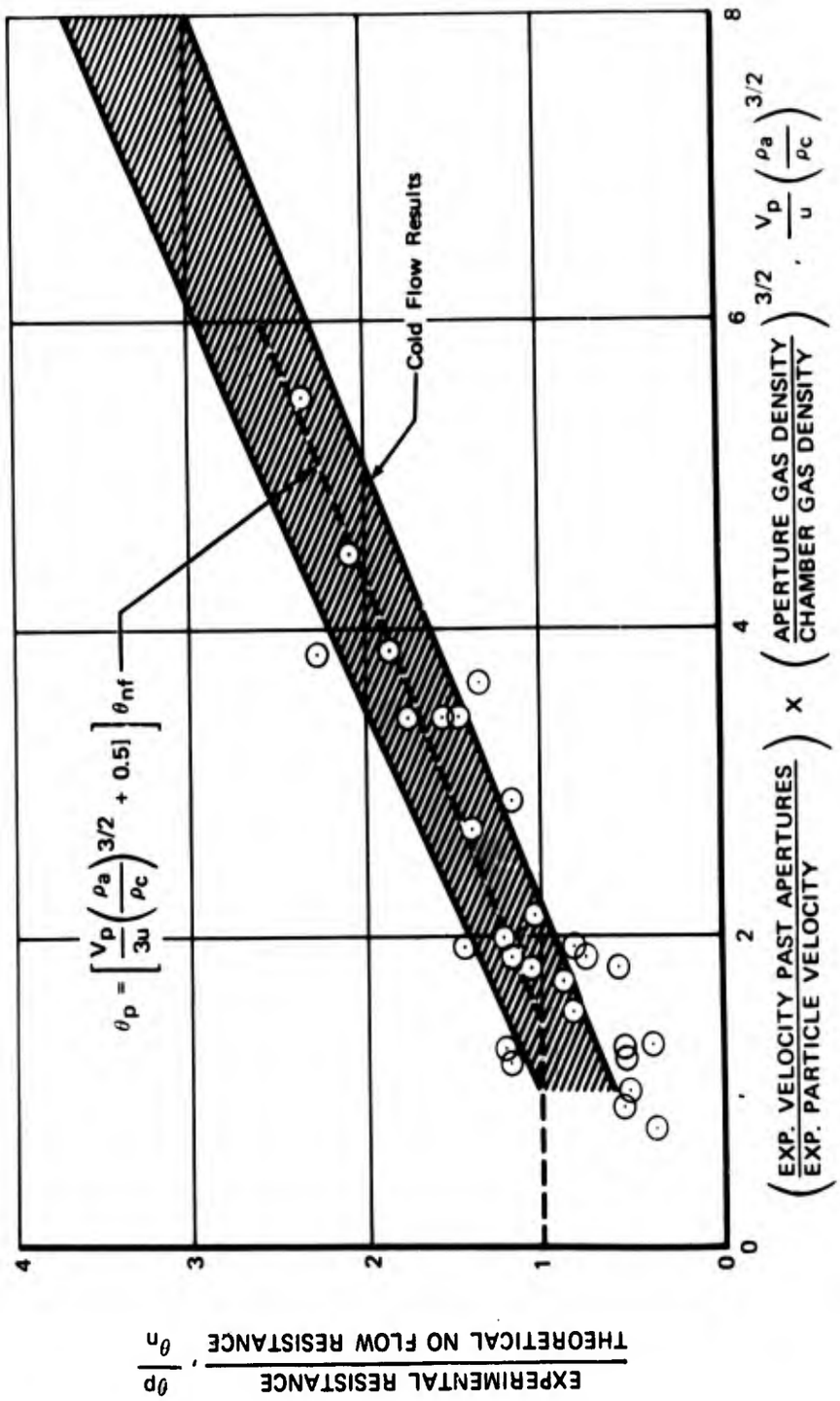

FD 53772

Figure 68. Comparison of High Particle Velocity Resistance Data From Rocket Firings and From Cold Flow Tests Using Phillips Equation for Effective Length

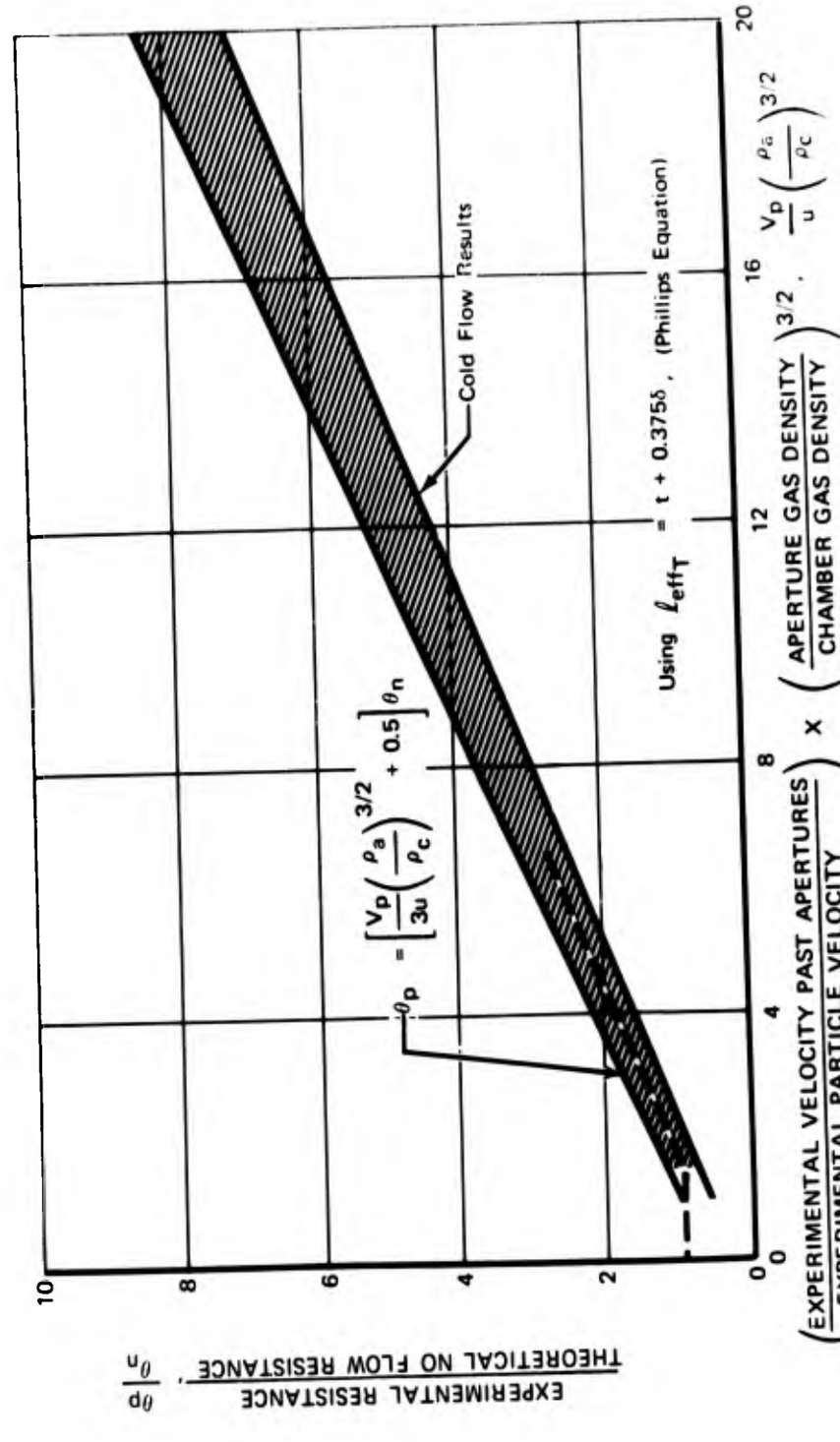

FD 53773

Figure 69. Comparison of Resistance Correlation With Entire Range of Cold Flow Data

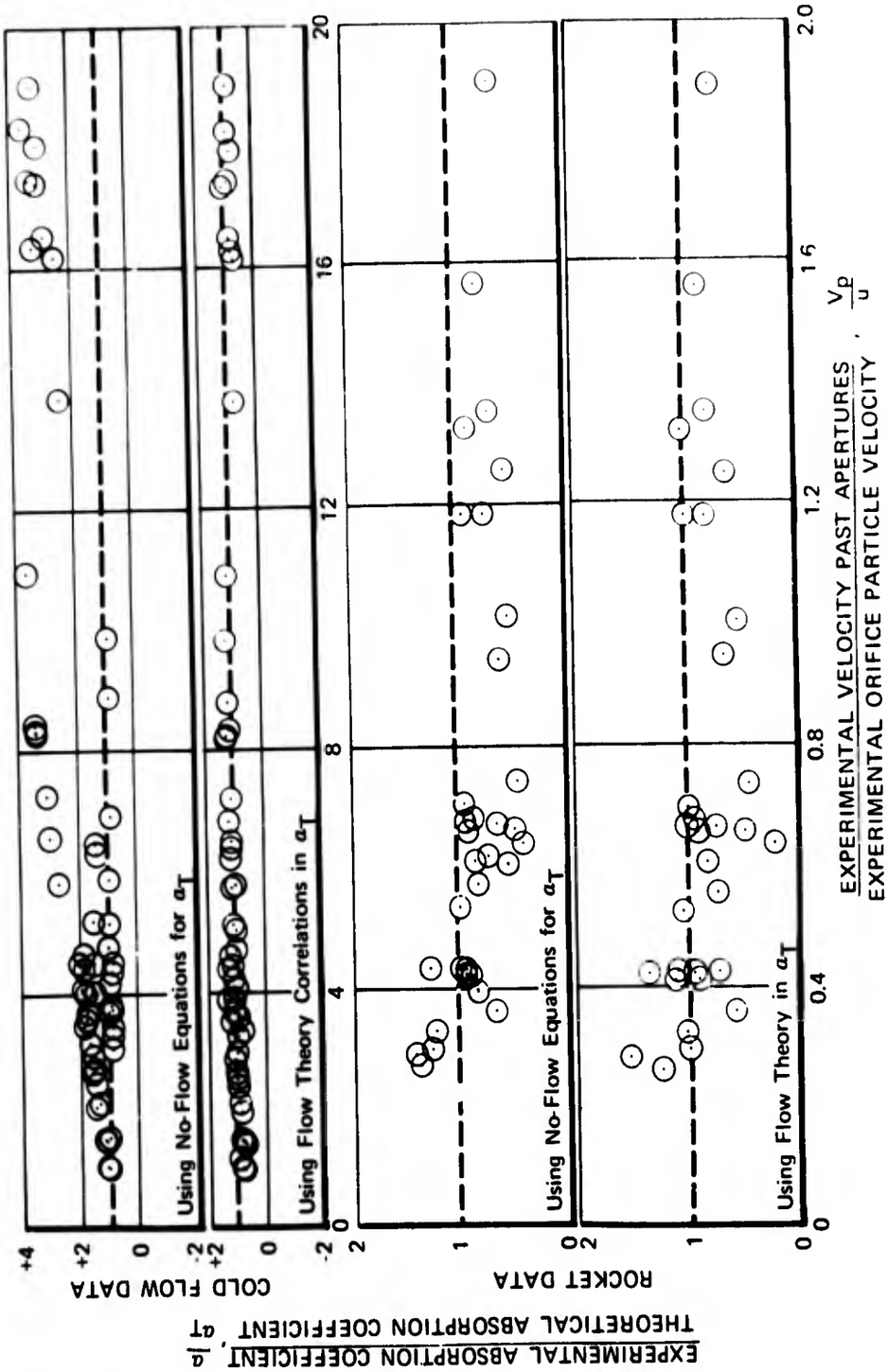

FD 53774

Figure 70. Comparison of Experimental Absorption Coefficient With Flow Ratio

F. VERIFICATION TEST PROGRAM

1. Hardware

The verification test program was conducted to investigate the effectiveness of liners designed using the high velocity absorbing liner design theory. The test motor (figure 71) consisted of a triplet impinging (fuel-oxidizer-fuel) injector and an outer pressure shell into which both solid and perforated liner sections were installed; the motor was fabricated for use under both phases of the previous program (References 1 and 2). Extensive testing with and without absorbing liners under that program has shown the following: (1) combustion in the motor is extremely rough with spontaneous, high amplitude pops occurring at closely spaced intervals, (2) with chamber Mach numbers of 0.14 and 0.23, acoustic liners with absorption coefficients greater than 17% will suppress the spontaneous instability that the pops trigger for all frequencies up to 5000 Hz, (3) with the exception of one dual-array ablative liner that structurally failed within 6.6 sec, no liner has successfully suppressed all modes of instability up to 10,000 Hz, (4) the most predominant mode of instability in the motor is the 2nd transverse mode, which has a characteristic frequency of 3300 Hz.

Modifications to the hardware that were necessary for use in the verification tests included:

1. Changing the throat diameter of an existing uncooled 1000-psia nozzle to operate at 100-psia and with an average chamber velocity of 1250 ft/sec (M = 0.32).

2. Addition of a pulse gun boss to the chamber wall to accept the guns developed during Phase I of the present program.

3. Remachining of existing acoustic liners to the desired configurations.

The design of the acoustic liners for the motor was based on the flow correlations derived from the analysis of Section III-E, which are used in the design computer program of Appendix III for predicting the specific acoustic resistance, specific acoustic reactance, and the absorption coefficients of liners with high flow velocities past the apertures. The results of the design analysis conducted using the program indicated that a liner with wide bandwidth characteristics was a possible configuration. A second liner was designed with a dual acoustic array, i.e., a liner with two distinct resonant frequencies; the frequencies chosen were 3000 and 7000 Hz. The dual array liner is shown in figure 72. The test conditions used in the liner design analysis are listed in table XIII.

In figures 73 and 74 the theoretical absorption coefficients are shown as function of frequency for each of the liner designs. It was believed that the absorption characteristics of either liner were sufficient to suppress combustion instability in the motor over the entire range of possible frequencies to 10,000 Hz.

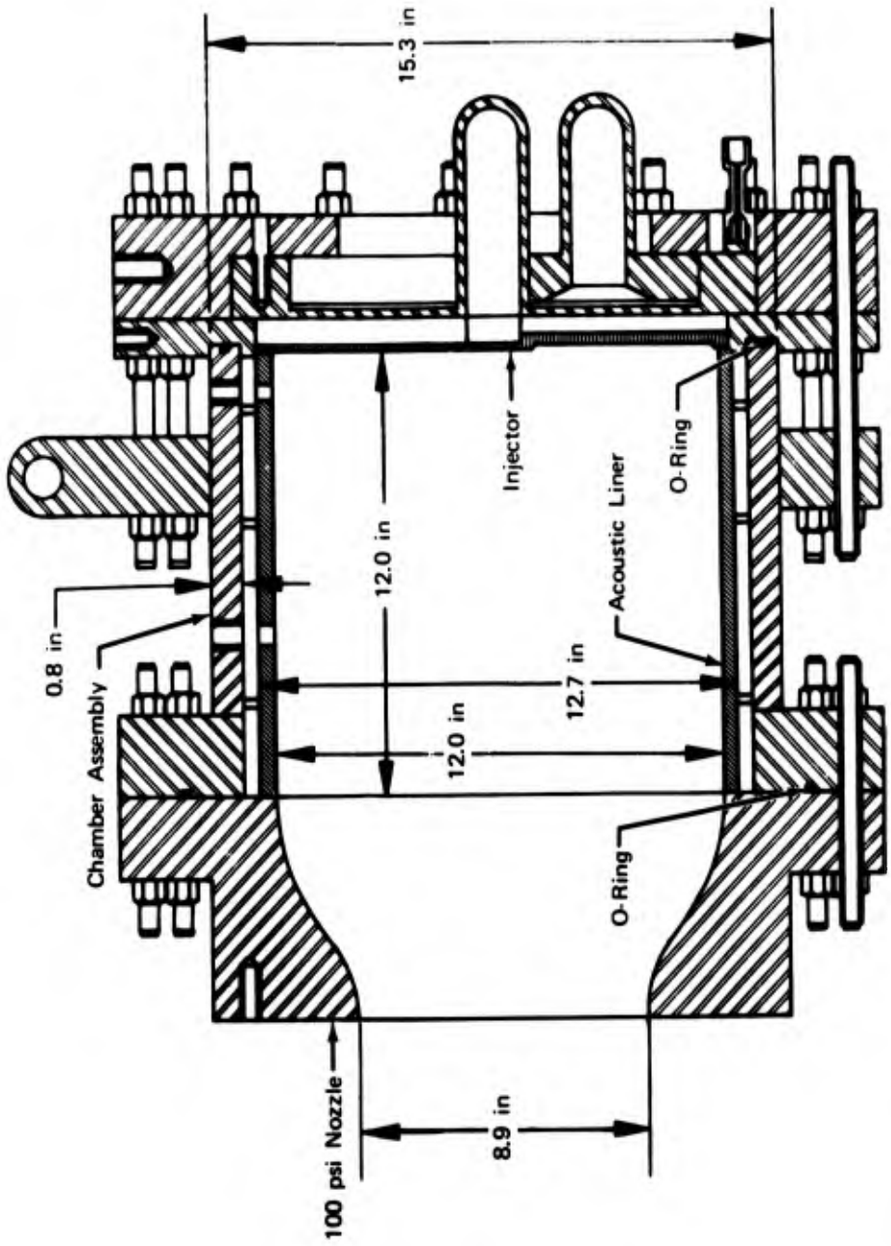

FD 53775

Figure 71. Uncooled Verification Liner Test Motor Assembly

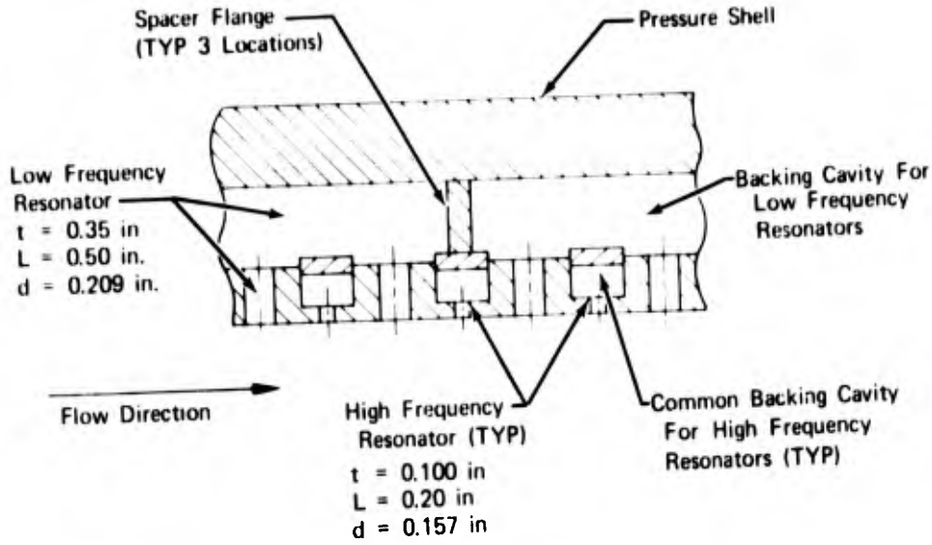

Figure 72. Dual Array Acoustic Liner FD 53776

Table XIII. Verification Motor, Nominal Test Conditions

Thrust, lb_f	5000
Chamber pressure, psia	100
Fuel	N_2H_4 and UDMH (50-50 blend)
Oxidizer	N_2O_4
Mixture ratio	2
Aperture gas temperature, °R	3000
Cavity gas temperature, °R	1500
Incident pressure amplitude, db	170
Velocity past apertures, ft/sec	1250
Mach number	0.318

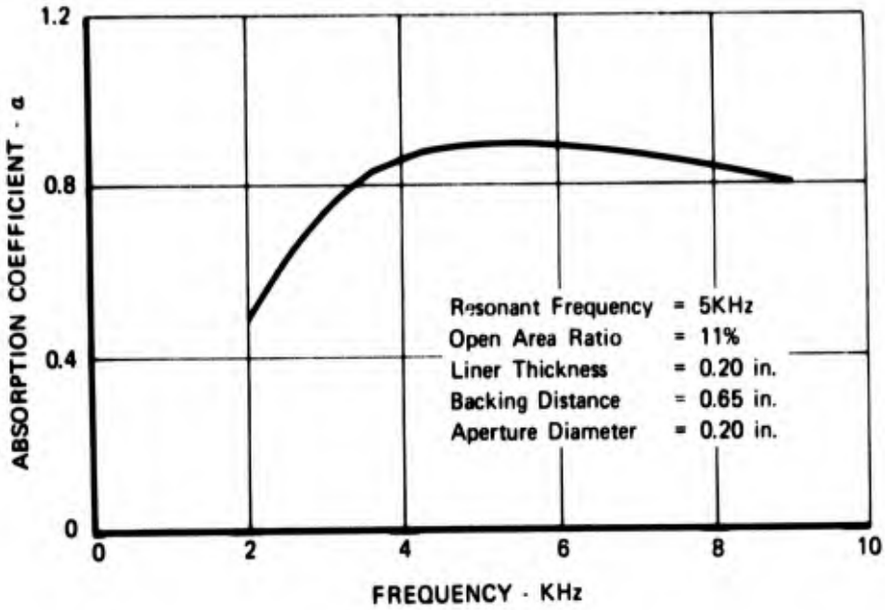

Figure 73. Theoretical Absorption Coefficient of Wide-Band Liner FD 53777

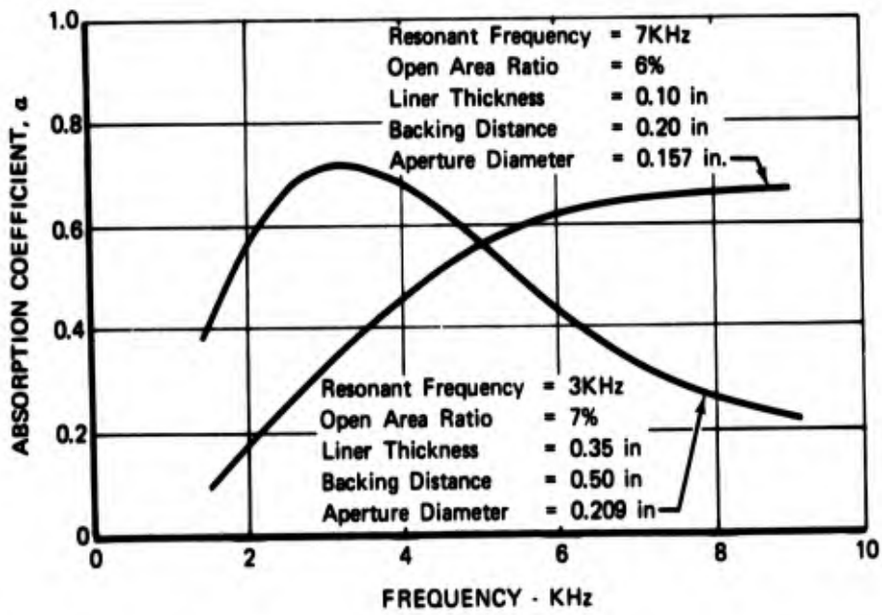

Figure 74. Theoretical Abosrption Coefficient of Dual Array Liner FD 53778

2. Test Program

A series of five tests was conducted with the verification hardware; a summary of test results is listed in table XIV. Tests 1 and 2 were conducted using a solid liner to determine the baseline stability characteristics of the motor with high chamber velocity. As noted in previous firings with this injector (References 1 and 2) pops occurred during the ignition phase of the test; amplitude spikes of 30 and 50 psi were recorded. The pops triggered steady-state instability, with amplitudes in excess of 30-psi peak-to-peak at several frequencies, which caused the rough combustion cutoff (RCC) system to abort the test.

Test 3 was conducted with the dual array liner; it was also aborted by the RCC. The motor survived several ignition pops and remained stable at full chamber pressure for 0.15 sec before a pop of 120-psi amplitude resulted in 7400 Hz steady-state instability.

Tests 4 and 5 were conducted with the wide-bandwidth liner. Both firings were aborted by the RCC. During each test, the liner was able to damp pops at steady-state chamber pressure for a short period of time (0.2 and 0.4 sec, respectively); however, in each case pops with peaks of between 100 and 115 psi triggered high-frequency steady-state instability.

Figures 75 through 78 show the dual array liner, the wider-bandwidth liner, the injector face, and the nozzle after the final firing. On disassembly of the motor no damage to any of the hardware was found.

3. Analysis

A comparison of the baseline stability characteristics of the verification test motor with data from firings of the motor with the dual array liner and the wide band liner are shown in figures 79 and 80. With the solid liner combustion instability occurred at several frequencies; the maximum amplitude, 61% of chamber pressure, occurred at 3300 Hz (2T mode). Both absorbing liners suppressed all the low-frequency modes including the predominate 2T mode, but neither liner was completely effective at high frequency. The wide band liner failed at 6400 Hz and at higher frequencies. The dual array liner was effective beyond 6400 Hz but failed at 7500 Hz.

Past experience with this particular injector (References 1 and 2) shows that high frequency instability (7200 to 7800 Hz) occurred with liners in firings having nominal chamber gas velocity past the liner of 500 and 850 ft/sec. Because the verification liners suppressed the most predominate mode of instability and performed at higher frequencies similar to other liners tested at lower chamber velocities, it was concluded that the high flow past the liner was not the cause of liner failures.

Table XIV. Verification Liner Test Summary

Test No.	Duration, sec	Chamber Pressure, psia	Disturbance Device	Mixture Ratio	C* Efficiency %(1)	Comments
1	0.87	93.0	25 gr Radial Pulse Gun*	1.8	95.4	Solid Liner - RCC abort. 30 and 50 psi pops occurred at +0.63 and +0.68 sec triggering steady-state instability.
2	0.81	90.0	25 gr Radial Pulse Gun*	1.75	92.8	Solid Liner - RCC abort. 90 psi pop occurred at +0.66 sec. 70 psi pop, at +0.69 sec triggered steady-state instability.
3	0.90	96.0	25 gr Radial Pulse Gun*	1.84	97.3	Dual Array Liner - RCC abort. 95 psi pop, at +0.42 sec damped in 0.003 sec 110 psi pop, at +0.66 sec damped in 0.007 sec 120 psi pop, at +0.78 sec resulted in steady-state instability.
4	1.20	98.0	25 gr Radial Pulse Gun*	1.87	98.3	Wide-Bandwidth Liner - RCC abort. Ten pops of amplitude up to 125 psi occurred between +0.65 and +0.85 sec. All were damped in 0.010 sec or less. A 115 psi pop, at +0.89 sec resulted in steady-state instability.
5	1.24	95.0	25 gr Radial Pulse Gun*	1.90	95.7	Wide-Bandwidth Liner - RCC abort. Sixteen pops of amplitude up to 115 psi occurred between +0.63 and +1.15 sec - all were damped in 0.015 sec or less. A 100 psi pop, at +1.17 sec resulted in steady-state instability.

*Pulse gun timed to detonate at +1.5 sec but did not detonate because of RRC Abort.
(1)Based on Chamber pressure.

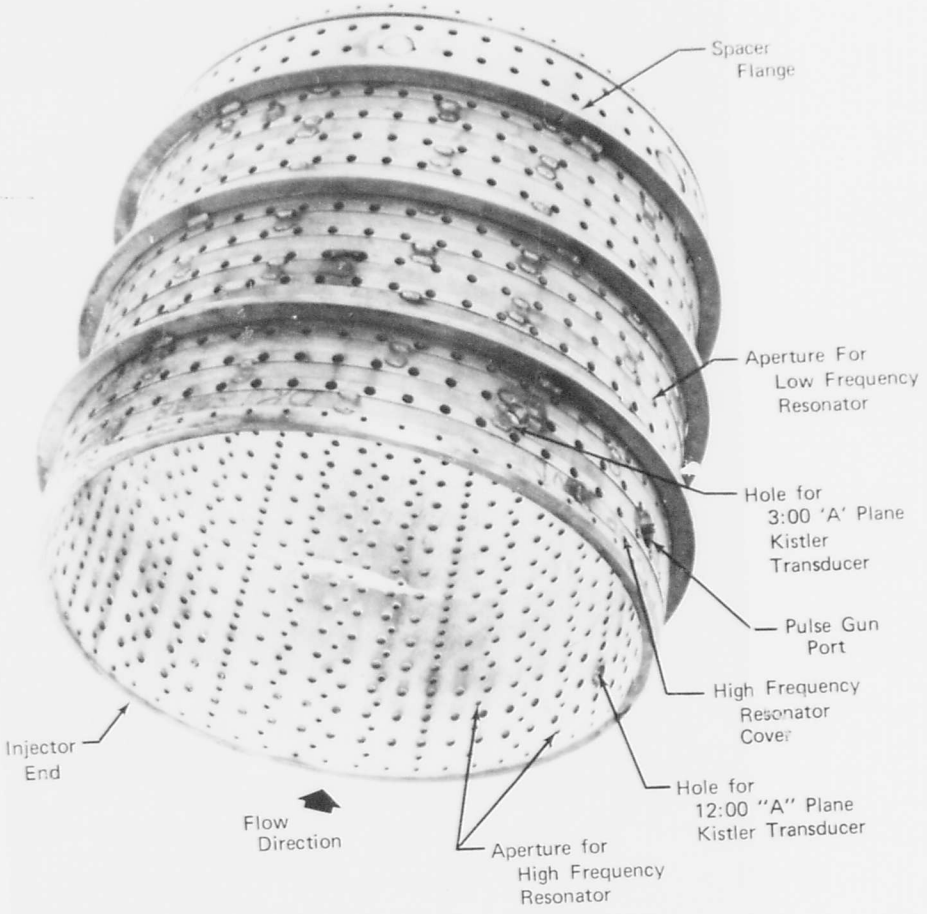

Figure 75. Dual Array Liner After Testing

FE 107343A

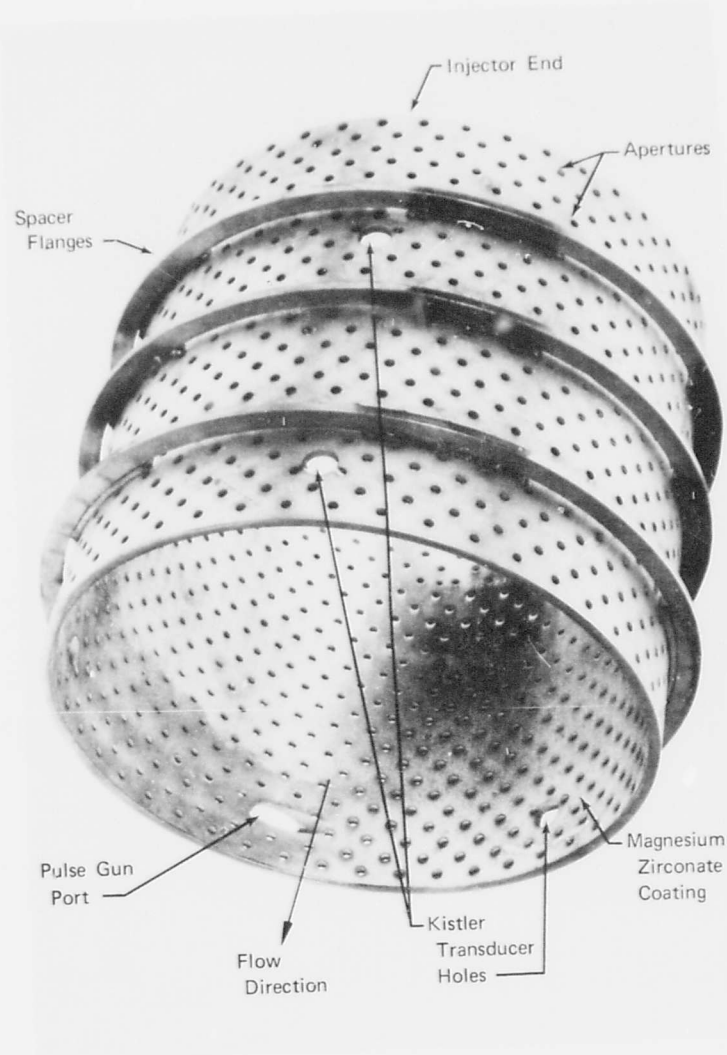

Figure 76. Wide-Bandwidth Liner After Testing FE 107344A

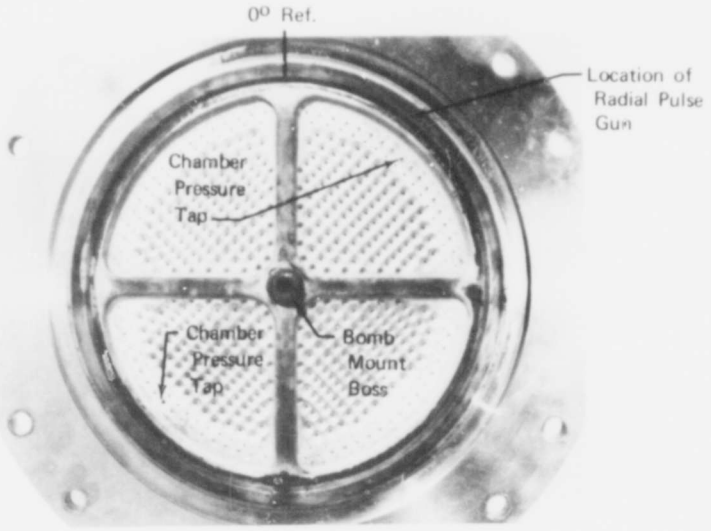

Figure 77. Verification Test Injector After Testing FE 107346A

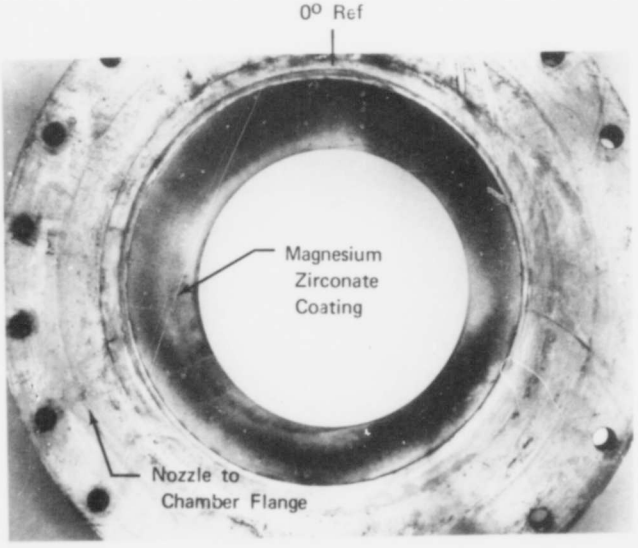

Figure 78. Downstream View of 100 psi Nozzle After Testing FE 107345A

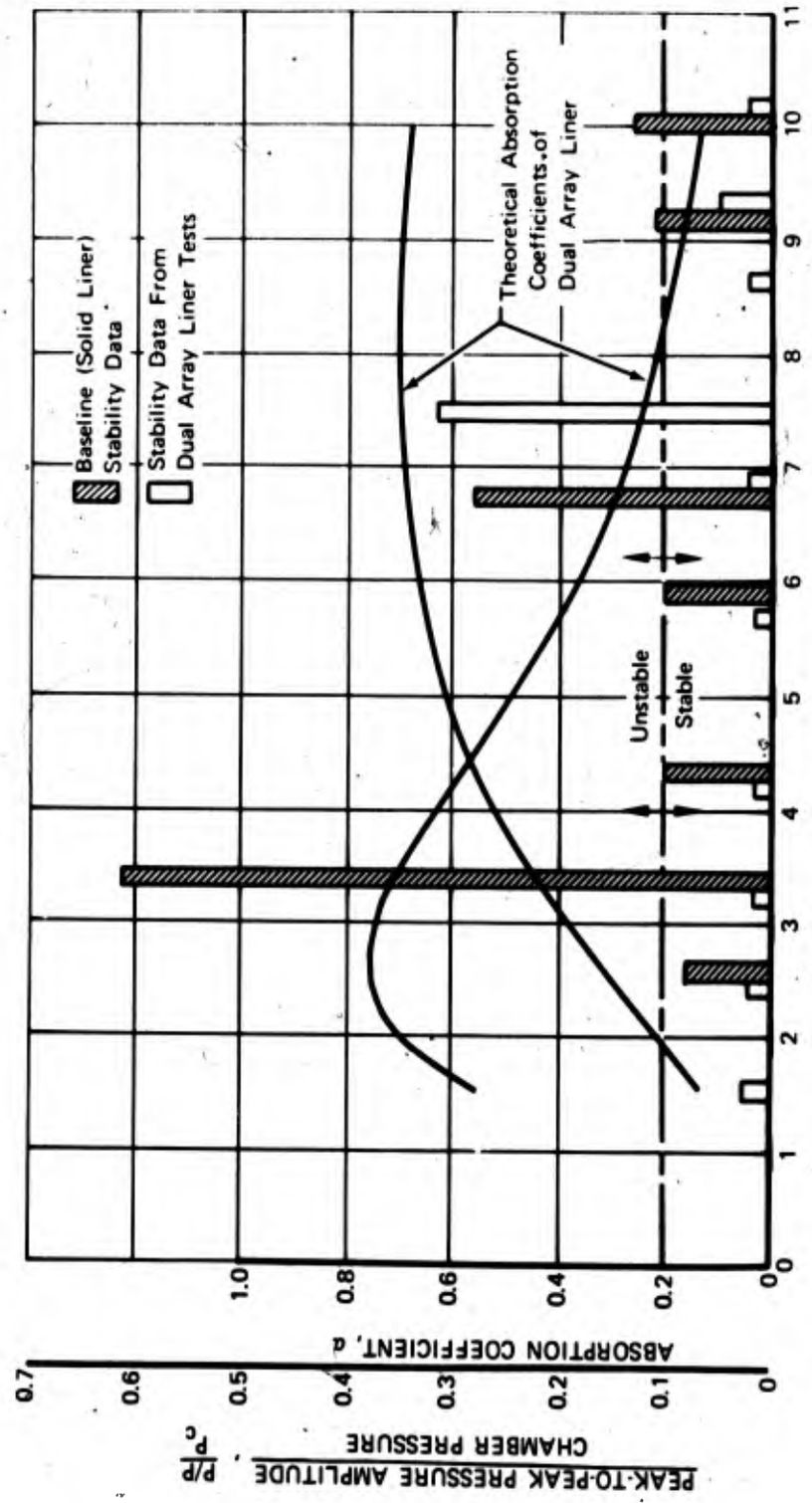

FD 53779

Figure 79. Stability Characteristics of Verification Motor: Comparison of Data From Baseline and Dual Array Liner Tests

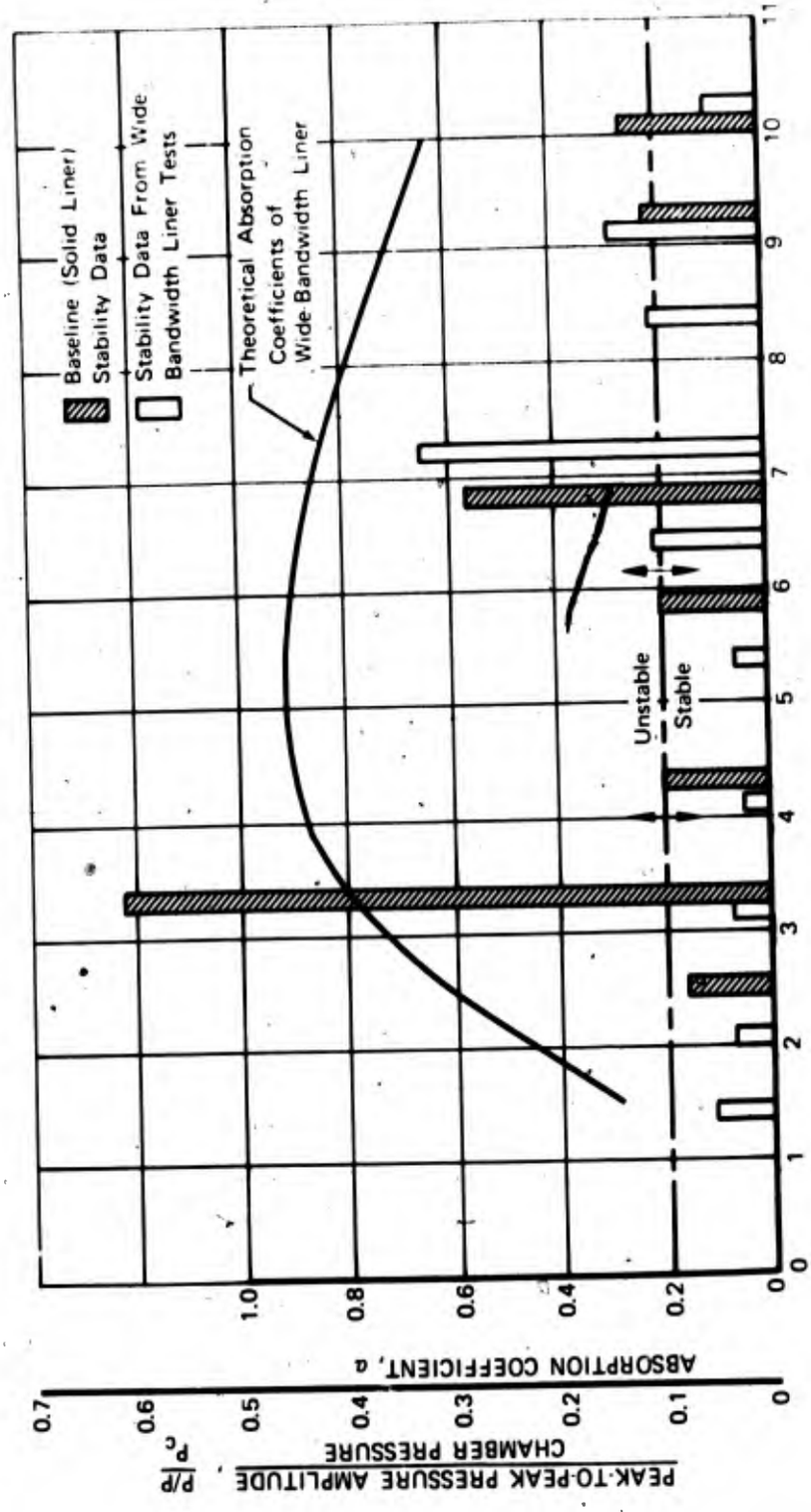

FD 53780

Figure 80. Stability Characteristics of Verification Motor: Comparison of Data From Baseline and Wide-Bandwidth Liner Tests

As shown in figures 79 and 80, the theoretical absorption coefficients of both liners at the higher frequencies was at least as great as those at the lower frequencies. The data used to develop the design theory for high flow past the liner were from cold flow and from rocket tests with flow velocities up to 1672 ft sec, but the frequency range of the data was relatively low; a maximum of 3300 Hz for the cold flow tests and a maximum of 2300 for the rocket firings. Therefore, to predict the absorption of both liners at frequencies greater than 3300 Hz extrapolations were necessary.

Although the exact reason for the failure of the liners to suppress the high frequency instability is not known, it is postulated that because of the extrapolations with frequency, the theoretical absorption was not as high as indicated thereby allowing the high frequency modes to appear.

It is recommended that additional acoustic data be generated at high frequencies with high flow velocity and high sound pressure level. Because it is extremely difficult to generate this type of acoustic data with conventional cold flow techniques, it is recommended that the 5K verification motor be instrumented with partitioned liner segments, as was done in the high chamber velocity program (Section III-D) and fired to generate the necessary acoustic data.

SECTION IV
REFERENCES

1. Garrison, G. D., Acoustic Liners for Storable Propellant Rocket Chambers - Phase I Final Report, Pratt & Whitney Aircraft, AFRPL-TR-67-295, Contract AF04(611)-11387, July 1967 (Confidential).

2. Garrison, G. D., Acoustic Liners for Storable Propellant Rocket Chambers - Phase II Final Report, Pratt & Whitney Aircraft, AFRPL-TR-68-114, Contract AF04(611)-11387, August 1968 (Confidential).

3. Thrust Chamber Injector Combustion Stability Evaluation, Bell Aerosystems Co., Report No. 8533-910012, December 1967.

4. Garrison, G. D., Absorbing Liners for Rocket Combustion Chambers, Theory and Design Techniques, Pratt & Whitney Aircraft, AFRPL-TR-66-234, August 1966 (Confidential).

5. Bartz, D. R., A Simple Equation for Rapid Estimation of Rocket Nozzle Convective Heat Transfer Coefficients, Jet Propulsion Laboratory, Volume 27, 1957, p. 49-51.

6. Birdseye, D. F., Experimental Investigation of Heat-Transfer Characteristics of Liquid Nitrogen Tetroxide, Jet Propulsion Laboratory Technical Report No. 32-37, October 1969.

7. Witte, A. B., Experimental Investigation of Heat Flux at the Upper Limit of Nucleate Boiling for Two Mixtures of Hydrazine and Unsymmetrical Dimethylhydrazine, Jet Propulsion Laboratory Technical Report No. 32-75, April 1971.

8. Improvement of Bombs and Pulse Guns as Combustion Stabilizing Rating Devices, Final Report, Rocketdyne Report No. AFRPL-TR-68-13, March 1969.

9. Elliott, D. G., D. R. Bartz, and S. Silver, Calculation of Turbulent Boundary-Layer Growth and Heat Transfer in Axi-Symmetric Nozzles, Jet Propulsion Laboratory Technical Report No. 32-387, February 1963.

10. Dipprey, D. F, and R. H. Saversky, Heat and Momentrum Transfer in Smooth and Rough Tubes at Various Prandtl Numbers, Jet Propulsion Laboratory Technical Report No. 32-269.

11. Kraus, A. D., Heat Flow Theory and Extended Surfaces for Heat Transfer, C-M Technical Publication Corporation, New York 17, New York 1961.

12. Garrison, G. D., Suppression of Combustion Oscillations With Mechanical Damping Devices, Phase II Interim Report, Pratt & Whitney Aircraft, PWA FR-3880, June 1970.

REFERENCES (Continued)

13. Garrison, G. D., Suppression of Combustion Oscillations With Mechanical Damping Devices, Interim Report, Pratt & Whitney Aircraft, PWA FR-3299, August 1969.

14. Garrison, G. D., A Study of the Suppression of Combustion Oscillations With Mechanical Damping Devices, Phase II Summary Report, PWA FR-1922, July 1966.

15. Garrison, G. D., A Study of the Suppression of Combustion Oscillations With Mechanical Damping Devices, Final Report, Pratt & Whitney Aircraft Report No. PWA FR-2596, November 20, 1967.

16. Phillips, B., "Recent Advances in Acoustic Liner Technology at Lewis Research Center", 5th ICRPG Combustion Conference CPIA Pub. No. 183, December 1968.

APPENDIX I
PRESSURE-PHASE DATA REDUCTION EQUATIONS

A typical Helmholtz resonator at the end of a tube is shown in figure 81. Shown also are two microphones, one mounted in the side wall to measure the sound pressure in front of the sample, P_1[3], and one on the rear wall to measure the sound pressure in the cavity, P_2. The phase difference between the two sound pressures is designated as ϕ.

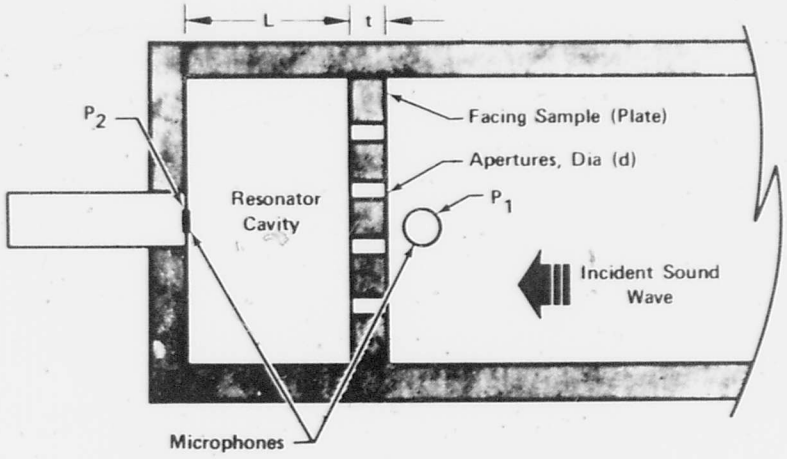

Figure 81. Helmholtz Resonator in Impedance Tube FD 23080C

The total impedance of the resonator assembly is composed to two parts:

$$Z_{total} = Z_{plate} + Z_{air\ cavity} \tag{20}$$

If u is the oscillatory gas velocity amplitude in the apertures and ρ and c are the density and sonic velocity, respectively, of the test media, by definition

$$Z_{plate} = \frac{P_1 - P_2}{u\rho c} \tag{21}$$

and also

$$Z_{air\ cavity} = \frac{P_2}{u\rho c} = \frac{i}{kL} \tag{22}$$

Solving (21) for u, substituting into (22) and solving for Z_{plate} gives:

$$Z_{plate} = \frac{i}{kL}\left[\frac{P_1}{P_2} - 1\right] \tag{23}$$

where k, the wave number, is defined as $k = \omega/c$.

[3] In this appendix, the time dependent variables P, and u, are peak values.

Using a mathematical identify, the ratio of the complex pressures can be expressed as:

$$\frac{P_1}{P_2} = \left|\frac{P_1}{P_2}\right| e^{-i\phi} = \left|\frac{P_1}{P_2}\right| \cos\phi - i \left|\frac{P_1}{P_2}\right| \sin\phi$$

Substituting the identity into (23):

$$Z_{plate} = \frac{i}{kL}\left|\frac{P_1}{P_2}\right| \sin\phi - \frac{i}{kL}\left[1 - \left|\frac{P_1}{P_2}\right| \cos\phi\right]$$

Solving (20) for Z_{total} gives:

$$Z_{total} = \frac{i}{kL}\left|\frac{P_1}{P_2}\right| \sin\phi - \frac{i}{kL}\left[1 - \left|\frac{P_1}{P_2}\right| \cos\phi\right] + \frac{i}{kL} \qquad (24)$$

or

$$Z_{total} = \frac{1}{kL}\frac{P_1}{P_2} \sin\phi - i\left[\frac{1}{kL}\left|\frac{P_1}{P_2}\right| \cos\phi\right] \qquad (25)$$

The total impedance is a complex sum; the real part is the resistance θ, and the imaginary part is the reactance, χ. By inspection of equation (25) it is evident that the resistance can be determined from

$$\theta = \frac{1}{kL}\left|\frac{P_1}{P_2}\right| \sin\phi \qquad (26)$$

and the reactance from

$$\chi = -\frac{1}{kL}\left|\frac{P_1}{P_2}\right| \cos\phi \qquad (27)$$

Additional acoustic parameters that can now be computed are:

Absorption coefficient

$$\alpha = \frac{4\theta}{(\theta+1)^2 + \chi^2} \qquad (28)$$

Oscillatory flow velocity in apertures (particle velocity), computed using equation (22)

$$u = kLP_2/(\sigma\rho c) \qquad (29)$$

and the aperture effective length

$$\ell_{eff} = \frac{\sigma c Z_{plate}}{2\pi f} = \frac{\sigma c}{2\pi f kL}\left[\frac{P_1}{P_2} - 1\right] \qquad (30)$$

APPENDIX II
ACOUSTIC DATA

Acoustic data obtained under the present program are listed in the following tables. For simplicity, the IBM printouts from the data reduction computer program are used.

A brief title describing the type of data precedes each individual listing. Next the properties of the gaseous medium and the dimensions of the resonator assembly that are input into the program are listed. The following list identifies each symbol used on the data sheets.

1. Gas conditions and test sample configuration

   RGAS - Gas constant of gas medium

   GAMM - Ratio of specific heats (cavity gas)

   MOLW - Molecular weight (cavity gas)

   CF - Aperture flow coefficient (Steady flow discharge coefficient)

   SIG - Open area ratio

   XL - Cavity backing distance, in.

   T - Liner thickness, in.

   D - Aperture diameter, in.

2. Input data from test

   FREQ - Frequency, Hz

   PA1 - Chamber or facing pressure amplitude, db

   PA2 - Cavity pressure amplitude, db

   PHASE - Phase difference between PA1 and PA2, deg

3. Calculated data

   RESIS - Specific Acoustic Resistance

   REACT - Specific Acoustic Reactance

   IMPED - Specific Acoustic Impedance

   ABSOR - Absorption Coefficient

   UORF - Particle Velocity in Orifice, ft/sec

   VELPT - Velocity of Steady flow past Apertures, ft/sec

AF HELIUM FLOW 3 LING

RGAS	GAMM	MOLW	CF	SIG	XL		D
386.0	1.66	4.00	0.850	0.0270	0.507	0.300	0.099

FREQ	PA1	PA2	PHASE	RESIS	REACT	IMPED	ABSOR	UORF	VELPT
2500.	158.6	162.[illegible]	93.7	3.030	0.195	3.037	0.744	277.9	897.3
2500.	158.6	162.5	93.5	3.107	0.190	3.113	0.735	291.0	870.9
2500.	157.0	161.1	95.3	2.998	0.278	3.011	0.746	269.8	956.8
2500.	158.6	161.3	95.5	3.503	0.337	3.519	0.687	310.2	1047.2
2500.	158.6	161.5	96.0	3.447	0.362	3.466	0.692	295.5	1079.8
2500.	158.6	161.0	92.0	3.678	0.128	3.680	0.671	263.6	1113.7
2500.	158.6	161.1	94.5	3.562	0.280	3.573	0.681	256.1	1125.4
2500.	148.0	154.5	113.0	2.134	0.905	2.318	0.802	131.7	529.0
2500.	149.0	156.0	106.0	2.107	0.604	2.192	0.841	93.7	538.9
2500.	149.0	156.2	106.0	2.039	0.594	2.121	0.851	107.3	537.0
2500.	149.0	156.1	107.0	2.051	0.627	2.145	0.845	117.5	548.0
2500.	149.0	156.2	108.0	2.018	0.655	2.122	0.846	135.0	506.3
2500.	148.0	154.6	109.0	2.146	0.738	2.269	0.821	131.6	474.1
2500.	149.0	152.1	97.0	3.207	0.406	3.322	0.706	107.5	1050.2
2500.	149.0	152.3	98.0	3.238	0.455	3.269	0.712	116.5	1020.8
2500.	149.2	153.5	101.0	2.903	0.564	2.958	0.746	143.2	973.8
3300.	150.0	145.7	129.0	4.772	3.864	6.141	0.395	88.5	1672.8
3300.	150.0	145.1	131.0	4.705	4.090	6.235	0.381	88.8	1585.5
3300.	150.0	145.2	133.0	4.527	4.221	6.189	0.374	91.8	1503.1
3300.	150.0	144.7	134.5	4.699	4.618	6.588	0.349	87.4	1401.1
3300.	150.0	145.2	136.5	4.302	4.534	6.250	0.353	94.1	1288.5
3300.	150.0	145.5	124.0	4.955	3.342	5.977	0.425	90.8	1650.1
3300.	150.0	145.2	125.0	5.024	3.518	6.133	0.412	90.1	1559.9
3300.	150.0	145.2	125.5	5.003	3.568	6.145	0.410	91.5	1479.3

GP. FLOW PAST TESTS 100 DH 2/24/70

RGAS	GAMA	VOLM	CF	SIG	XL	T	D
55.0	1.40	28.0	0.850	0.0270	0.507	0.300	0.099

FREQ	PA1	PA2	PHASE	RESIS	REACT	IMPED	ABSOR	UCRF	VELPT
1100.	159.3	161.2	158.0	1.131	2.800	3.020	0.365	150.0	155.1
1100.	159.3	161.0	158.0	1.160	2.871	3.097	0.359	159.4	162.0
1100.	159.3	161.2	163.0	0.882	2.887	3.019	0.297	120.6	174.1
1100.	159.3	160.5	155.0	1.420	3.046	3.361	0.375	140.8	208.6
1100.	159.3	162.0	157.0	1.090	2.567	2.789	0.397	105.7	212.3
1100.	159.3	159.0	145.0	2.191	3.129	3.820	0.438	170.4	364.0
1100.	159.3	159.0	141.0	2.398	2.952	3.811	0.472	184.6	398.0
1100.	159.3	159.0	138.0	2.574	2.839	3.848	0.491	158.2	418.0
1100.	159.3	158.8	135.0	2.747	2.747	3.885	0.508	151.8	435.3
1100.	159.3	158.7	133.0	2.868	2.674	3.921	0.518	146.2	451.1
1100.	159.3	158.6	128.0	3.116	2.434	3.954	0.545	136.3	477.1
1100.	159.3	158.3	123.0	3.426	2.225	4.085	0.558	124.7	499.2
1100.	159.3	158.3	120.0	3.529	2.037	4.075	0.572	117.3	515.4
1100.	159.3	159.0	136.0	2.638	2.732	3.798	0.509	159.6	416.8
1100.	159.3	157.7	115.0	3.970	1.851	4.380	0.564	152.5	527.8
1100.	159.3	157.7	114.0	3.989	1.776	4.367	0.568	150.7	543.3
1100.	159.3	157.7	112.0	4.040	1.632	4.357	0.575	149.8	559.7
1100.	159.3	157.6	111.0	4.109	1.577	4.401	0.574	146.7	574.7
1100.	159.3	157.5	110.0	4.177	1.520	4.445	0.573	144.2	589.7
1100.	159.3	157.3	109.0	4.292	1.478	4.540	0.568	139.7	602.9
1100.	159.3	157.1	108.5	4.399	1.471	4.639	0.561	135.7	616.4
1100.	159.3	157.7	113.0	4.015	1.704	4.362	0.572	149.9	560.3
1100.	159.3	157.7	113.0	4.013	1.703	4.360	0.572	149.8	560.0
1100.	159.3	156.7	106.0	4.802	1.377	4.995	0.540	136.8	538.0
1100.	159.3	156.5	104.0	5.001	1.247	5.154	0.532	129.7	571.6
1100.	159.3	155.8	101.0	5.405	1.050	5.506	0.513	119.3	602.3
1100.	159.3	154.8	97.0	6.162	0.756	6.208	0.475	104.4	646.7

GN FLOW PAST TESTS, SPL VARIATION, CONSTANT VELOCITY

RGAS	GAMM	MOLW	CF	SIG	XL	T	D
55.0	1.40	28.00	0.850	0.0270	0.507	0.300	0.099

FREQ	PA1	PA2	PHASE	RESIS	REACT	IMPED	ABSOR	UORF	VELPT
1100.	151.5	151.0	113.0	3.537	1.501	3.843	0.619	68.4	560.3
1100.	159.3	157.7	113.0	4.013	1.703	4.360	0.572	149.8	560.0
1100.	171.8	167.4	118.0	5.322	2.829	6.027	0.443	457.7	560.9
1100.	149.5	146.0	98.0	5.473	0.769	5.527	0.515	37.5	646.1
1100.	159.3	154.8	97.0	6.162	0.756	6.208	0.475	104.4	646.7
1100.	159.3	154.6	97.0	6.311	0.774	6.359	0.466	102.1	647.3
1100.	169.1	162.6	101.0	7.679	1.492	7.823	0.396	256.4	647.3
1100.	176.4	167.7	102.0	9.815	2.086	10.034	0.323	453.4	681.3
1100.	149.5	149.7	127.0	2.907	2.191	3.640	0.579	57.0	409.6
1100.	159.3	159.0	141.0	2.398	2.962	3.811	0.472	164.6	398.0

GN FLOW PAST TESTS 1500R 2/24/70

RGAS	GAMM	MOLW	CF	SIG	XL	T	D
55.0	1.40	28.00	0.850	0.0270	0.507	0.300	0.099

FREQ	PA1	PA2	PHASE	RESIS	REACT	IMPED	ABSOR	UORF	VELPT
1100.	149.5	152.1	162.0	0.864	2.662	2.799	0.327	60.8	202.1
1100.	149.5	150.0	129.0	2.769	2.242	3.563	0.575	59.7	385.1
1100.	149.5	149.7	127.0	2.904	2.188	3.637	0.579	57.0	409.2
1100.	149.5	149.7	124.0	3.004	2.026	3.623	0.596	53.9	448.0
1100.	149.5	149.0	119.0	3.459	1.917	3.955	0.587	45.4	492.4
1100.	149.5	150.1	135.0	2.469	2.469	3.491	0.544	62.8	357.9
1100.	149.5	146.0	98.0	5.473	0.769	5.527	0.515	37.5	646.1
1100.	151.5	151.0	113.0	3.537	1.501	3.842	0.619	68.8	561.8

TEST 05.01-36 6 ELEMENT [illegible]-.36 NOZZLE

RGAS	GAMM	WGLW	CF	SIG	XL	T	D
69.0	1.22	22.40	0.950	[illegible]	[illegible]	.2	0.120

FREQ	PA1	PA2	PHASE	RESIS	REACT	IMPED	ABSOR	UORF	VELPT
2250.	200.9	195.7	25.3	3.070	-6.496	7.185	0.208	1484.1	950.0

TEST 05.01-36 4.5 ELEMENT [illegible]-.36 NOZZLE

RGAS	GAMM	WGLW	CF	SIG	XL	T	D
69.0	1.22	22.40	0.950	[illegible]	.800	0.200	0.110

FREQ	PA1	PA2	PHASE	RESIS	REACT	IMPED	ABSOR	UORF	VELPT
2150.	201.1	193.3	35.2	5.827	-8.261	10.110	0.202	1437.0	950.0
2150.	204.2	198.6	33.8	4.352	-6.501	7.823	0.245	2547.2	950.0
2150.	198.6	197.2	41.8	3.178	-3.554	4.768	0.422	2269.0	950.0

TEST 05.01-36 2.5 ELEMENT [illegible]-.36 NOZZLE

RGAS	GAMM	WGLW	CF	SIG	XL	T	D
69.0	1.22	22.40	0.950	0.0250	0.600	0.200	0.100

FREQ	PA1	PA2	PHASE	RESIS	REACT	IMPED	ABSOR	UORF	VELPT
2200.	200.2	189.3	64.8	12.649	-5.952	13.979	0.228	1671.7	950.0
2200.	203.5	194.9	71.8	10.228	-3.362	10.766	0.297	3204.1	950.0
2200.	204.2	195.7	72.3	10.197	-3.254	10.704	0.299	3487.7	950.0

TEST 07.01-36 6 ELEMENT [illegible]-.6 NOZZLE

RGAS	GAMM	MOLW	CF	SIG	XL	T	D
69.0	1.22	22.40	0.950	0.0600	[illegible]	[illegible]	0.120

FREQ	PA1	PA2	PHASE	RESIS	REACT	IMPED	ABSOR	CORF	VELPT
2200.	201.5	196.1	42.8	5.016	-5.417	7.383	0.356	2158.6	1450.0
2200.	202.0	197.0	53.9	5.747	-4.190	7.112	0.364	2307.6	1450.0
2200.	201.9	198.2	58.6	5.195	-3.171	6.086	0.429	2747.4	1450.0
2200.	201.0	196.1	69.5	6.575	-2.458	7.020	0.414	2158.6	1450.0
2200.	197.3	190.1	70.6	8.676	-3.055	9.198	0.337	1079.3	1450.0

TEST 07.01-36 4.5 ELEMENT [illegible]-.6 NOZZLE

RGAS	GAMM	MOLW	CF	SIG	XL	T	D
69.0	1.22	22.40	0.950	0.0450	[illegible]	[illegible]	0.110

FREQ	PA1	PA2	PHASE	RESIS	REACT	IMPED	ABSOR	CORF	VELPT
2200.	198.6	197.6	56.2	3.829	-2.374	4.506	0.529	3401.5	1450.0
2200.	204.3	199.8	56.9	5.607	-3.655	6.693	0.393	4404.6	1450.0
2200.	201.6	201.0	49.8	3.267	-2.761	4.278	0.505	5058.7	1450.0
2200.	199.4	197.6	39.4	3.120	-3.798	4.915	0.397	3401.5	1450.0

TEST 07.01-36 2.5 ELEMENT [illegible]-.6 NOZZLE

RGAS	GAMM	MOLW	CF	SIG	XL	T	D
69.0	1.22	22.40	0.950	0.0250	[illegible]	[illegible]	0.100

FREQ	PA1	PA2	PHASE	RESIS	REACT	IMPED	ABSOR	CORF	VELPT
2150.	185.5	184.8	99.9	4.361.	0.761	4.427	0.594	1380.8	1450.0
2150.	182.7	193.5	127.1	2.944	2.226	3.691	0.574	1149.0	1450.0
2150.	181.7	187.7	131.1	1.539	1.343	2.043	0.746	1917.8	1450.0

TEST 09.01-36 8 ELEMENT M=.36 NOZZLE

RGAS	GAMM	VOLM	CF	SIG	XL	T	D
69.0	1.25	22.40	0.950	0.0800	0.500	0.300	0.139

FREQ	PA1	PA2	PHASE	RESIS	REACT	IMPED	ABSOR	UORF	VELPT
2300.	199.3	196.6	37.6	3.834	-4.979	6.285	0.318	1003.5	950.0
2300.	203.7	198.8	29.7	4.015	-7.039	8.104	0.214	1290.2	950.0
2300.	201.1	199.5	55.6	4.605	-3.153	5.581	0.445	1397.8	950.0

TEST 11.01-36 5 ELEMENT M=.36 NOZZLE

RGAS	GAMM	VOLM	CF	SIG	XL	T	D
69.0	1.22	22.40	0.950	0.0500	0.500	0.300	0.116

FREQ	PA1	PA2	PHASE	RESIS	REACT	IMPED	ABSOR	UORF	VELPT
2300.	205.0	199.3	83.9	0.757	-0.935	0.807	0.364	2184.6	950.0
2300.	204.8	199.3	88.0	0.681	-0.303	0.686	0.370	2184.6	950.0
2300.	205.2	199.5	82.2	0.735	-1.196	0.816	0.363	2242.1	950.0

TEST 11.01-36 2.5 ELEMENT M=.36 NOZZLE

RGAS	GAMM	VOLM	CF	SIG	XL	T	D
69.0	1.22	22.40	0.950	0.0250	0.500	0.300	0.100

FREQ	PA1	PA2	PHASE	RESIS	REACT	IMPED	ABSOR	UORF	VELPT
2200.	200.8	190.6	57.9	13.050	-8.186	15.406	0.197	1539.7	950.0
2200.	205.1	194.8	56.2	13.397	-8.968	16.121	0.186	2419.5	950.0
2200.	204.3	190.9	47.0	16.439	-15.329	22.477	0.121	1594.7	950.0

TEST 10.01-36 A ELEMENT M=.6 NOZZLE

RGAS	GAMM	MCLA	CF	SIG	XL	T	D
69.0	1.22	22.40	0.950	0.0250	0.500	0.300	.0139

FREQ	PA1	PA2	PHASE	RESIS	REACT	IMPED	ABSOR	CORF	VELPT
2150.	198.4	194.7	36.7	4.494	-6.029	7.521	.271	1153.6	1450.0
2150.	201.5	196.6	36.3	5.081	-4.917	7.072	0.239	1431.7	1450.0
2150.	201.5	199.8	57.0	4.976	-3.231	5.943	.431	2176.9	1450.0
2150.	198.1	195.3	48.0	5.057	-4.553	6.804	0.352	1231.7	1450.0
2150.	195.3	191.2	50.0	6.011	-5.744	8.317	0.322	749.2	1450.0
2150.	196.8	195.3	62.0	5.142	-2.734	5.824	0.455	1231.7	1450.0
2150.	202.0	200.4	51.0	4.609	-3.730	5.93	.446	22 5.0	1450.0
2150.	197.5	194.3	56.4	7.057	-5.444	7.071	0.439	1102.5	1450.0
2150.	195.7	192.9	56.2	5.661	-3.789	6.811	0.345	923.0	1450.0

TEST 10.01-3 5 ELEMENT M=.6 NOZZLE

RGAS	GAMM	MCLA	CF	SIG	XL	T	D
69.0	1.22	22.40	0.950	0.0500	0.500	0.300	.0116

FREQ	PA1	PA2	PHASE	RESIS	REACT	IMPED	ABSOR	CORF	VELPT
2150.	199.7	181.1	62.2	36.922	-19.467	41.740	0.081	385.6	1450.0
2150.	199.2	181.1	83.0	39.182	2.053	39.235	0.096	385.6	1450.0
2150.	200.0	185.4	148.3	14.545	23.550	27.680	0.073	598.9	1450.0

TEST 10.01-3 2.5 ELEMENT M=.6 NOZZLE

RGAS	GAMM	MCLA	CF	SIG	XL	T	D
69.0	1.22	22.40	0.950	0.0250	0.500	0.300	0.100

FREQ	PA1	PA2	PHASE	RESIS	REACT	IMPED	ABSOR	CORF	VELPT
2150.	190.5	180.9	21.7	5.440	-13.670	14.713	0.095	754.9	1450.0
2150.	184.2	182.5	14.8	1.537	-5.817	6.017	0.152	902.5	1450.0

APPENDIX III
LINER DESIGN COMPUTER PROGRAM

The contents of this appendix appear in the following order:

A. Source Program Listing

B. Sample Input

C. Output Symbol Description

D. Output for Example Case

The Sample input sheet may be used as the input for a program test case; results identical to those of the Example Case will be obtained.

A. SOURCE PROGRAM LISTING

The program was written in FORTRAN IV for the IBM 1130 computer. The following listing includes the program coding instructions, with a brief description of the input data, and a source listing of the program.

```
PAGE    1

// JOB

LOG DRIVE    CART SPEC    CART AVAIL    PHY DRIVE
  0000         0D22         0D22          0000

V2 M06   ACTUAL  8K  CONFIG  8K

// FOR
*IOCS(CARD,1132 PRINTER)
*  ONE WORD INTEGERS
*LIST SOURCE PROGRAM
*
**     HIGH FLOW VELOCITY DESIGN PROGRAM
```

```
C
C
C                    INPUT SYMBOL NOMENCLATURE
C
C   CARD  COLS  VARIABLE        DESCRIPTION
C
C     1  01-05    CASES     NO. OF COMPLETE SETS OF INPUT
C     2  01-80    TITLE     ANY TITLE INFORMATION
C
C     3  01-10    PRESS     COMBUSTION PRESSURE (PSIA).
C        11-20    GASCN     GAS CONSTANT IN RESONATOR (LBF-FT/LBM/R).
C        21-30    TEMP      GAS TEMPERATURE IN RESONATOR APERATURES
C                           (DEGREES RANKINE).
C        31-40    GAMA      RATIO OF SPECIFIC HEATS OF GAS IN RESONATOR.
C        41-50    VELPT     VELOCITY OF FLOW PAST APERTURES.
C                           FOR NO FLOW INPUT VELPT=0.0
C                           FOR FLOW THRU. INPUT VELPT AS NEGATIVE.
C        51-60    TEMPC     CHAMBER GAS TERMPERATURE (DEG. R).
C        61-70    TEMCA     CAVITY TEMPERATURE (DEG.R)
C
C     4  01-10    FMIN      MINIMUM FREQUENCY OF OSCILLATIONS (HZ)
C        11-20    DELF      FREQUENCY INCREMENT (HZ)
C        21-30    FMAX      MAXIMUM FREQUENCY OF OSCILLATIONS (HZ)
C        31-40    SIGN      MINIMUM LINER OPEN AREA RATIO (PERCENT)
C        41-50    DELS      LINER OPEN AREA RATIO INCREMENT (PERCENT)
C        51-60    SIGM      MAXIMUM LINER OPEN AREA RATIO (PERCENT)
C
C     5  01-10    SPLN      MINIMUM CHAMBER PRESSURE OSCILLATIONS
C                           (DECIBELS REFERENCE 0.0002 MICROBAR)
C        11-20    DELP      PRESSURE OSCILLATION INCREMENT (DB)
C        21-30    SPLM      MAXIMUM CHAMBER PRESSURE OSCILLATIONS (DB)
C        31-40    CFMIN     MINIMUM FLOW COEFFICIENT OF LINER APERTURES
C        41-50    DELCF     FLOW COEFFICIENT INCREMENT
C        51-60    CFMAX     MAXIMUM FLOW COEFFICIENT OF LINER APERATURES
C
C     6  01-10    XLMIN     MINIMUM RESONATOR CAVITY DEPTH (INCHES)
C        11-20    DELXL     RESONATOR CAVITY DEPTH INCREMENT (INCHES)
C        21-30    XLMAX     MAXIMUM RESONATOR CAVITY DEPTH (INCHES)
C        31-40    TMIN      MINIMUM LINER THICKNESS (INCHES)
C        41-50    DELT      LINER THICKNESS INCREMENT (INCHES)
C        51-60    TMAX      MAXIMUM LINER THICKNESS (INCHES)
C
C     7  01-10    DMIN      MINIMUM LINER APERATURE DIAMETER (INCHES)
C        11-20    DELD      APERATURE DIAMETER INCREMENT (INCHES)
C        21-30    DMAX      MAXIMUM LINER APERTURE DIAMETER (INCHES)
C
C  NOTE. CARD 2,3,4,5,6 AND 7 WILL BE REPEATED CASES (CARD 1) TIMES
C
C
      REAL IMPED
      DIMENSION TITLE(20)
  100 FORMAT(8E10.0)
      READ(2,100) CASES
      NCASE=CASES+.05
      DO 299 MWH=1,NCASE
      READ(2,101) TITLE
```

```
  101 FORMAT(20A4)
      READ (2,100) PRESS,GASCN,TEMP,GAMA,VELPT,TEMPC,TEMCA
      READ(2,100)  FMIN,DELF,FMAX,SIGN,DELS,SIGM
      READ(2,100) SPLM,DELP,SPLM,CFMIN,DELCF,CFMAX
      READ(2,100) XLMIN,DELXL,XLMAX,TMIN,DELT,TMAX
      READ(2,100) DMIN,DELD,DMAX
      SIGMA = SIGM
  301 P1=SPLM
  302 CF=CFMIN
  303 XL=XLMIN
  304 T=TMIN
  305 D=DMIN
  306 CONTINUE
      FREQ=FMIN
      G=32.1725
      SONC=SQRT(GAMA*G*GASCN*TEMPC)
      FLMAC=VELPT/SONC
      WRITE(3,200) TITLE
  200 FORMAT('1',1X,20A4// 21X'INPUT LINER PROPERTIES AND DIMENSIONS'//1
      WRITE(3,201) PRESS,GASCN,TEMP,GAMA,FLMAC
  201 FORMAT(10X'COMBUSTION STATIC PRESSURE (PSIA)'F27.3/
     110X'GAS CONSTANT IN RESONATOR (LBF*FT/LBM/R)'F20.3/
     210X'GAS TEMPERATURE IN RESONATOR APERATURES (DEGREE R)'F10.3/
     310X'RATIO OF SPECIFIC HEATS'F37.3/
     410X'MACH NUMBER OF FLOW'F41.3)
      WRITE(3,202) SIGMA,P1,CF,XL,T
  202 FORMAT(10X'LINER OPEN AREA RATIO (PERCENT)'F29.3/
     110X'CHAMBER PRESSURE OSCILLATIONS (DECIBELS)'F20.3/
     210X'FLOW COEFFICIENT OF LINER APERTURES'F25.3/
     310X'RESONATOR CAVITY DEPTH (INCHES)'F29.3/
     410X'LINER THICKNESS (INCHES)'F36.3)
      WRITE(3,203) D
  203 FORMAT(10X'LINER APERTURE DIAMETER (INCHES)'F28.3)
      WRITE(3,210) TEMCA
  210 FORMAT(10X'LINER CAVITY TEMPERATURE (DEGREE R)'F25.3)
      PI2=6.2832
      DEN=144.*PRESS/GASCN/TEMP
      SONIC=SQRT(GAMA*GASCN*TEMP*G)
      SONCC=SQRT(GAMA*GASCN*G*TEMCA)
      IF(FLMAC) 307,308,308
C
C     FLOW PAST OR NO FLOW CALCULATIONS
C
  308 CONTINUE
      REAFO=0.0
      P1A=4176.0*SQRT(2.0)*(10.0**(P1/20.0-10.0))
      UORFO=SQRT((P1A*CF**2*G/(0.37*DEN)))
      DENC=144.*PRESS/GASCN/TEMPC
      VPOR=(VELPT/UORFO)*(DEN/DENC)**1.5
      SIGIM = (SIGMA/100.0)/(1.0-(SIGMA/100.0)**2)
  315 RESFO=0.37*UORFO/((CF**2)*SIGIM*SONIC)
      IF(VPOR-1.5) 499,499,498
  498 RESFO=RESFO*(.33*VPOR+.5)
  499 CONTINUE
      ABSFO=4.*RESFO/((RESFO+1.)**2)
      ABSFO = ABSFO * 100.0
      IF(FLMAC) 324,325,325
  324 XLEFF=(T/12.)+(D/12.)
      GO TO 326
  325 XLEFF=T/12.+.375*(.85*D/12.*(1.-.7*SQRT(SIGMA)))
```

```
  326 FO = SQRT(SONCC*SONIC*SIGIM/(XLEFF*(XL@12.)))/PI2
      XLEFF=XLEFF*12.
      WRITE(3,204)
  204 FORMAT(/////8X'CALCULATED GAS PROPERTIES AND ACOUSTIC PROPERTIES
     1 AT RESONANCE'/)
      WRITE(3,205) DEN,SONIC,XLEFF,P1A,UORFO
  205 FORMAT(10X'DENSITY OF APERTURE GAS (LBM/FT**3)'F25.3/
     1 10X'SONIC VELOCITY OF APERATURE GAS (FT/SEC)'F20.3/
     2 10X'EFFECTIVE APERTURE LENGTH (INCHES)'F26.3/
     3 10X'CHAMBER PRESSURE OSCILLATION (LBF/FT**2)'F20.3/
     4 10X'ORIFICE PARTICLE VELOCITY AT RESONANCE (FT/SEC)'F13.3)
      WRITE(3,206) FO,REAFO,RESFO,ABSFO
  206 FORMAT(10X'LINER RESONANT FREQUENCY (HZ)'F31.3/
     1 10X'ACOUSTIC REACTANCE AT RESONANCE'F29.3/
     2 10X'ACOUSTIC RESISTANCE AT RESONANCE'F28.3/
     3 10X'ABSORPTION COEFFICIENT AT RESONANCE (PERCENT)'F15.3)
      WRITE(3,207)
  207 FORMAT(///2X'FREQ'7X'RESIS'7X'REACT'7X'IMPED'7X'UORFX'7X'ABSOR'/)
      WRITE(3,208)
  208 FORMAT(3X'(HZ)'41X'(FT/SEC)'4X'(PERCENT)'/)
      XLEFF=XLEFF/12.
      GO TO 312
  309 CONTINUE
      IF (FMAX-FREQ) 311,311,310
  310 FREQ=FREQ+DELF
  312 REACT=PI2*XLEFF*FREQ/SONIC/SIGIM-COS(PI2*FREQ*XL/SONCC/12.)/(SIN(
     1PI2*FREQ*XL/SONCC/12.))
      UORFX=(-(2.7*SIGIM*SONIC*REACT*(CF**2))**2+SQRT((2.7*SIGIM*SONIC*
     1 REACT*(CF**2))**4+4.0*(UORFO**4)))/2.0
      UORFX=SQRT(UORFX)
      IF(FLMAC) 328,329,329
  328 IF(-FLMAC-0.5*UORFX/SONIC) 329,327,327
  329 RESIS=0.37*UORFX/(SIGIM*SONIC*(CF**2))
      VPOR=(VELAT/UORFX)*(DEN/DENC)**1.5
      IF(VPOR-1.5) 501,501,500
  500 RESIS=RESIS*(.33*VPOR+.5)
  501 CONTINUE
      IMPED=SQRT((RESIS**2)+(REACT**2))
      ABSOR=4.*RESIS/((RESIS+1.)**2+(REACT**2))
      ABSOR=ABSOR*100.
      WRITE(3,209) FREQ,RESIS,REACT,IMPED,UORFX,ABSOR
  209 FORMAT(F8.1,5F12.3)
      GO TO 309
C
C     FLOW THROUGH CALCULATIONS
C
  307 CONTINUE
      REAFO=0.0
      P1A=4176.0*SQRT(2.0)*(10.**(P1/20.-10.))
      UORFO=SQRT((P1A*CF**2)*G/(0.37*DEN))
      SIGIM = (SIGMA/100.0)/(1.0-(SIGMA/100.0)**2)
      IF(-FLMAC-0.5*UORFO/SONIC) 315,316,316
  316 RESFO = FLMAC * (-1.0)/(SIGIM*(CF**3))
      XLEFF=(AT/12.)+(D/12.)
      ABSFO=4.*RESFO/(RESFO+1.)**2
      ABSFO = ABSFO * 100.0
      FO = SONIC*SQRT(SIGIM/(XLEFF*(XL/12.0)))/PI2
      XLEFF=XLEFF*12.
      WRITE(3,204)
```

```
      WRITE(3,205) DEN,SONIC,XLEFF,P1A,UOREO
      WRITE(3,206) FO,REAFO,RESFO,AHSFO
      WRITE(3,207)
      WRITE(3,208)
      XLEFF = XLEFF/12.0
      GO TO 312
  327 RESIS=FLMAC/(SIGIM*(CF**3))*(-1.0)
      UOREX=FLMAC*SONIC*(-1.0)
      IMPED=SQRT((RESIS**2)+(REACT**2))
      ABSOR=4.*RESIS/((RES.S+.)**2+REACT**2)
      ABSOR=ABSOR*.00.
      WRITE(3,209) FREQ,RESIS,REACT,IMPED,UOREX,ABSOR
      GO TO 309
  311 CONTINUE
      IF(D-DMAX) 401,402,402.
  401 D=D+DELD
      GO TO 306
  402 IF(T-TMAX) 403,404,404
  403 T=T+DELT
      GO TO 305
  404 IF(XL-XLMAX) 405,406,406
  405 XL=XL+DELXL
      GO TO 304
  406 IF(CF-CFMAX) 407,408,408
  407 CF=CF+DELCF
      GO TO 303
  408 IF(P1-SPLM) 409,410,410
  409 P1=P1+DELP
      GO TO 302
  410 IF(SIGMA-SIGM) 411,299,299
  411 SIGMA=SIGMA+DELS
      GO TO 301
  299 CONTINUE
      CALL EXIT
      END

FEATURES SUPPORTED
 ONE WORD INTEGERS
 IOCS

CORE REQUIREMENTS FOR
 COMMON       0  VARIABLES    170  PROGRAM    1856

 END OF COMPILATION

// XEQ
```

B. SAMPLE INPUT

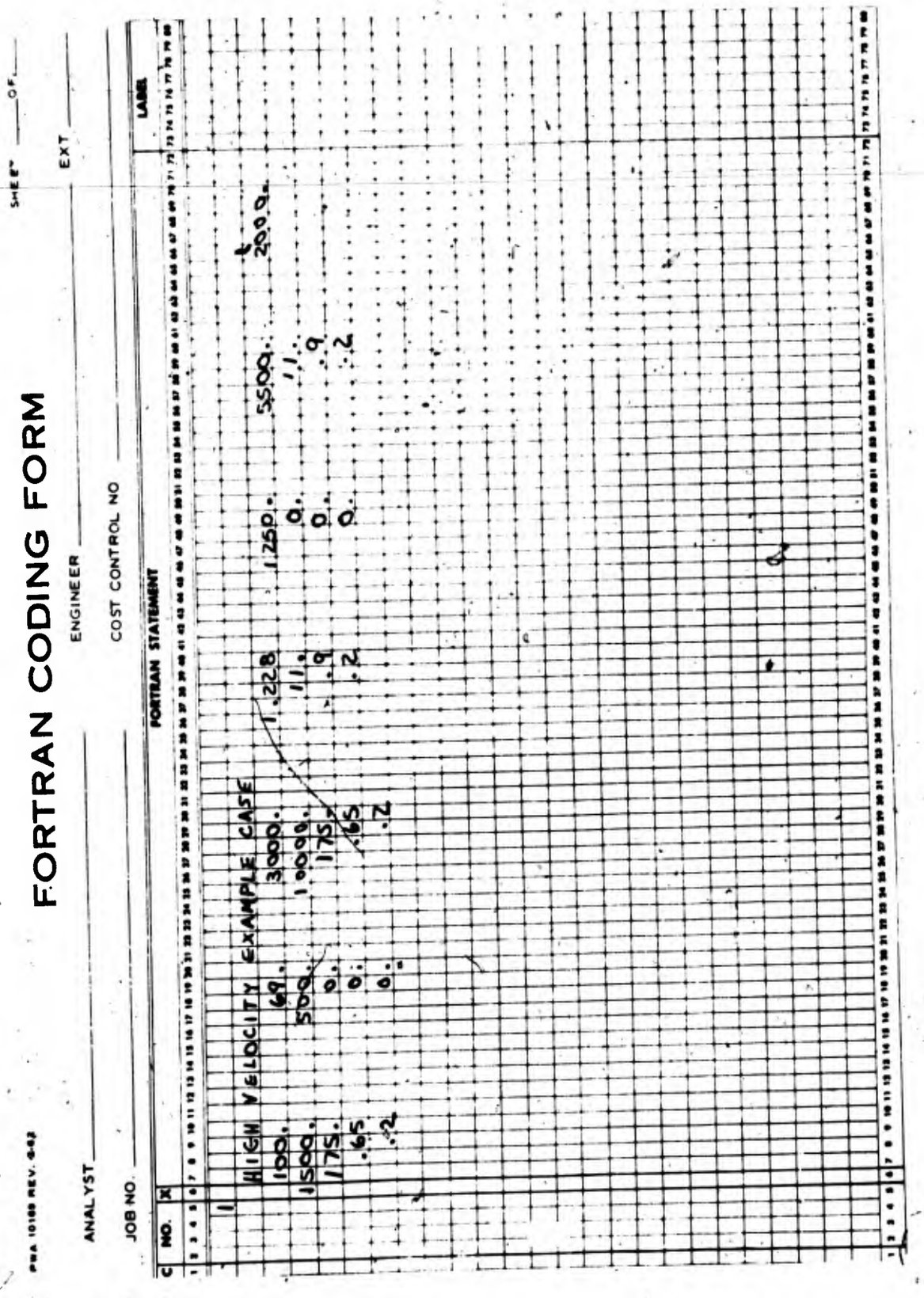

C. OUTPUT SYMBOL DESCRIPTION

The symbols used for the output format are described below.

Symbol	Description
FREQ	Frequency, Hz
RESIS	Specific acoustic resistance
REACT	Specific acoustic reactance
IMPED	Specific acoustic impedance
UORFX	Orifice particle velocity, ft/sec
ABSOR	Absorption coefficient, %

D. OUTPUT FOR EXAMPLE CASE

HIGH VELOCITY EXAMPLE CASE

INPUT LINER PROPERTIES AND DIMENSIONS

COMBUSTION STATIC PRESSURE (PSIA)	100.000
GAS CONSTANT IN RESONATOR (LBF*FT/LBM/R)	69.000
GAS TEMPERATURE IN RESONATOR APERATURES (DEGREE R)	3000.000
RATIO OF SPECIFIC HEATS	1.228
MACH NUMBER OF FLOW	0.322
LINER OPEN AREA RATIO (PERCENT)	11.000
CHAMBER PRESSURE OSCILLATIONS (DECIBELS)	175.000
FLOW COEFFICIENT OF LINER APERTURES	0.900
RESONATOR CAVITY DEPTH (INCHES)	0.650
LINER THICKNESS (INCHES)	0.200
LINER APERTURE DIAMETER (INCHES)	0.200
LINER CAVITY TEMPERATURE (DEGREE R)	2000.000

CALCULATED GAS PROPERTIES AND ACOUSTIC PROPERTIES AT RESONANCE

DENSITY OF APERTURE GAS (LBM/FT**3)	0.069
SONIC VELOCITY OF APERATURE GAS (FT/SEC)	2859.741
EFFECTIVE APERTURE LENGTH (INCHES)	0.115
CHAMBER PRESSURE OSCILLATION (LBF/FT**2)	332.105
ORIFICE PARTICLE VELOCITY AT RESONANCE (FT/SEC)	579.863
LINER RESONANT FREQUENCY (HZ)	6003.922
ACOUSTIC REACTANCE AT RESONANCE	0.000
ACOUSTIC RESISTANCE AT RESONANCE	1.884
ABSORPTION COEFFICIENT AT RESONANCE (PERCENT)	90.592

FREQ (HZ)	RESIS	REACT	IMPED	UOREX (FT/SEC)	ABSOR (PERCENT)
1500.0	1.551	-4.215	4.491	114.457	25.556
2000.0	1.505	-2.951	3.350	169.050	41.189
2500.0	1.628	-2.145	2.693	222.546	56.575
3000.0	1.681	-1.568	2.299	297.080	69.701
3500.0	1.745	-1.120	2.074	386.084	79.390
4000.0	1.809	-0.754	1.960	474.686	85.523
4500.0	1.856	-0.442	1.908	540.382	88.872
5000.0	1.880	-0.169	1.888	573.956	90.345
5500.0	1.883	0.078	1.885	578.566	90.538
6000.0	1.871	0.306	1.895	560.619	89.775
6500.0	1.846	0.518	1.917	526.681	88.231
7000.0	1.815	0.718	1.952	483.329	86.008
7500.0	1.782	0.909	2.001	436.881	83.197
8000.0	1.750	1.094	2.064	392.314	79.908
8500.0	1.721	1.273	2.141	352.417	76.277
9000.0	1.697	1.448	2.230	318.007	72.439
9500.0	1.676	1.619	2.330	288.766	68.514
10000.0	1.658	1.789	2.432	263.950	64.593

APPENDIX IV
HEATED FUEL FACILITY

Combustion stability has in some instances been a problem in motors burning heated 50-50 blend fuel. Thus, to establish the effectiveness of the acoustic liner configuration chosen for the regeneratively cooled chamber, it was necessary to conduct firings at the same injector fuel inlet temperature as would be encountered when the cooled chamber was fired. To accomplish this a heated fuel system was fabricated and installed on the B-5 test stand. A schematic of the heated fuel system is shown in figure 82. The system consisted of an enlarged section of run line that held approximately eight gallons of fuel, immersed in an open vat of ethylene glycol. The vat was heated with external electrical heaters and wrapped with thermal insulation.

Thermocouples were installed at several locations through the enlarged run line to determine when the desired fuel temperature was reached.

The procedure used for a firing was as follows: the run line up to the fuel control valve was filled with fuel and the ethylene glycol was heated. When the fuel in the heated section reached 250°F, the heaters were shut off, the ethylene glycol drained, and the firing commenced. After 2.0 sec the control valve was closed and the vat was filled with cold water. The system was then allowed to cool to approximately ambient conditions before the water was drained and the vat filled with ethylene glycol in preparation for the next test.

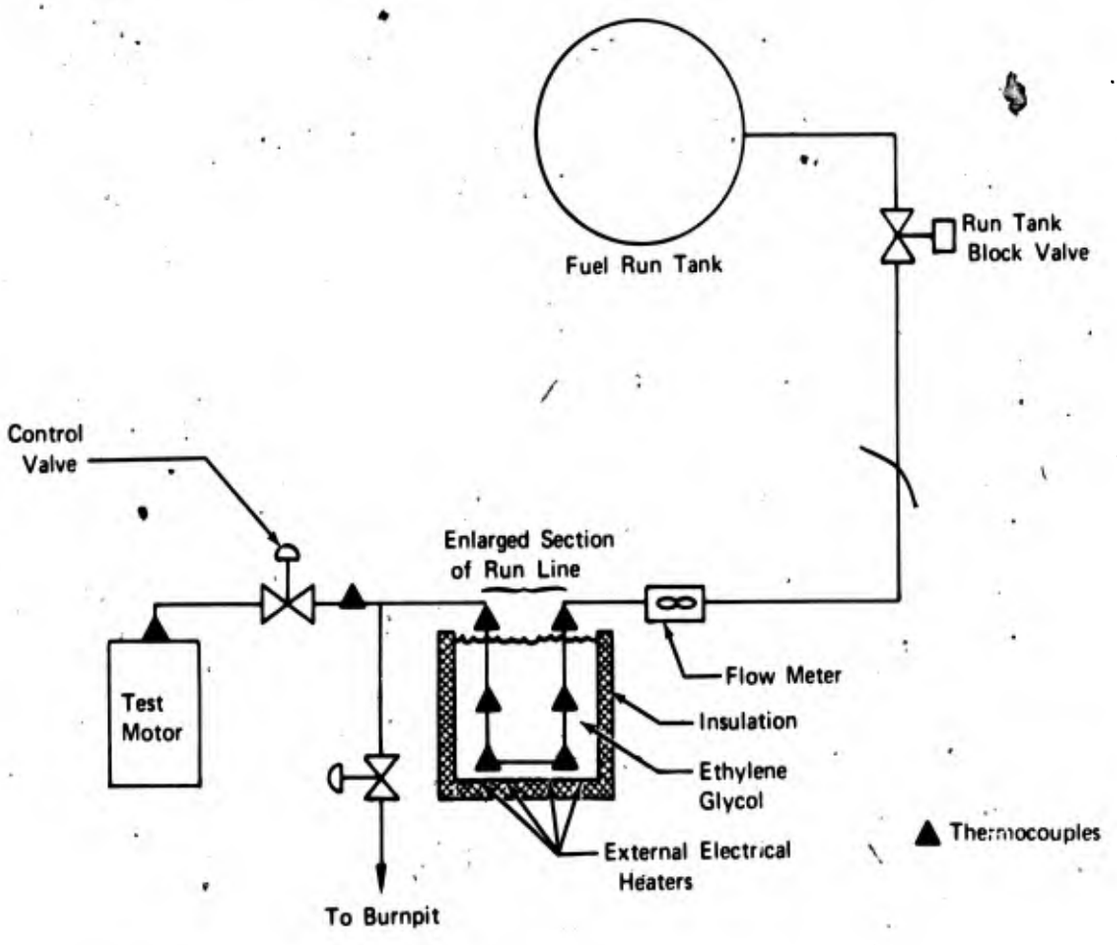

Figure 82. Heated Fuel Facility FD 53781

Unclassified

Security Classification

DOCUMENT CONTROL DATA - R & D

(Security classification of title, body of abstract and indexing annotation must be entered when the overall report is classified)

1 ORIGINATING ACTIVITY (Corporate author)
Pratt & Whitney Aircraft
Division of United Aircraft Corporation

2a. REPORT SECURITY CLASSIFICATION
Confidential

2b GROUP
4

3 REPORT TITLE
Acoustic Liner Design and Demonstration Final Report

4 DESCRIPTIVE NOTES (Type of report and inclusive dates)
Final Report, Inclusive Dates: 15 November 1968 through 30 April 1971

5 AUTHOR(S) (First name, middle initial, last name)
Gary D. Garrison

6 REPORT DATE
28 August 1971

7a. TOTAL NO OF PAGES

7b NO OF REFS
16

8a CONTRACT OR GRANT NO
F04611-69-C-0017

b PROJECT NO
Air Force Project No. 3058

c
Program Structure No. (BPSN): 623058

d

9a. ORIGINATOR'S REPORT NUMBER(S)
AFRPL-TR-71-75

9b. OTHER REPORT NO(S) (Any other numbers that may be assigned this report)
PWA FR-4515

10 DISTRIBUTION STATEMENT
In addition to security requirements which must be met, this document is subject to special export controls and each transmittal to foreign governments or foreign nationals may be made only with prior approval of AFRPL (RPPR/STINFO), Edwards, California 93523.

11 SUPPLEMENTARY NOTES

12 SPONSORING MILITARY ACTIVITY
Air Force Rocket Propulsion Laboratory
Air Force Systems Command
United States Air Force
Edwards Air Force Base, California

13 ABSTRACT

The objectives of this two-phase exploratory development program were (1) to demonstrate the effectiveness for suppressing combustion instability of a regeneratively cooled acoustic liner installed in flight-type hardware, and (2) to extend the acoustic liner design theory to include rocket chamber applications with high combustion gas velocities and high dynamic pressure amplitudes. Phase I consisted of the design, fabrication and firing of a fuel cooled, 15,000 lb thrust chamber incorporating an integral acoustic liner, using an Agena injector known to be dynamically unstable with N_2O_4 50 / N_2H_4-50 / UDMH propellants. Before fabrication of the chamber was initiated adequate suppression characteristics of the liner design was demonstrated in short duration tests of uncooled hardware. The uncooled test series included firings during which both the baseline heat transfer rates and the effects of liner apertures on the heat transfer rates were measured. Other uncooled firings were conducted to measure the dynamic stability characteristics of the potential flightweight liner design, to determine the minimum required liner length, and to supply data for the final liner design. Thirty uncooled firings and thirteen firings of the regeneratively cooled chamber were made; combustion in the regeneratively cooled chamber was demonstrated to be dynamically stable. Results under this phase of the program demonstrated that regeneratively cooled acoustic liners are feasible for flightweight thrust chamber applications. The necessary acoustic data for the Phase II theory extension were obtained from high Mach number cold-flow impedance experiments, and from firings of an uncooled rocket motor using a technique based on the measurement of the complex pressure difference across the absorbing liner surface. The acoustic data formed the basis for appropriate theory extensions, and using the extended theory, two different types of resonant absorbing liners were designed for a spontaneously unstable, existing uncooled thrust chamber having a chamber Mach number of 0.32. Five firings were made with N_2O_4 50 / UDMH-50 / N_2H_4 propellants at a nominal thrust level of 5000 lb_f. The liners suppressed the most prevalent modes of combustion instability, but spontaneous pops triggered instability at frequencies greater than 6400 Hz. Both liners theoretically had sufficient absorption to suppress the high frequency modes. It was concluded that failure of the liners to suppress high frequency modes of instability in the particular test motor used was not caused by the high net flow past the liners, but was the result of errors from extrapolation of the liner design theory with frequency. Additional firings of the motor with liner elements instrumented for high frequency acoustic impedance measurements are recommended.

DD FORM 1 NOV 65 1473

Unclassified

Security Classification

14 KEY WORDS	LINK A		LINK B		LINK C	
	ROLE	WT	ROLE	WT	ROLE	WT
Acoustic Liners						
Combustion Instability						
Agena Injectors						
Flightweight Rocket Motor						
Regenerative (Fuel) Cooling						
N_2O_4/UDMH-N_2H_4 (50-50 Blend) Propellants						
Acoustic Liner Design Computer Program						
Refractory Coating						
Combustion Perturbation Devices						
Dynamic Combustion Stability						
High Mach No. Acoustic Experiments						
High Mach No. Impedance Data						
Pressure-Phase Impedance Measuring Techniques						